RSC Advances

REVIEW

View Article Online
View Journal | View Issue

Cite this: *RSC Adv.*, 2024, **14**, 21706

Recent trends and future perspectives of thermoelectric materials and their applications

Pavithra Baskaran and Mani Rajasekar *

This review explores the ever-evolving landscape of thermoelectric materials, focusing on the latest trends and innovations in ceramics, thermally conductive gel-like materials, metals, nanoparticles, polymers, and silicon. Thermoelectric materials have garnered significant attention for their capability to convert waste heat into electrical power, positioning them as promising candidates for energy harvesting and cooling applications. This review distinguishes itself by highlighting recent advancements in synthesis methods, advanced doping strategies, and nanostructuring techniques that have markedly enhanced material performance. It provides a comprehensive analysis of the controlled properties concerning their synthesis parameters, such as electrical conductivity, Seebeck coefficient, and thermal conductivity. Furthermore, this work delves into the emerging applications of thermoelectric devices across diverse fields, including automotive, aerospace, wearable electronics, and industrial waste heat recovery. By offering forward-looking insights, this review outlines thermoelectric devices' challenges and future prospects, underscoring their potential to contribute to sustainable energy solutions and efficient thermal management systems. By integrating current trends with future projections, this review offers a timely and comprehensive roadmap for researchers and engineers dedicated to advancing next-generation thermoelectric technologies.

Received 17th May 2024
Accepted 3rd July 2024

DOI: 10.1039/d4ra03625e

rsc.li/rsc-advances

1. Introduction

Recent years have witnessed a surge of interest in thermoelectric devices and their applications, driven by the pressing need for sustainable energy solutions and efficient thermal management systems.[1] Thermoelectric materials have become more attractive as potential solutions to these problems because of their exceptional capacity to transform waste heat into useful electrical power. This paper aims to provide a comprehensive overview of the recent trends in thermoelectric devices and their diverse applications across various industries, while also delving into the future prospects and potential impact of these advancements. The field of thermoelectric materials and devices has undergone significant evolution, marked by a growing emphasis on enhancing performance, scalability, and applicability.[2–5] Recent advancements in materials science have led to the development of novel thermoelectric materials, including nanostructured materials, organic and hybrid materials, and the utilization of advanced manufacturing techniques. These innovations have opened new avenues for improving the efficiency and cost-effectiveness of thermoelectric devices, thereby expanding their potential applications.[6–8]

One of the key future prospects in the realm of thermoelectric devices lies in the continued refinement of materials and manufacturing processes to achieve higher thermoelectric conversion efficiencies. The pursuit of materials with enhanced thermoelectric properties, such as high thermoelectric figure of merit (ZT), remains a focal point for researchers and industry stakeholders. Additionally, the exploration of scalable and cost-effective manufacturing methods holds promise for enabling the widespread adoption of thermoelectric technology in diverse settings.[9–11] The potential applications of thermoelectric devices span a wide spectrum of industries, each presenting unique opportunities for leveraging waste heat recovery and efficient thermal management. In the automotive sector, thermoelectric generators offer the prospect of harnessing waste heat from exhaust systems to power vehicle electronics and reduce fuel consumption. Similarly, in aerospace applications, thermoelectric devices hold the potential to enhance energy efficiency and provide reliable power sources for critical systems. The integration of thermoelectric modules in wearable electronics presents an intriguing avenue for self-powered, energy-autonomous wearable devices, catering to the burgeoning demand for portable and sustainable technologies. Furthermore, in industrial settings, thermoelectric systems offer the prospect of recovering waste heat from various

Centre for Molecular and Nanomedical Sciences, International Research Centre, Sathyabama Institute of Science and Technology (Deemed to be University), Chennai 600 119, Tamilnadu, India. E-mail: mrajasekar_83@yahoo.com; drmrajasekar.irc@sathyabama.ac.in; Tel: +91-9710230530

processes, thereby improving overall energy efficiency and reducing environmental impact.[12]

The future prospects of thermoelectric devices extend beyond their immediate applications, encompassing broader implications for sustainable energy solutions and environmental conservation. As the global focus on renewable energy and energy efficiency intensifies, thermoelectric technology stands poised to play a pivotal role in realizing these objectives.[13–15] By enabling the conversion of waste heat into useable electrical power, thermoelectric devices have the potential to contribute significantly to the reduction of greenhouse gas emissions and the overall sustainability of energy systems. Moreover, the integration of thermoelectric devices into existing infrastructure and energy systems holds promise for enhancing overall energy efficiency and reducing reliance on traditional energy sources.[16] The prospect of utilizing thermoelectric technology (**1**) in conjunction with solar panels or other renewable energy sources to create hybrid energy systems represents an exciting avenue for achieving greater energy autonomy and resilience (Fig. 1).

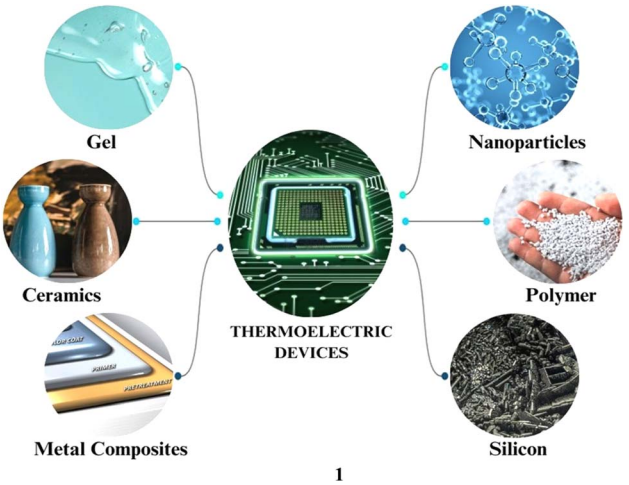

1

Fig. 1 Schematic representation of thermoelectrical materials and applications.

Pavithra Baskaran

Pavithra Baskaran was born in 1998, Cuddalore district, Tamilnadu, India. She is currently working as a Project Fellow in the Centre of Nanoscience and Nanotechnology, International Research Centre, Sathyabama Institute of Science and Technology (deemed to be University), Chennai, under the guidance of Dr M. Rajasekar., Scientist-C/Assistant Professor (Research). After completing her Undergraduate degree in Physics at Saradha Gangadharan College of Arts and Science (an affiliated college of Pondicherry University), Pondicherry, in 2018. She started her Post-Graduate degree in physics at Annamalai University, Chidambaram, Tamilnadu. Additionally, she has pursued her BEd degree in M. K. Raman of Education, (affiliated to Tamil Nadu Teachers Education University, Chennai). Her research interest generally includes Electrical Power & Energy Systems and materials applications.

Mani Rajasekar

Dr M. Rajasekar is currently working as Scientist-C/Assistant Professor (Research) of Chemistry at the Centre for Molecular and Nanomedical Sciences, International Research Centre, Sathyabama Institute of Science and Technology (deemed to be University), Chennai since 2018. He was born in Agatheripattu village, Tiruvannamalai district in Tamil Nadu, India, and his main research interest is in the area of material chemistry. He received his BSc degree from the Department of Chemistry, Arignar Anna Govt. Arts College, Cheyyar, affiliated to the University of Madras in 2005 and MSc Degree from the Department of Chemistry, C. Abdul Hakeem College of Arts and Science, Vellore, affiliated to Thiruvalluvar University in 2007. He received his M. Phil degree from the Department of Chemistry, The New College, affiliated with the University of Madras, Chennai, in 2008. He worked as a Visiting Lecturer at the Department of Chemistry, Anna University, Chennai from 26.06.2008 to 30.12.2008 and a PhD degree from the Department of Organic Chemistry, the University of Madras in 2015. He worked as a National Postdoctoral (DST-SERB) at Sathyabama University, Chennai from 2016–2018. He received his BEd (2021) and MEd (2023) degrees from Arunachala College of Education, affiliated with Tamil Nadu Teachers Education University, Chennai. He was awarded NET, SLET, SET, NPDF, DSKPDF, Nehru PDF, Young Scientist, RSC Advances panel reviewer, and National Educational Star Award by "The Glorious Organization for Accelerated to Literacy (GOAL)", New Delhi. Additionally, he has been granted five patents, published twelve books, and has authored two monographs.

In the context of thermal management, the future prospects of thermoelectric devices are equally compelling. The ability of thermoelectric modules to provide precise and localized cooling or heating presents opportunities for improving the efficiency and reliability of thermal control systems in various applications, ranging from electronics cooling to temperature regulation in medical devices.[17–20] The potential impact of thermoelectric technology on sustainable energy solutions and thermal management systems is underscored by the growing interest and investment in research and development in this field. As governments, industries, and research institutions increasingly recognize the significance of addressing energy sustainability and efficiency, the momentum behind thermoelectric technology continues to build.

2. Ceramic based thermoelectric devices

Researchers are increasingly focusing on processing technologies to enhance thermoelectric generator (TEG) production. A quick and scalable method for producing TEGs involves spray coating and laser structuring, which offers flexibility. The process combines both additive and subtractive technologies to create a versatile ceramic-based TEG suitable for high temperatures with significant potential for optimization. A prototype of a TEG based on Ca_3Co_4O (CCO) and Ag on a ceramic substrate (**2**) was fabricated. The microstructural and thermoelectric analyses demonstrate achievement of up to 1.65 μW cm^2 at 673 K with a ΔT of 100 K. Additionally, the developed process offers high controllability facilitating adaptation for various thermoelectric materials (Fig. 2a).[21] Furthermore, plate-like microcrystal particles of $Ca_3Co_4O_9$ (**3**) were synthesized using molten salt synthesis. Morphologically optimized particles were used as template seeds to fabricate denser $Ca_3Co_4O_9$ thermoelectric ceramics. The effects of $Ca_3Co_4O_9$ template seeds on the ceramics microstructure and thermoelectric performance were studied. The findings demonstrated that varying the weight ratios of salt to oxides (s/o) significantly influenced the composition, microstructure, and grain size of the template seeds. When the s/o ratio reached a certain level, the particles exhibited desirable morphology and uniform grain size, with an average diameter of 7.92 μm and a thickness of 1.13 μm. Incorporating 40 wt% of the template seed resulted in a bulk density of 92.5% for $Ca_3Co_4O_9$ ceramics. Thermoelectric properties were assessed within a temperature range spanning from 50 °C to 800 °C. The findings revealed an electrical resistivity of 20.3 mΩ cm a Seebeck coefficient of 179 μV K^{-1}, and a power factor of 0.16 mW m^{-1} K^{-2} (Fig. 2b).[22]

A highly densified CCO-based ceramics (**4**) were prepared utilizing Bi_2O_3 additive *via* liquid-phase sintering processing. With increasing Bi_2O_3 additive the bulk densities of the samples rose from 92.1% to 95.5%. A band gap of 2.21 eV was observed for the sample containing 6 wt% Bi_2O_3 additive. Furthermore, the concentration and mobility of charge carriers showed

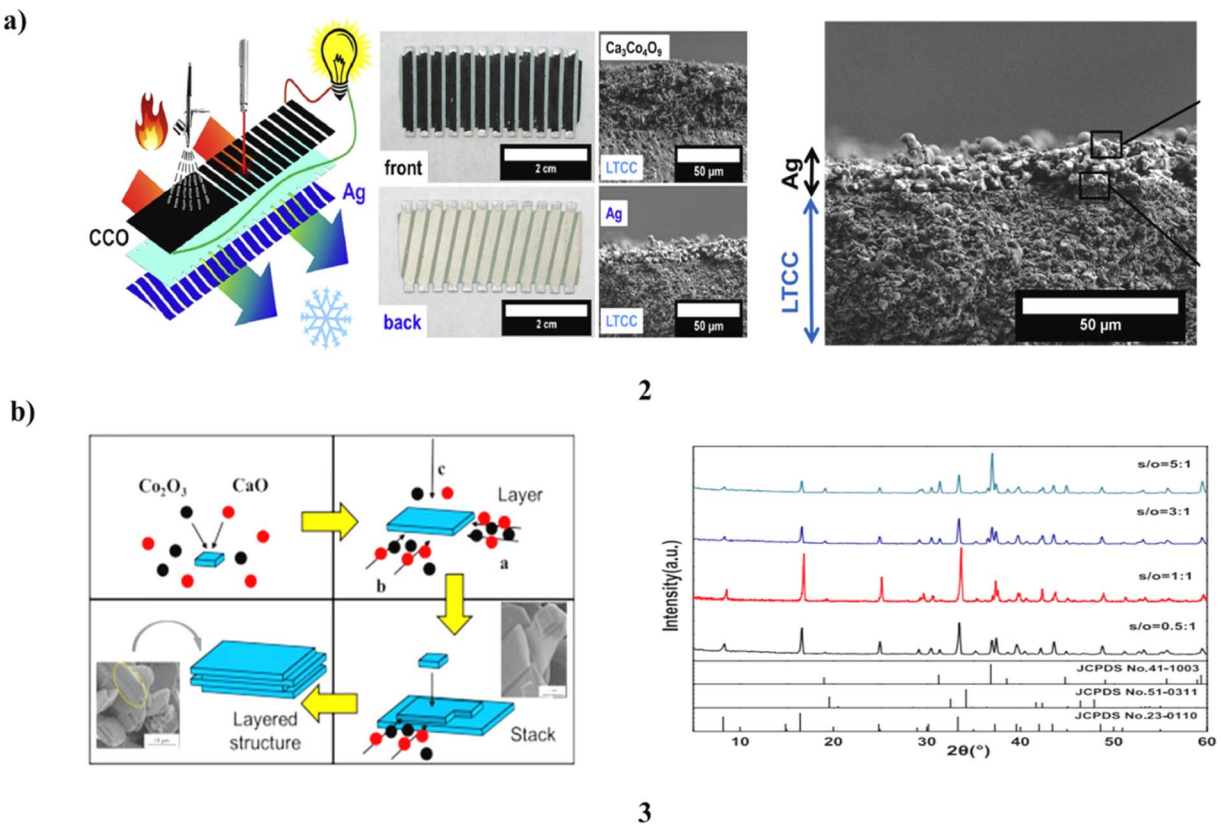

Fig. 2 (a) Spray-coating of ceramic-based thermoelectric generator (**2**). (b) Thermoelectric study of $Ca_3Co_4O_9$ ceramics (**3**).

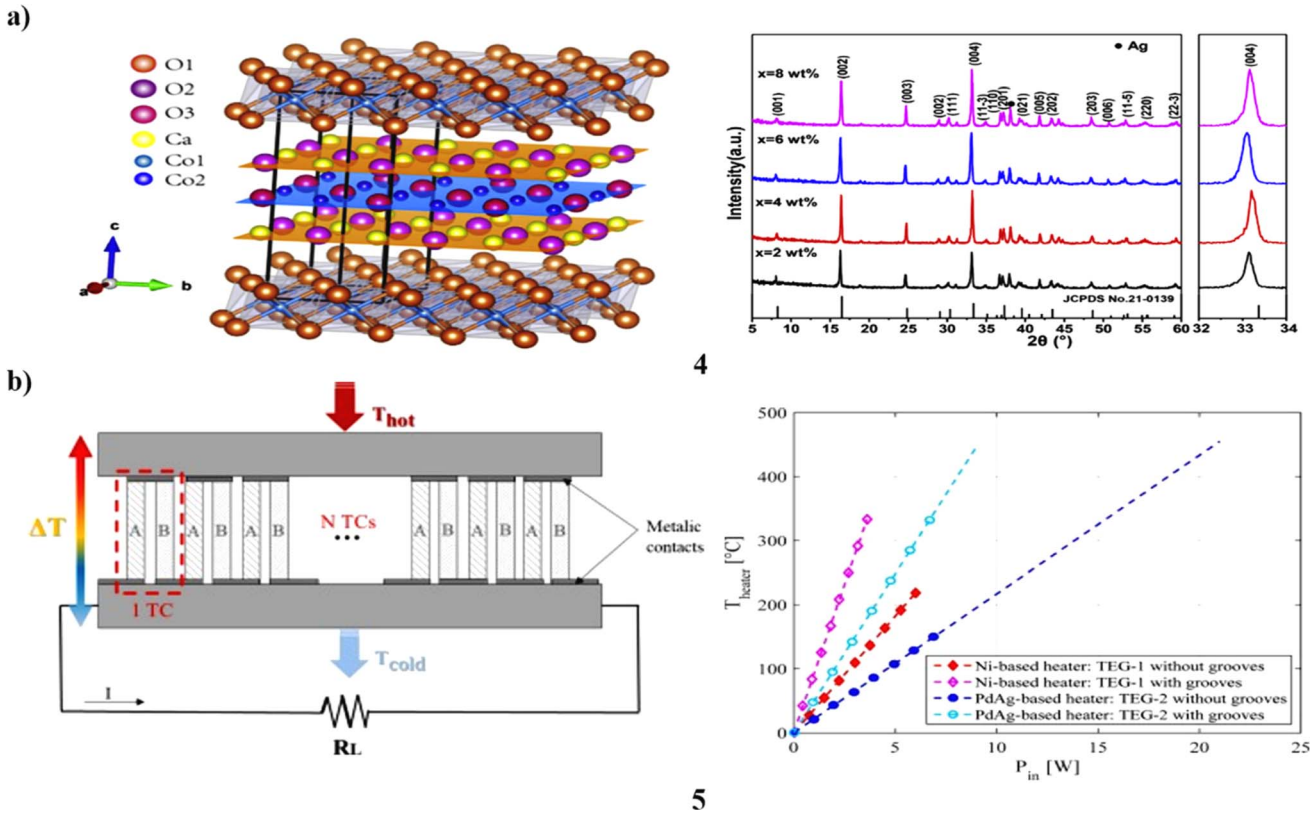

Fig. 3 (a) Liquid-phase sintering study of $Ca_3Co_4O_9$–Bi_2O_3 based ceramics (**4**). (b) LTCC technology of Ag/PdAg-based ceramic-based thermoelectric generator (**5**).

temperature-dependent behavior at 723 K, reaching values of 22.26 × 10^{20} cm^{-3} and 103.2 cm^2 V^{-1} s^{-1} respectively. These results were utilized to estimate the charge carrier transport characteristics. The electrical resistance would inevitably drop and the Seebeck coefficient would rise as the Bi_2O_3 addition increased. Moreover, a maximum power factor of 0.23 mW m^{-1} K^{-2} was achievable at 1073 K. With a lower thermal conductivity of 0.92 W m^{-1} K^{-1} the sample containing 6 wt% Bi_2O_3 additive exhibited a high *ZT* value of 0.25. Bi_2O_3 additive effectively enhanced both the sintering characteristics and thermoelectric properties of CCO ceramics (Fig. 3a).[23] Thermal heat recovered from electrical power components installed on ceramic substrates is possible with an ideal design. The thick-film/low-temperature co-fired ceramic (LTCC)-based multilayer thermoelectric micro-generators (TEGs) (**5**) were built upon in terms of the fabrication methods and characterization. Thus, two separate TEGs were fabricated based on the Seebeck effect each utilizing different thermocouple materials (Ag/Ni and Ag/PdAg) followed by simulation, analytical examination, and comparative analysis. Each generator design incorporates 104 thermocouples, each with a width and spacing of 300 μm. A meander-shaped planar heater was employed to generate the necessary heating, simulating the conditions of an electronic power device. Furthermore, a comparison was conducted between two heaters constructed from Ni and PdAg. Each heater was tested with and without cylindrical grooves added to the back side of the LTCC substrate. The addition of grooves surrounding the hot element has demonstrated an average improvement of 160% in the temperature difference along the generator. In terms of TEGs, the Ag/PdAg-based variation was able to produce an output power that was greater than the Ag/Ni-based TEG, which was able to obtain an output power of 4.6 μW at $\Delta T = 62$ °C. This variant reached an output power of 81 μW with a temperature difference of 114 °C. The Ag/PdAg-based TEG exhibited a conversion efficiency of 0.5%, while the Ag/Ni-based TEG showed a conversion efficiency of 0.08% (Fig. 3b).[24]

The thermoelectric properties of SiC/AlN ceramic composites (**6**) were analyzed across a broad temperature range. Simulation and analysis were conducted to evaluate the thermal stress durability of the composites. SiC/AlN composites containing 0–30 wt% of AlN were manufactured using the pressureless sintering method. The obtained composites underwent inspection for phase analysis, densification, and microstructure characterization. The porous structure of the SiC/AlN ceramics was observed with porosity levels varying between 23.77% and 31.74%. A 2Hss SiC/AlN solid solution was produced in its entirety with the content growing in step with the increase in the percentage of AlN weight. The incorporation of AlN into SiC ceramics resulted in a structured composition with elongated grain morphology. The electrical resistivity and thermoelectric properties of the examined ceramics were assessed across a temperature range from 25 to 1000 K. The outcomes were primarily influenced by the AlN content, microstructure, and temperature. Moreover, SiC/AlN composites exhibited

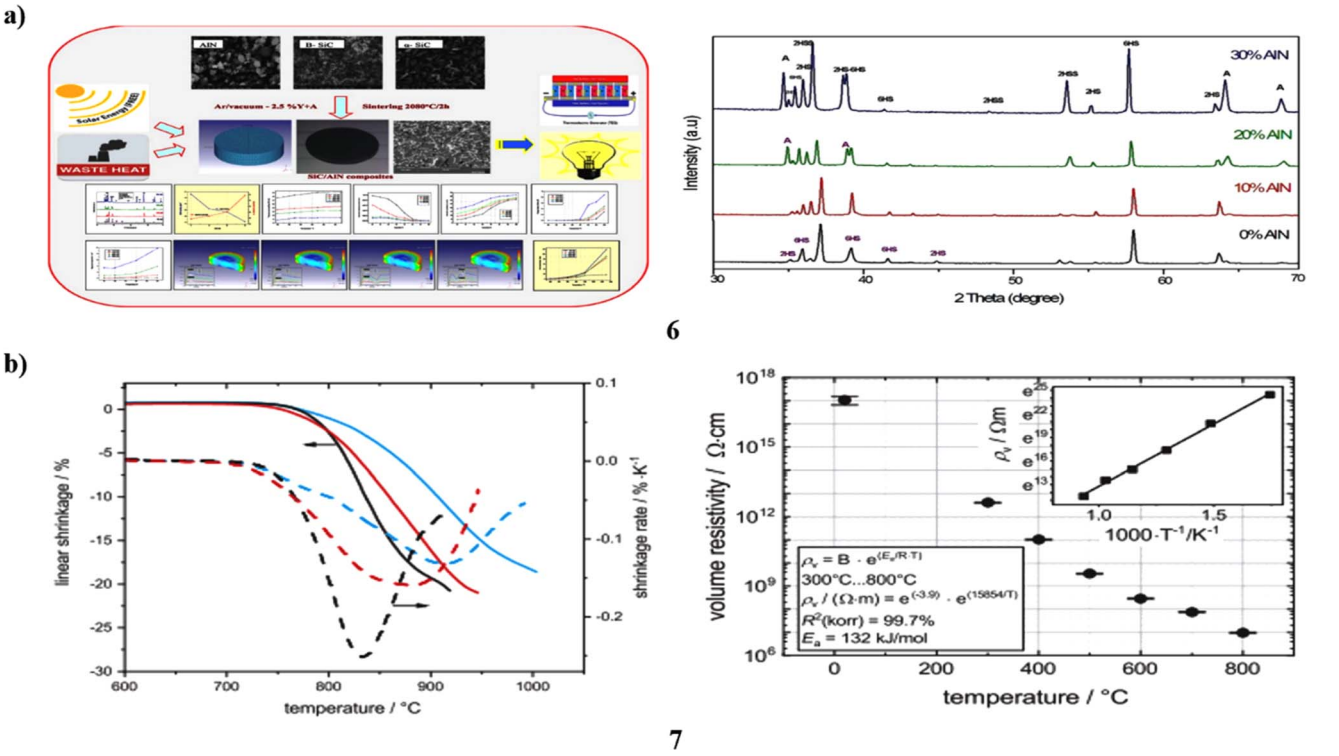

Fig. 4 (a) SiC/AlN ceramic composites (**6**). (b) Thermoelectric study of glass-ceramic composites (**7**).

consistent behavior as p-type semiconductors showcasing exceptional thermoelectric properties, particularly at elevated temperatures. At 1000 K, the 30% AlN composite displayed the lowest electrical resistivity of 1.5×10^5 μΩ × cm and the highest Seebeck coefficient of 370 μV K^{-1}. The figure of merit (*ZT*) exhibited a remarkable increase with the augmentation of AlN content. The 30% AlN composites attained a *ZT* value 130 times greater than that of the 0% AlN composite. Increasing the weight percentage of AlN significantly improved the thermoelectric power factor. A finite element technique simulation was used to analyze the thermal stress of different ceramics up to 1773 K in temperature. The homogeneous transition and dispersion of heat in SiC/AlN composites demonstrated exceptional thermal stress resilience. They are highly recommended for effective utilization in thermoelectric power generation and high-temperature applications (Fig. 4a).[25] Additionally, the fabrication of thermoelectric generators automatically is made possible by ceramic multilayer technology, which is advantageous for energy harvesting in sensor applications. In such multilayer thermoelectric generators, the electrical insulation material plays a critical role in enhancing device performance. It needs to be carefully matched to the thermoelectric material in terms of its coefficient of thermal expansion α and its sintering temperature while maintaining a high resistivity to optimize overall efficiency. A glass-ceramic composite material (**7**) was developed for use in multilayer thermoelectric generators, starting from theoretical calculations. This composite material was synthesized from a combination of calcium manganate and calcium cobaltite. The optimization process focused on achieving a coefficient of thermal expansion (α) of 11 $\times 10^{-6}$ K^{-1} over a temperature range of 20–500 °C, a sintering temperature of 900 °C, and maintaining high resistivity up to 800 °C. The calculated and measured coefficients of thermal expansion (α) exhibit strong agreement validating the accuracy of the theoretical predictions in the development of the glass-ceramic composite material for multilayer thermoelectric generators. The selected glass-ceramic composite, containing 45 vol% quartz demonstrates a resistivity of 1×10^7 Ω cm and maintains an open porosity of less than 3%. The sintered multilayer samples, consisting of tape-cast thermoelectric oxides and screen-printed insulation, exhibit minimal reaction layers. This suggests that glass-ceramic composites are highly suitable for insulation layers in such applications. Moreover, the physical properties of these composites can be precisely adjusted by modifying glass composition or introducing dispersion phases highlighting their versatility and effectiveness in optimizing device performance (Fig. 4b).[26]

Furthermore, Oscillatory Pressure Sintering (OPS) has proven to be a beneficial manufacturing method for achieving precise control over the fine and uniform distribution of grains across different ceramic systems. This capability facilitates improved densification, thereby enhancing the physical and mechanical properties of the materials involved. This study utilized Oscillatory Pressure Sintering (OPS) to fabricate pure $Ca_3Co_4O_9$ thermoelectric material (**8**). The findings reveal that the electrical and thermoelectric properties of $Ca_3Co_4O_9$ prepared *via* OPS outperform those of samples sintered using conventional hot pressing (HP) without oscillation. The

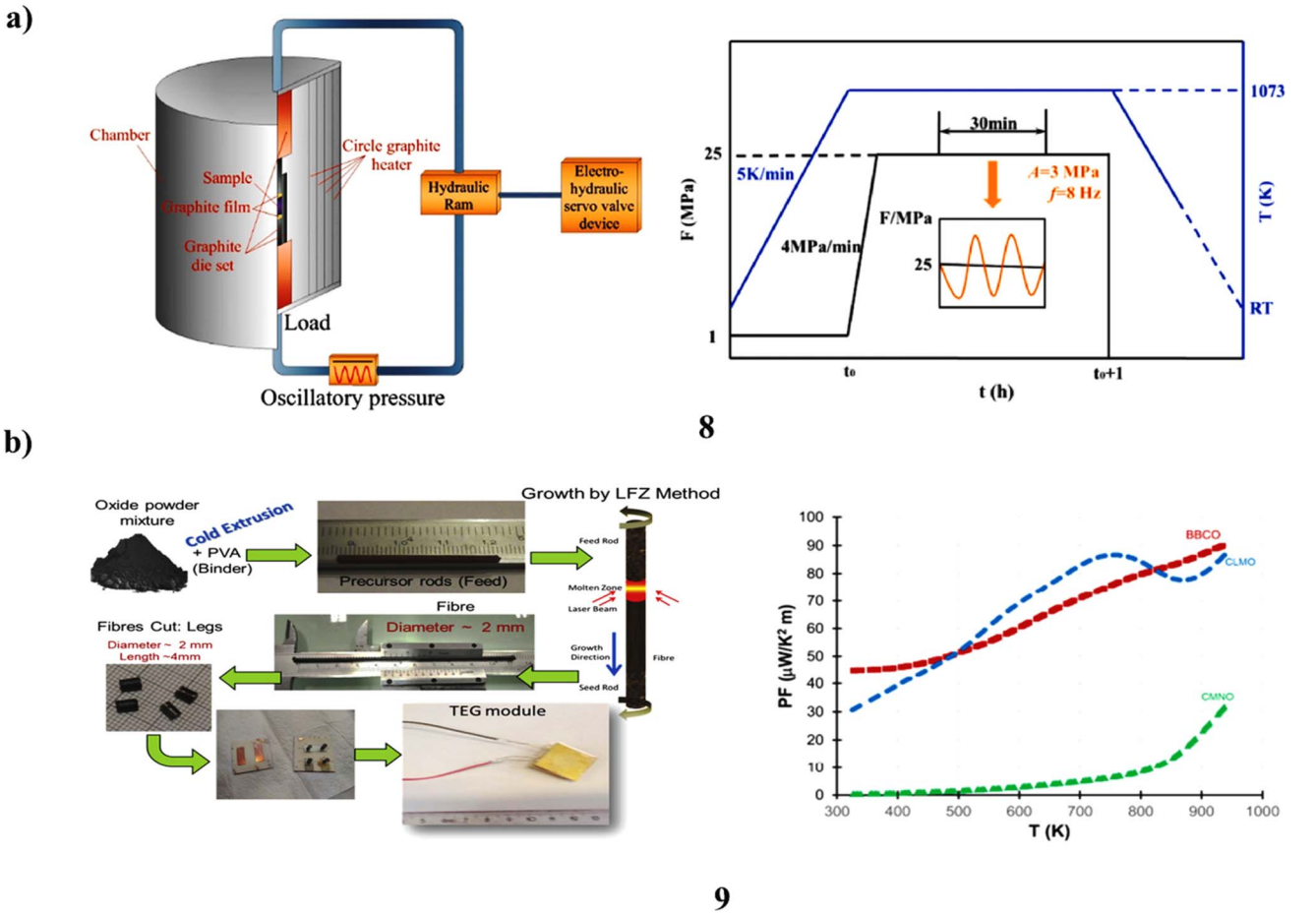

Fig. 5 (a) Thermoelectric study of $Ca_3Co_4O_9$ based ceramics (**8**). (b) Ceramic legs-based thermoelectric modules (**9**).

improved performance of the OPS samples can be attributed to several factors. Firstly, OPS facilitates better alignment of plate-like grains, leading to enhanced electrical conductivity. Additionally, OPS results in higher grain boundary density, which effectively increases phonon scattering, thereby reducing thermal conductivity. This study suggests that employing a simple oscillatory pressure sintering approach can yield high-quality and high-performance thermoelectric materials, eliminating the necessity for doping, templating, or high-temperature sintering methods (Fig. 5a).[27] The first attempt at thermoelectric module design was based on oxide materials fabricated using the laser floating zone technique. Two modules with four-leg thermoelectric configurations were constructed, incorporating $Bi_2Ba_2Co_2O_y$ fibers as the p-type legs, and $Ca_{0.9}La_{0.1}MnO_3$ and $CaMn_{0.95}Nb_{0.05}O_3$ fibers (**9**) as the n-type legs. Structural and electrical characterization of the individual fibers was conducted. The evolution of open-circuit voltage during heating and cooling up to 723 K followed the expected trends based on the Seebeck coefficient of the individual fibers. This observation suggests the excellent reliability of the modules during temperature cycling. The power generation performance was assessed across a temperature difference of up to 500 K under various electric loads. The maximum measured power output reached approximately 2.2 mW with a module volume of approximately 39 mm^3 (Fig. 5b).[28]

The precise and adaptable technique combining spray-coating and laser structuring is employed to engineer ceramic layers on a versatile substrate, suitable for various applications. A thermoelectric material $Ca_3Co_4O_9$ (**10**), was employed in the process and affixed onto a flexible ceramic substrate. The resultant structures exhibit highly controllable shapes and possess favorable thermoelectric properties. They are suitable for fabricating a printable thermoelectric generator (TEG). Employing a flexible ceramic substrate and benefiting from the high feasibility of the process, this approach offers a universally applicable procedure for processing ceramics with distinctive structures and designs (Fig. 6a).[29] Pyroelectric energy harvesting has garnered significant interest for its capacity to transform low-grade waste heat into electrical energy. Despite the limitations posed by low-grade temperature the practical applications of pyroelectric energy harvesting have been expanded with the introduction of a high-performance hybrid BNT-BZT-*x*GaN pyroelectric ceramic (**11**). This system incorporates an environmentally friendly lead-free BNT-BZT pyroelectric matrix, complemented by high thermal conductivity GaN as a dopant. Theoretical analysis of BNT-BZT and BNT-BZT-*x*GaN with $x = 0.1$ wt% indicates that incorporating GaN promotes resonance

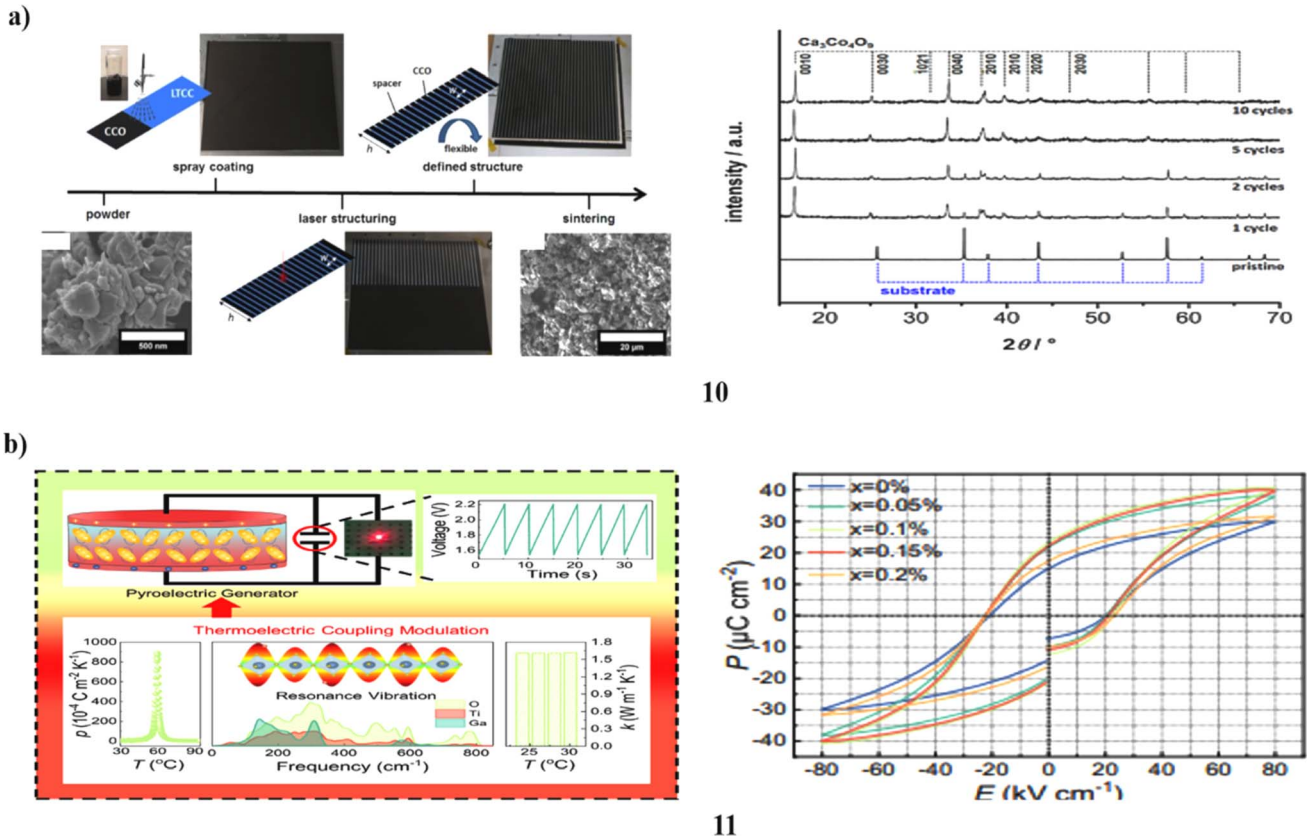

Fig. 6 (a) Laser structuring of thermoelectric ceramics (**10**). (b) BNT-BZT-*x*GaN pyroelectric ceramics-based thermoelectric properties (**11**).

vibration between Ga and Ti, O atoms. This phenomenon not only enhances lattice heat conduction but also improves the vibration of TiO_6 octahedra. Accordingly, there is a simultaneous improvement in both thermal conductivity and pyroelectric coefficient. Therefore, BNT-BZT-*x*GaN ceramics with $x =$ 0.1 wt% have achieved an enhanced energy harvesting density of 80 μJ cm^{-3} through thermoelectric coupling. This performance is achieved under a temperature variation of 2 °C and an optical load resistance of 600 MΩ (Fig. 6b).[30]

Ceramics are known for their high thermal stability and electrical insulation properties. Optimizing thermoelectric performance in ceramics involves enhancing their electrical conductivity while maintaining low thermal conductivity. This can be achieved through doping, which introduces charge carriers, and by creating nanostructured ceramics that scatter phonons effectively, thereby reducing thermal conductivity. The balance between electrical and thermal properties is key to improving the figure of merit (*ZT*).

3. Gel based thermoelectrical devices

The role of interfacial phenomena involving conducting polymer PEDOT electrodes has been highlighted in enhancing the thermoelectric efficiency of integrated thermoelectric (iTE) devices. In the development of integrated thermoelectric energy conversion systems (ITESCs) PEDOT-based electrodes were utilized alongside a gradient of poly-styrene sulfonate (PSS) content. These electrodes were paired with an ionic-liquid polymer (IL-p) gel (**12**) as the electrolytes. The thermo-induced voltage coefficient ($\Delta V/\Delta T$) of the ionic thermoelectric supercapacitor/battery (ITESCs) exhibited an increase with the addition of higher PSS contents in the electrodes. The potential at the interface between the PEDOT:PSS electrode and the electrolyte is influenced by a Donnan-like exclusion effect leading to a concentration disparity of the anion between the interior and exterior of the electrode. The thermo-voltage is influenced by changes in the interfacial potential caused by variations in temperature. The ionic Seebeck effect that the electrolyte exhibits is coupled with this phenomenon. This study underscores the crucial significance of the interfacial potential in the design of ionic thermoelectric supercapacitors featuring conducting polymer electrodes. These discoveries hold paramount importance in comprehending and enhancing the interfacial characteristics of polymers and electrolytes essential for various organic electrochemical devices. Additionally, the exceptional suitability of PEDOT:PSS as an electrode in ionic thermoelectric energy harvesting devices (Fig. 7a).[31] Furthermore, the gel electrolyte-based thermogalvanic generator (**13**) employing Fe^{3+}/Fe^{2+} as a redox pair showcases both moderate thermoelectric efficiency and exceptional flexibility. Introducing a PVDF diaphragm with widespread micropores into the gel created a thermal barrier between the two halves leading to an effective enhancement of the Seebeck coefficient through the reduction of thermal

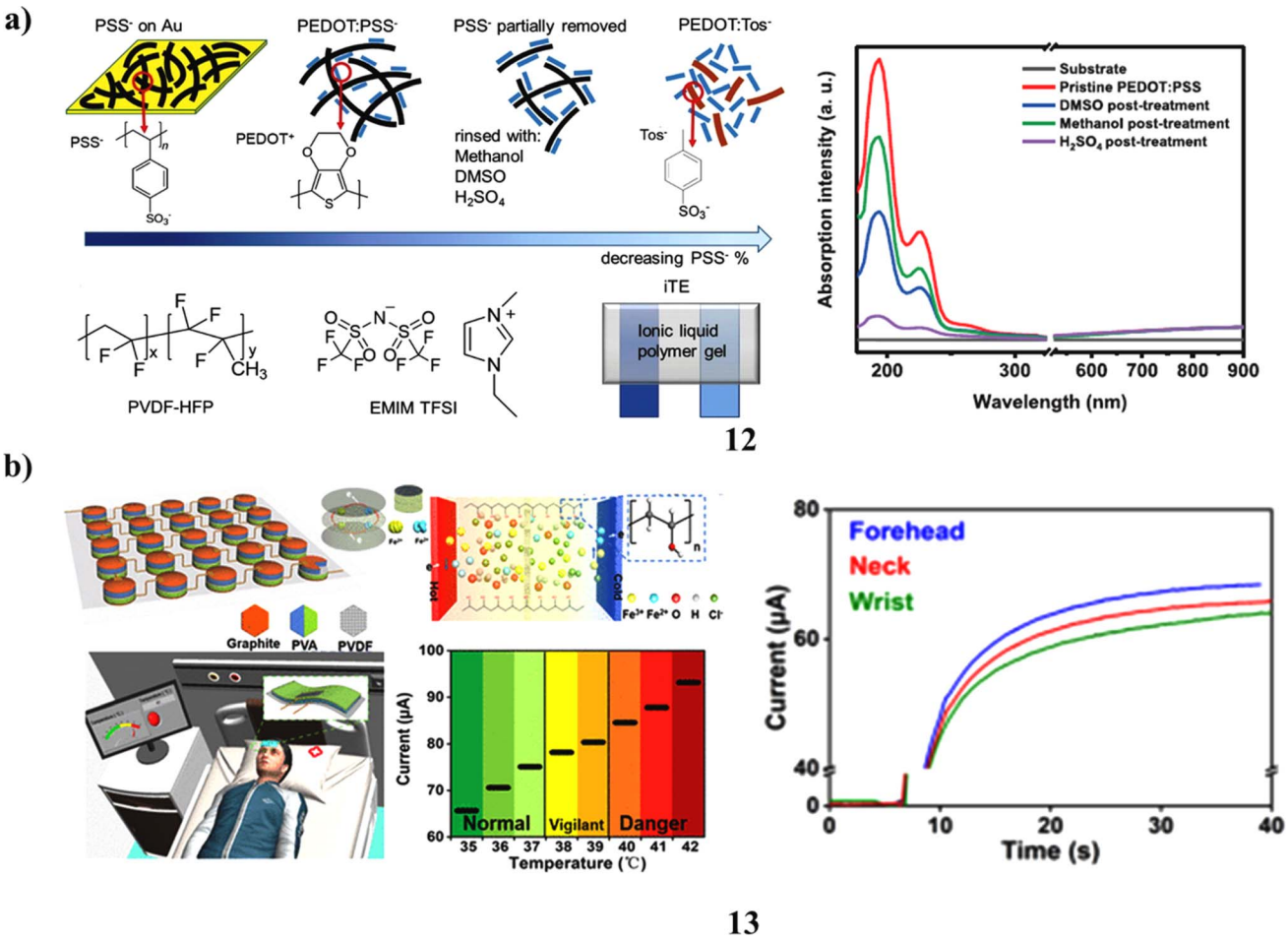

Fig. 7 (a) IL-p gel-based thermoelectric devices (**12**). (b) Gel electrolyte-based thermoelectric devices (**13**).

conductivity. Leveraging the exceptional temperature responsiveness of the gel patch a self-powered body temperature monitoring system was developed by securely attaching it to the forehead in a conformal manner. At the same time, the gel patch boasting a high specific heat capacity proves highly effective in efficiently reducing the body temperature of fever patients (Fig. 7b).[32]

Developing a technology capable of converting low-grade waste heat into useable electricity while simultaneously storing it necessitates a novel approach enabling the directed migration of electrons or ions in response to temperature disparities leading to their accumulation on the electrodes. Despite the growing demand for energy conversion and storage (ECS) in wearable electronics creating an integrated bifunctional device remains challenging due to the distinct mechanisms governing electrical transportation and storage. The ionic thermoelectric supercapacitor harnesses the synergistic capabilities of thermoelectricity and supercapacitors within a thermoelectric ionogel electrolyte and high-performance hydrogel electrodes to optimize ECS performance in the presence of a thermal gradient. The thermoelectric electrolyte comprises a polyacrylamide hydrogel and sodium carboxymethyl cellulose (PMSC) (**14**) featuring a cross-linked network that exhibits outstanding cation selectivity. Moreover, the ionic thermoelectric properties are enhanced with the addition of NaCl. In the NaCl-PMSC electrolyte, the Seebeck coefficient and ionic conductivity achieve values of 17.1 mV K^{-1} and 26.8 mS cm^{-1}, respectively. The ionic thermoelectric supercapacitor a fully stretchable integrated electrochemical sensor (ECS) device exhibits a remarkable thermal-charge storage capacity of roughly 1.3 mC at a temperature difference of approximately 10 K. This is attributed to the excellent stretchability of both the gel-based electrode and electrolyte. Accordingly, it shows significant potential for wearable energy harvesting applications (Fig. 8a).[33] In addition, the development of efficient self-powered energy harvesting and storage technologies represents a crucial milestone in meeting the demands of the Internet of Things (IoT) landscape. The creation of an interdigital planar all-in-one thermally chargeable supercapacitor (IPTS) marks the successful integration of energy harvesting and storage technologies. This intelligent device was fabricated using a photolithography process, which combined carbon nanotubes as the electrode material with polyvinyl alcohol (PVA) doped with H_3PO_4 (**15**) to form a solid-gel polyelectrolyte. By adjusting the quantity of H_3PO_4 incorporated into the PVA matrix, the ionic conductivity of the

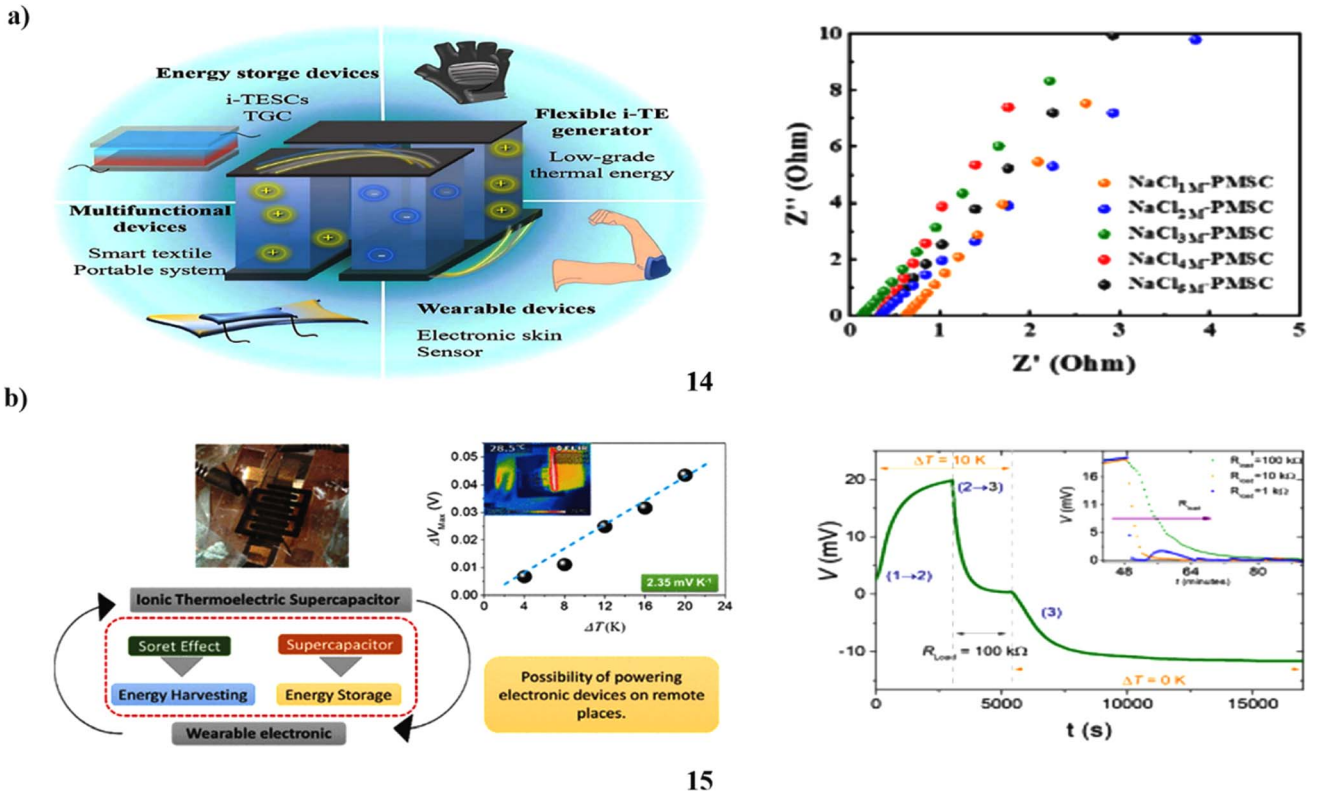

Fig. 8 (a) Voltage curve of the ionic thermoelectric supercapacitor (**14**). (b) Ionic solid-gel polymer based thermoelectric device (**15**).

resulting material was tailored. This investigation revealed an optimal ratio of PVA to H_3PO_4 at 1 : 1 (m/m). The power generation capabilities of the IPTS were assessed revealing a Soret coefficient of 2.35 mV K^{-1}. This value is noteworthy as it is approximately an order of magnitude higher than those typically observed in thermoelectric materials, which usually range in the few hundreds of μV K^{-1}. Furthermore, the device achieved a voltage generation output of up to 45 mV when subjected to a temperature difference of 20 K. Regarding its energy storage capabilities, the device functioned as an electric double-layer capacitor delivering an energy density of 1.05 mW h cm^{-3} at a power density of 1.21 W cm^{-3}. The customized interdigital structure along with its remarkable flexibility and energy efficiency, make the IPTS an exceptional candidate for flexible electronics. Furthermore, its cost-effective production process allows for scalable manufacturing opening up new horizons in this field (Fig. 8b).[34]

The organic thermoelectric devices (OTEDs) emerge as highly promising platforms for efficiently harvesting electricity from low-temperature heat sources. The integration of zinc oxide (ZnO) particles into hybrid composites with poly(3,4-ethylenedioxythiophene):poly(styrene sulfonate) (PEDOT:PSS) (**16**) significantly boosts the performance of OTEDs. This enhancement arises from the ZnO particles bridging role leading to improved electrical conductivity. The comprehensive investigation revealed that incorporating ZnO particles into aqueous solutions of PEDOT:PSS resulted in increased viscosity due to specific interactions between sulfonic acid groups in PSS and hydroxyl groups leading to the formation of a gel-like state. The wearable thermal sensors incorporating PEDOT:PSS/ZnO hybrid composite films demonstrated rapid thermoelectric responses when exposed to both heat and cool sources (Fig. 9a).[35] A dire need exists for wearable thermoelectric generators (TEGs) based on fibers, prioritizing exceptional thermoelectric performance, robust mechanical durability, and superior wearer comfort to effectively harness low-grade human body heat. In this study, a wearable ionogel fiber-based ionic thermoelectric device was devised and fabricated to achieve a high thermo-voltage. To synergistically boost both the ionic conductivity and ionic Seebeck coefficient, ethanol and sodium bis(trifluoromethyl sulfonyl)imide (NaTFSI) are introduced into the poly(vinylidene fluoride-*co*-hexafluoropropylene)/1-ethyl-3-methylimidazolium dicyanamide (PVDF-HFP/EMIM:DCA, PH/ED) ionogel (**17**). This addition serves to enhance ionic mobility and augment the diffusion disparity between cations and anions. The study comprehensively analyzes the morphology, structure, transmittance, crystallization, rheological properties, mechanical characteristics, and thermoelectric performances of the material. Subsequently, a mechanism is proposed to elucidate the enhancements observed in performance. Following the modification, the PH/ED-ethanol-NaTFSI (PH/ED-E-NaTFSI) ionogel achieves significantly enhanced properties with high ionic conductivity, ionic Seebeck coefficient, and ionic power factor of 17.5 mS cm^{-1}, 22.9 mV K^{-1}, and 870.26 μW m^{-1} K^{-2}, respectively. These values notably surpass those of the pristine PH/ED ionogel. Meanwhile, the tensile

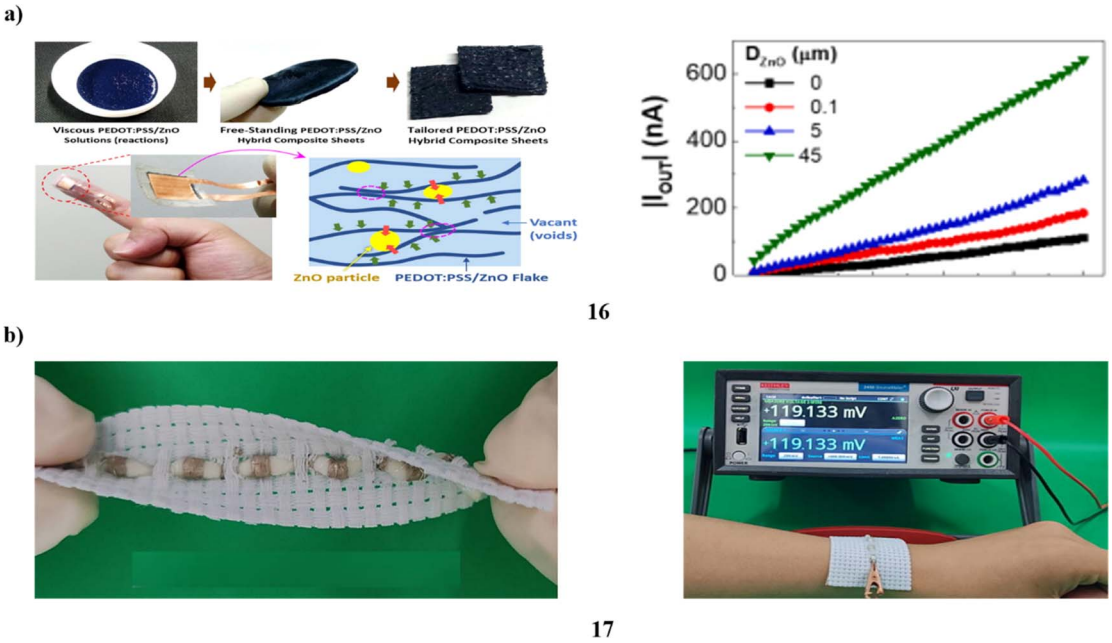

Fig. 9 (a) PEDOT:PSS/ZnO hybrid composites for organic thermoelectric devices (**16**). (b) Low-grade human body heat gathering device based on ionogel fiber (**17**).

stress of the ionogel fiber was significantly enhanced to 18.15 MPa from 0.19 MPa of PH/ED-E-NaTFSI ionogel film. Then, a wearable ionogel fiber-based wristband with synergistically improved TE performance, mechanical properties, and wearing comfort was prepared by a weaving process. Wearing the i-TE wristband (5-legs) at room temperature results in a remarkably high thermo-voltage output of 119.133 mV (Fig. 9b).[36]

The porous polymeric monoliths and their corresponding carbonized aerogels (**18**) exhibit favorable optical, thermal, and wetting characteristics making them well-suited for efficient solar-driven interfacial evaporation. A notable water production efficiency of 2.1 kg h^{-1} m^{-2} under 1 sun illumination was attained even in the absence of convective flow by using the aerogel-based solar-driven evaporation system. The solar-powered evaporation system was combined with a specially designed thermoelectric conversion device to generate electricity efficiently at the same time. The system produced an output power of about 66 W m^{-2} when exposed to 4 kW m^{-2} of solar radiation. Due to their simple fabrication process and outstanding performance in both solar energy conversion and water transportation, these materials offer promising avenues for solar energy utilization. They could serve as key components in the development of efficient solar-driven systems capable of generating clean water and electricity simultaneously (Fig. 10a).[37] In addition, the gel thermocells (**19**) are pivotal in the realm of low-grade heat harvesting, utilizing redox couple ions as carriers to efficiently convert heat into electricity. However, a significant hurdle is preserving the high ionic thermoelectric performance at temperatures outside of room temperature primarily due to the limited heat tolerance of gels. The approach to enhance both ionic thermopower and output power density at elevated temperatures involves optimizing the gel composition through the incorporation of graphene. The integration of graphene in a "bridge" structure has the potential to enhance the ion diffusion coefficient and exchange current density, consequently leading to improved performance. At 323 K, gels comprising gelatin-0.04/0.06 M $FeCN^{4-/3-}$-6 wt% Gr demonstrated a remarkable ionic thermopower of up to 13 mV K^{-1}, an output power density of 1.03 mW m^{-2} K^{-2}, and a continuous discharge energy density of 0.19 J m^{-2} K^{-2} over 1 hour. Moreover, a record-breaking output power density of 1.2 mW m^{-2} K^{-2} was achieved at the same temperature in a device constructed with four gel thermocells arranged in series (Fig. 10b).[38]

The Cu_2Se emerges as a promising thermoelectric system owing to its abundance of earth-friendly constituents and its high thermoelectric figure of merit particularly suited for mid-temperature range applications. The thermoelectric conversion efficiency of these materials can be enhanced through doping with carbon dots (CD) nanomaterials. Gel-like CD nanomaterials (**20**) were synthesized *via* a straightforward and swift solvothermal method. Cu_2Se powders were doped with these CDs and then subjected to spark plasma sintering to create hybrid thermoelectric systems. These hybrid systems exhibited significantly enhanced thermoelectric figure of merit compared to undoped Cu_2Se with the highest figure of merit reaching 2.1 at 880 K achieved with a CD dopant ratio of 2 wt%. The structural analysis conducted on the samples indicated a high level of purity, which played a crucial role in achieving the high thermoelectric figure of merit (*ZT*). The remarkable achievement can be attributed to several factors, including the synergetic presence of quasi-spherical CD nanoparticles the dense network of grain boundaries, and the high density of the

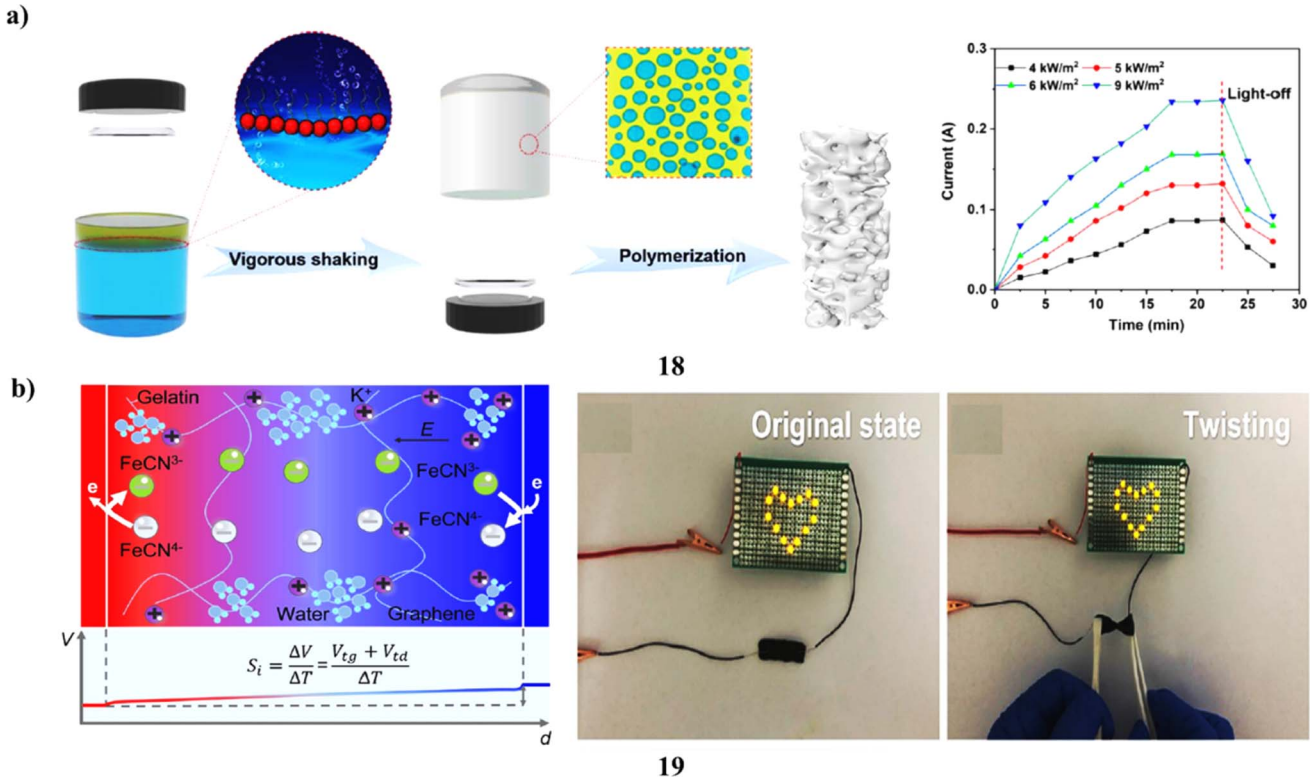

Fig. 10 (a) Electricity generation of the carbonized aerogels-based solar-driven system (18). (b) Gel thermocells based high-temperature ionic thermoelectric device (19).

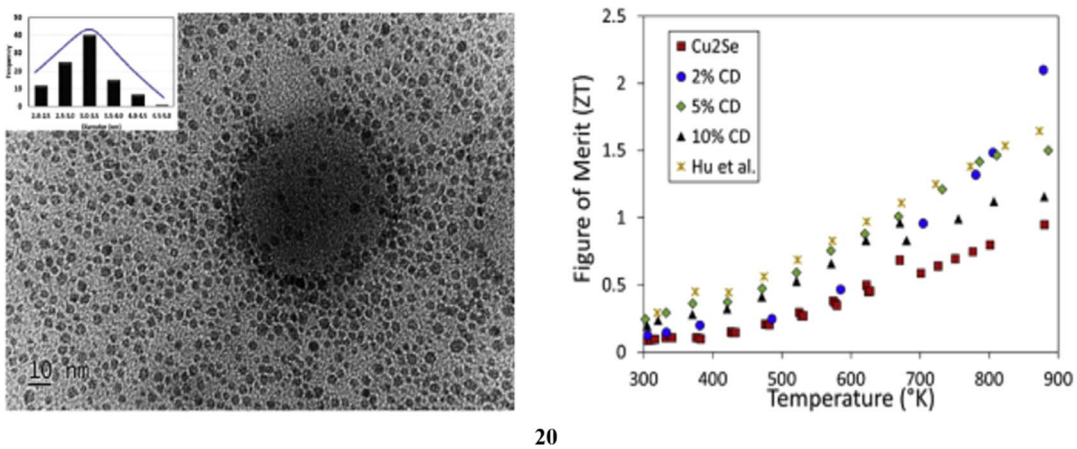

Fig. 11 Gel-like carbon dots based thermoelectric performance of Cu_2Se (20).

sintered Cu_2Se matrix. These factors collectively enhance phonon scattering and electrical conductivity leading to the observed high thermoelectric figure of merit. This study pioneers novel methodologies for fabricating gel-like CD-doped Cu_2Se material systems offering scaled-up nano-dopant preparation procedures and significantly enhancing thermoelectric conversion efficiencies (Fig. 11).[39]

Thermally conductive gel-like materials are emerging as flexible and efficient options for thermoelectric applications. They offer easy processing and adaptability, making them suitable for a variety of applications, including wearable devices and flexible electronics.

4. Metal composite-based thermoelectric devices

The high density of surface atoms with incomplete coordination can significantly influence the material's transport properties. To fully exploit the potential of nanocrystal building blocks for creating functional nanomaterials and thin films,

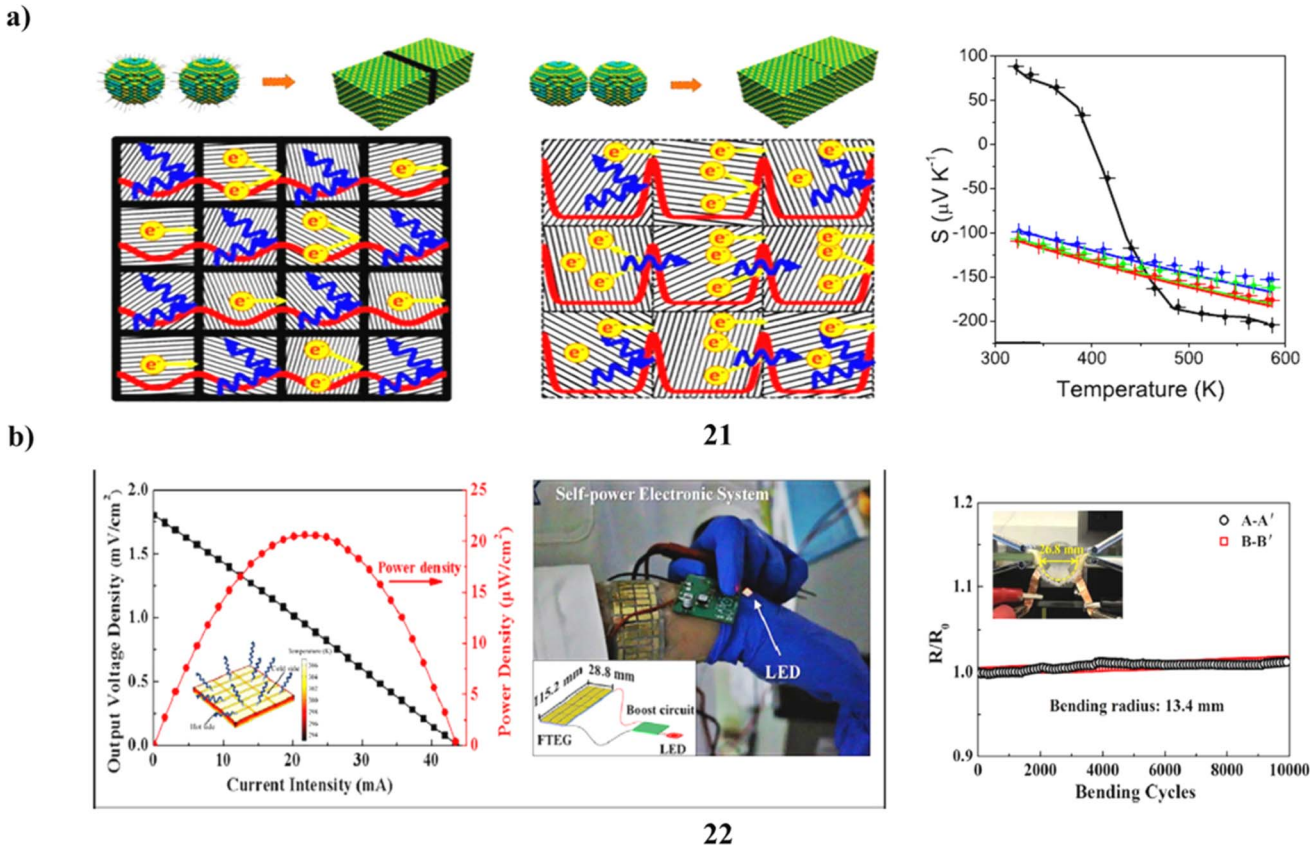

Fig. 12 (a) PbSe nanomaterials-based TE generator (**21**). (b) Mg_3Bi_2-based thermoelectric generator (**22**).

precise control over their surface chemistry is essential. The removal of native organic ligands through ligand stripping profoundly affects the charge and heat transport properties of sintered PbSe nanomaterials (**21**) formed from the assembly of colloidal PbSe nanocrystals. This process leaves behind carbon residues at crystal interfaces impeding crystal growth and hindering both charge and heat transport within the final nanomaterial structure. Furthermore, the displacement of ligands exposes the nanocrystal surface to oxidation and chalcogen evaporation exacerbating these effects. To understand the ligand displacement influences charge transport properties, researchers employ a two-band model based on the standard Boltzmann transport equation with the relaxation time approximation. Finally, the study showcases the practical application of these functional nanomaterials by designing, fabricating, and testing a simple thermoelectric device with a ring geometry utilizing PbSe as the primary material (Fig. 12a).[40] The construction of a specific type of wearable thermoelectric generator involves the design and fabrication process, incorporating n-type $Mg_{3.2}Bi_{1.498}Sb_{0.5}Te_{0.002}$ legs, p-type $Bi_{0.4}Sb_{1.6}Te_3$ legs (**22**), polyurethane matrices, and flexible Cu/polyimide electrodes. When applied to a human arm at an ambient temperature of 289 K, the suggested device achieves a peak power density of around ~20.6 mW cm^{-2} due to its minimized thermal bypass and highly efficient thermal contact interface. Also, it achieves a notable peak power density of 13.8 mW cm^{-2} with a temperature difference of 50 K. Moreover, its ability to endure 10 000 bending cycles at a bend radius of 13.4 mm implies that the suggested wearable thermoelectric generator holds promise as a reliable power source for specific wearable electronics used in everyday activities (Fig. 12b).[41]

All-oxide thermoelectric modules present an enticing option due to their stability at high temperatures, cost-effectiveness, and the ability to utilize non-scarce and non-toxic elements. Thermoelectric modules are commonly produced using the traditional π-design, which is accompanied by the difficulty of maintaining stable metallic interconnects under high-temperature conditions. Fabricating a thermoelectric module involves creating an *in situ* formed p–p–n junction using cutting-edge oxides such as $Ca_3Co_{4-x}O_{9+\delta}$ for the p-type component and a composite of $CaMnO_3$–$CaMn_2O_4$ for the n-type component (**23**). The $LaAlO_3$ was used as insulation between the p-type and n-type powders during the spark plasma co-sintering process used to create the module. This separation facilitated the formation of an *in situ* layer of p-type Ca_3CoMnO_6 at the interface where the n- and p-type materials were in contact. This resulted in the creation of a p–p–n junction demonstrating ohmic behavior, thereby enhancing the open-circuit voltage of the module through a transverse thermoelectric effect. The module's performance was assessed throughout a 700–900 °C temperature range producing a 160 K temperature differential and a peak power output of 5.7 mW at 900 °C.

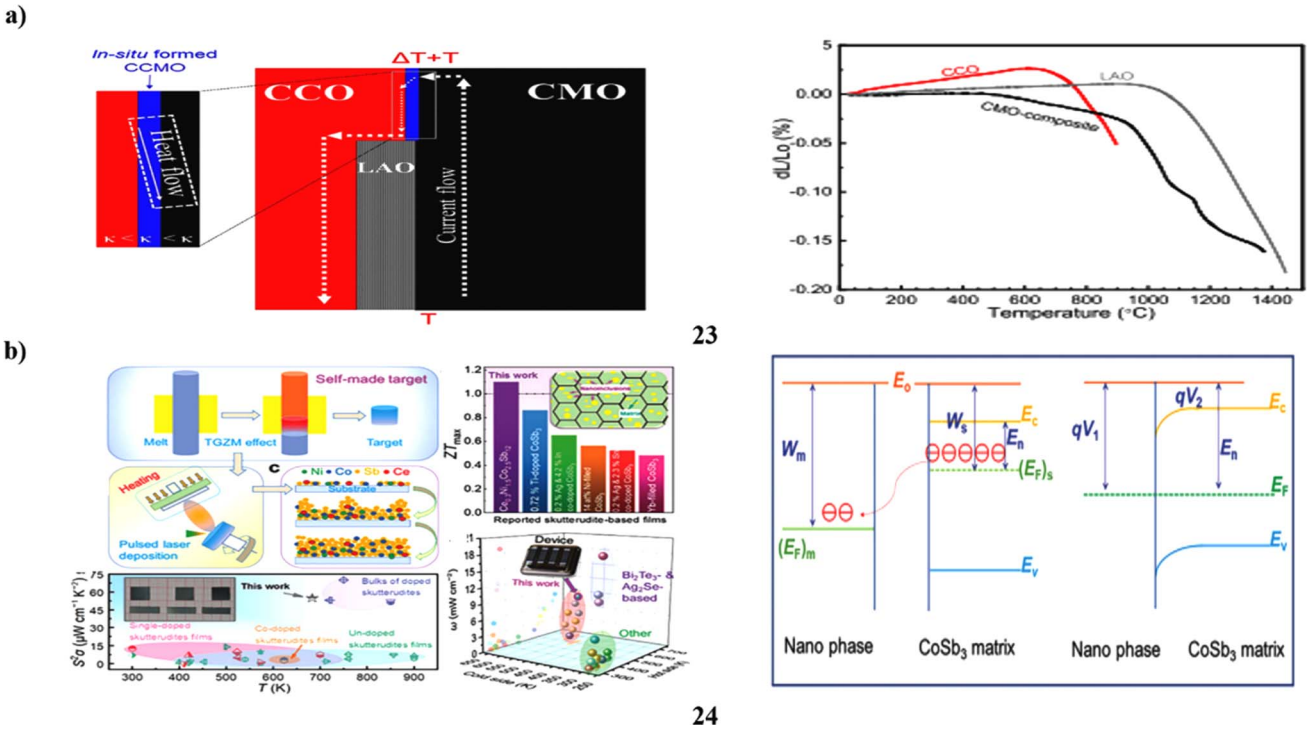

Fig. 13 (a) Current–voltage curves of CCO–CMO–CMO p–p–n junctions (**23**). (b) Nanoscale characterizations of $Ce_{0.3}Ni_{1.5}Co_{2.5}Sb_{12}$ thin film (**24**).

Concurrently, the thermoelectric properties of the p-type and n-type materials were analyzed across a temperature spectrum of 100–900 °C. It is noteworthy that the $Ca_3Co_{4-x}O_{9+\delta}$ and the $CaMnO_3$–$CaMn_2O_4$ composite had the greatest *ZT* values, 0.39 and 0.05, respectively (Fig. 13a).[42] Historically, the high thermoelectric performance in $CoSb_3$ skutterudite-based thin films and their associated devices has posed significant challenges particularly in developing thin-film-based devices capable of operating effectively at medium-to-high temperatures. In this study, a groundbreaking achievement was made with a record-high *ZT* of 1.1 attained at 683 K in an n-type thin film composed of $Ce_{0.3}Ni_{1.5}Co_{2.5}Sb_{12}$ (**24**). This remarkable result was achieved through the utilization of a self-designed target and advanced pulsed laser deposition techniques. It has been confirmed by both theoretical and experimental results that Ce-filling and metal-featured nanoinclusions (such CeSb) greatly increase electrical conductivity. Concurrently, Ni-doping intensifies the energy filtering effect at the dense interfaces between the $Ce_{0.3}Ni_{1.5}Co_{2.5}Sb_{12}$ matrix and the nanoinclusions. This augmentation leads to a substantial increase in the Seebeck coefficient, ultimately resulting in the exceptional *ZT* value achieved. Furthermore, a novel $CoSb_3$ thin-film-based device is developed successfully, demonstrating a remarkable output power density of 8.25 mW cm^{-2} with a temperature difference of 140 K and a cold-side temperature of 573 K. This achievement underscores the device's potential for utilization in power generation scenarios spanning medium-to-high temperatures (Fig. 13b).[43]

Nevertheless, there are growing difficulties when attempting to improve thermoelectric efficiency only by raising the figure of merit. A record-high thermoelectric efficiency of 16% has been reached by combining computer-aided design for geometry optimization with an increased figure of merit. The newly produced $Ge_{1-x-y}Cr_xSb_yTe$ alloy (**25**) and existing materials have been used to optimize the design of a segmented thermoelectric device through the use of finite element analysis simulations. This strategic geometry optimization has resulted in achieving remarkable levels of efficiency setting new records in thermoelectric performance. Additionally, simulations conducted on over 70 established n-type thermoelectric materials can serve as a comprehensive library. This library aids in bridging the gap between materials science and device engineering, facilitating the development of high-efficiency thermoelectric devices (Fig. 14a).[44] The soft electronics have highlighted the necessity for thermal management using deformable materials. New endeavors have concentrated on integrating microparticles of EGaIn (**26**) into elastomers to create thermally conductive composites. However, the shape deformation and coalescence propensity of EGaIn particles under mechanical stress sometimes leads to parasitic electrical conduction, which limits their use in thermal control. It is common for the composite to become brittle when EGaIn nanoparticle loading is increased beyond 20 vol%. A strategic approach is sought to achieve thermally conductive and pliable elastomers while maintaining a high volume ratio of EGaIn nanoparticles. By surface modifying EGaIn nanoparticles with carboxylic acid terminated polydimethylsiloxane (COOH-PDMS-

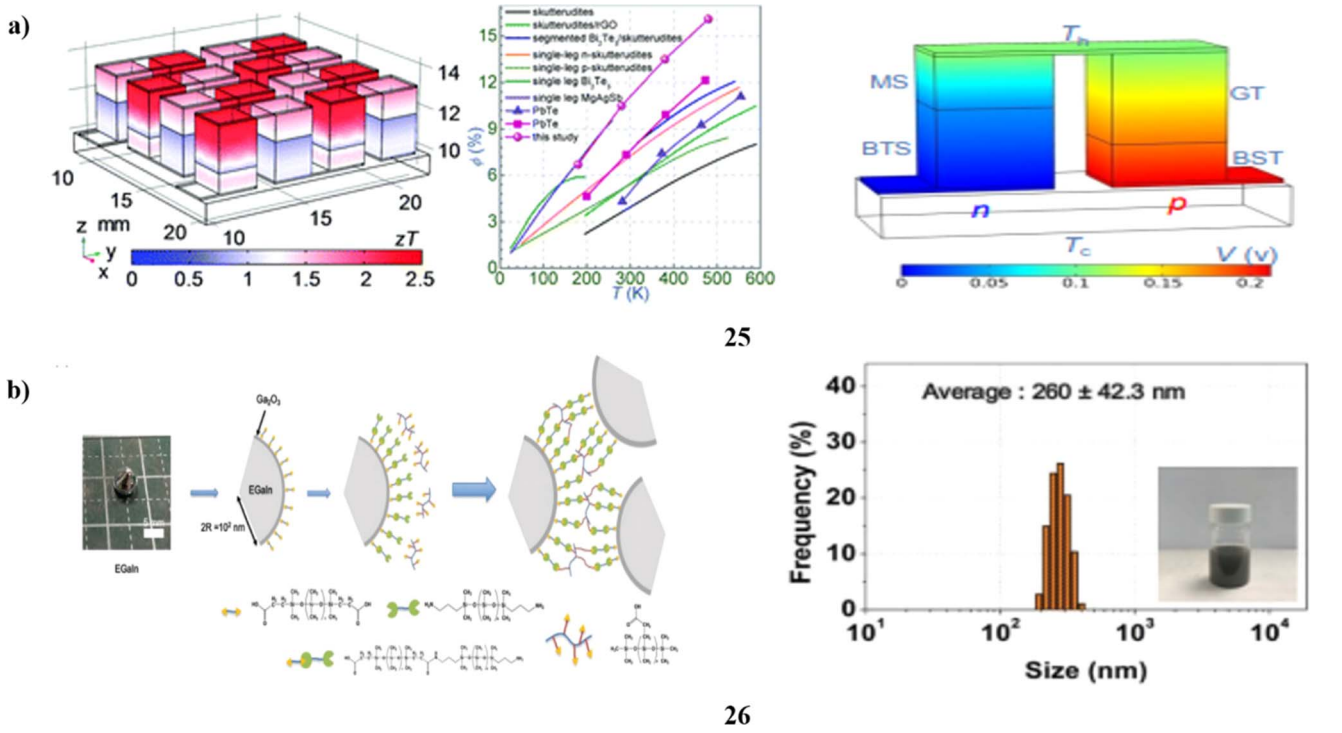

Fig. 14 (a) High-efficiency study of GeTe-based thermoelectric devices (**25**). (b) Thermal energy of liquid metal nanoparticles (**26**).

COOH) and inducing *in situ* formation of a PDMS matrix *via* crosslinking with the surface-treated EGaIn nanoparticles a dense EGaIn nanoparticle distribution within the PDMS matrix is achieved, thereby enhancing effective thermal transport. Significantly, despite the elevated volume ratio of EGaIn nanoparticles within the elastomer the composite retains a low elastic modulus of 6.91 kPa and maintains electrical insulation properties even when subjected to mechanical stress. Furthermore, the elastomer exhibits a unique anisotropic thermal conductivity when subjected to stretching. This property makes it suitable for use as a thermal interface layer in thermoelectric devices. The enhanced thermoelectric performance enabled by this elastomer holds potential applications in wearable devices for thermo-haptic thermal sensing (Fig. 14b).[45]

Nickel (Ni) metal has found extensive application as a barrier layer in Bi_2Te_3-based thermoelectric devices (**27**). This layer plays a crucial role in creating stable joints that effectively connect the Bi_2Te_3-based legs with the electrodes. Nevertheless, the joints formed by the Ni/Bi_2Te_3 interface tend to become extremely fragile under high-temperature conditions leading to significant deterioration in performance and potential device failure. Durable Ni/Bi_2Te_3 joints have been achieved through the arc spraying method, where the Ni barrier layer is applied to the Bi_2Te_3-based alloys. The research delves into the interface microstructure and contact performance of arc-sprayed Ni/Bi_2Te_3 joints focusing on parameters such as bonding strength and contact resistivity. The findings suggest that arc-sprayed Ni/Bi_2Te_3 joints exhibit significantly lower contact resistivity compared to traditional Ni/Bi_2Te_3 joints along with a notable 50% increase in bonding strength. Subjecting the joints to aging under high-temperature conditions reveals that arc-sprayed Ni/Bi_2Te_3 joints demonstrate superior resilience to thermal shock. They maintain stable bonding strength and contact resistivity despite exposure to elevated temperatures. The improved interfacial contact performance and enhanced thermal tolerance can be attributed to the presence of a thick Ni barrier layer and an interface reaction layer both of which facilitate a strong ohmic contact (Fig. 15a).[46] Researchers have conducted investigations into the structural parameters, and electronic band structure, as well as the half-metallic and thermoelectric properties of Sr_2EuReO_6 compound materials (**28**). Utilizing density-functional calculations within the framework of the generalized gradient approximation the computational analyses reveal a half-metallic nature in the electronic properties. Specifically, the majority spin channels exhibit metallic behavior, while the minority spin channels demonstrate semiconducting characteristics. The magnetic moment computed using GGA + U is determined to be 8.00 μB. The half-metallic behavior is attributed to the double-exchange interaction mechanism facilitated by the hybridization between Re(5d)–O(2p)–Eu(4f) orbitals. Utilizing Boltzmann theory, the thermoelectric response is evaluated revealing a Seebeck coefficient of 297.97 μV K^{-1}, electrical conductivity of 44.96 × 1019 Ω^{-1} m^{-1} s^{-1}, and lattice thermal conductivity of 5.94 × 1015 W m^{-1} K^{-1} s^{-1}. The thermoelectric efficiency determined through ZT calculation yields a value of 1 at 300 K. It exhibits potential for functioning in both low and high-temperature thermoelectric device operations. According to computational analyses, it showcases favorable characteristics in both spintronic and

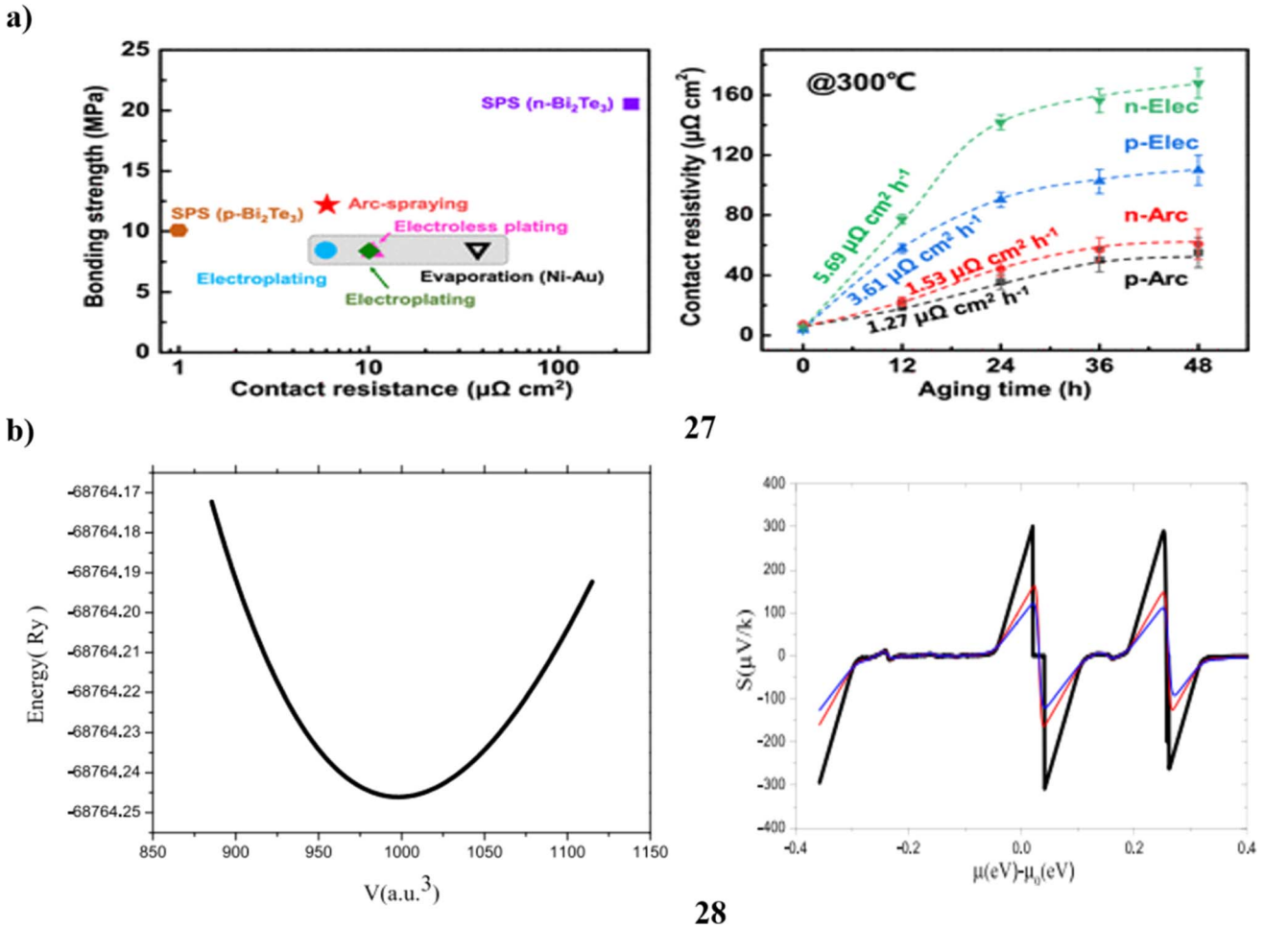

Fig. 15 (a) Thermal tolerance study of Ni/Bi Te based thermoelectric devices (**27**). (b) Thermoelectric study of Sr_2EuReO_6 (**28**).

thermoelectric properties making it a favorable candidate for spin injection applications (Fig. 15b).[47]

A flexible and ultralight planar thermoelectric generator comprising 15 thermocouples each composed of n-type bismuth telluride (Bi_2Te_3) and p-type antimony telluride (Sb_2Te_3) legs (**29**) with a thickness of 400 nm each connected in series on a Kapton® substrate with a thickness of 25 μm was successfully fabricated. The generator exhibits remarkable power factor values of 0.8 mW K^{-2} m^{-1} and 2.7 mW K^{-2} m^{-1} for Sb_2Te_3 and Bi_2Te_3 films, respectively. The p–n junction thermoelectric device exhibits impressive performance metrics generating a maximum open-circuit voltage of 210 mV and output power of 0.7 μW for a temperature difference of 35 K. Notably, this performance surpasses that observed for conventional thermoelectric devices with metallic contacts for p–n junctions. Additionally, the experimental findings are corroborated by numerical simulations demonstrating a strong agreement between the two sets of results. The *J*–*V* values of the fabricated p–n junctions display typical diode behaviour with a turn-on voltage close to ≈0.3 V and an exceptional rectifying ratio (I_{+1V}/I_{-1V}) of approximately ≈2 × 10^4 (Fig. 16a).[48] Furthermore, a highly flexible wearable thermoelectric generator (WTEG) comprising p-type MoS_2/CF and n-type Cu–Ni fabric-based TE legs (**30**) was fabricated for near-room temperature thermoelectric conversion. Initially, the thermoelectric properties of MoS_2/CF were improved by introducing a 1D MnO nanorod decoration, which induced an interface-induced energy filtering effect. The optimized barrier height of 0.035 eV in sample MMC10 resulted in the highest power factor surpassing that of pristine MoS_2 by 49.5% (Fig. 16b).[49]

The significant enhancements in the electrical conductivity and doping stability of poly(3-hexylthiophene) (P3HT) in ambient air are achieved through the utilization of a gold chloride dopant ($AuCl_4$) (**31**). The coexistence of $AuCl_4$- and Au nanoparticles plays a pivotal role in achieving both high electrical conductivity and doping stability simultaneously. Uniformly formed Au nanoparticles facilitate facile charge transfer within a thin film of $AuCl_3$-doped P3HT as confirmed by crystallography and transmission electron microscopy analysis. P3HT doped with $AuCl_3$ demonstrates impressive electrical conductivity of 207 S cm^{-1}, a Seebeck coefficient of 73.9 μV K^{-1}, and an optimized power factor of 110 μW m^{-1} K^{-2}. Crucially, $AuCl_3$-doped P3HT exhibits outstanding air stability. Even after 300 hours of exposure to ambient conditions, the optimized power factor of $AuCl_3$-doped P3HT remains above 80% of its initial value. In contrast, the power factor of $FeCl_3$-doped P3HT

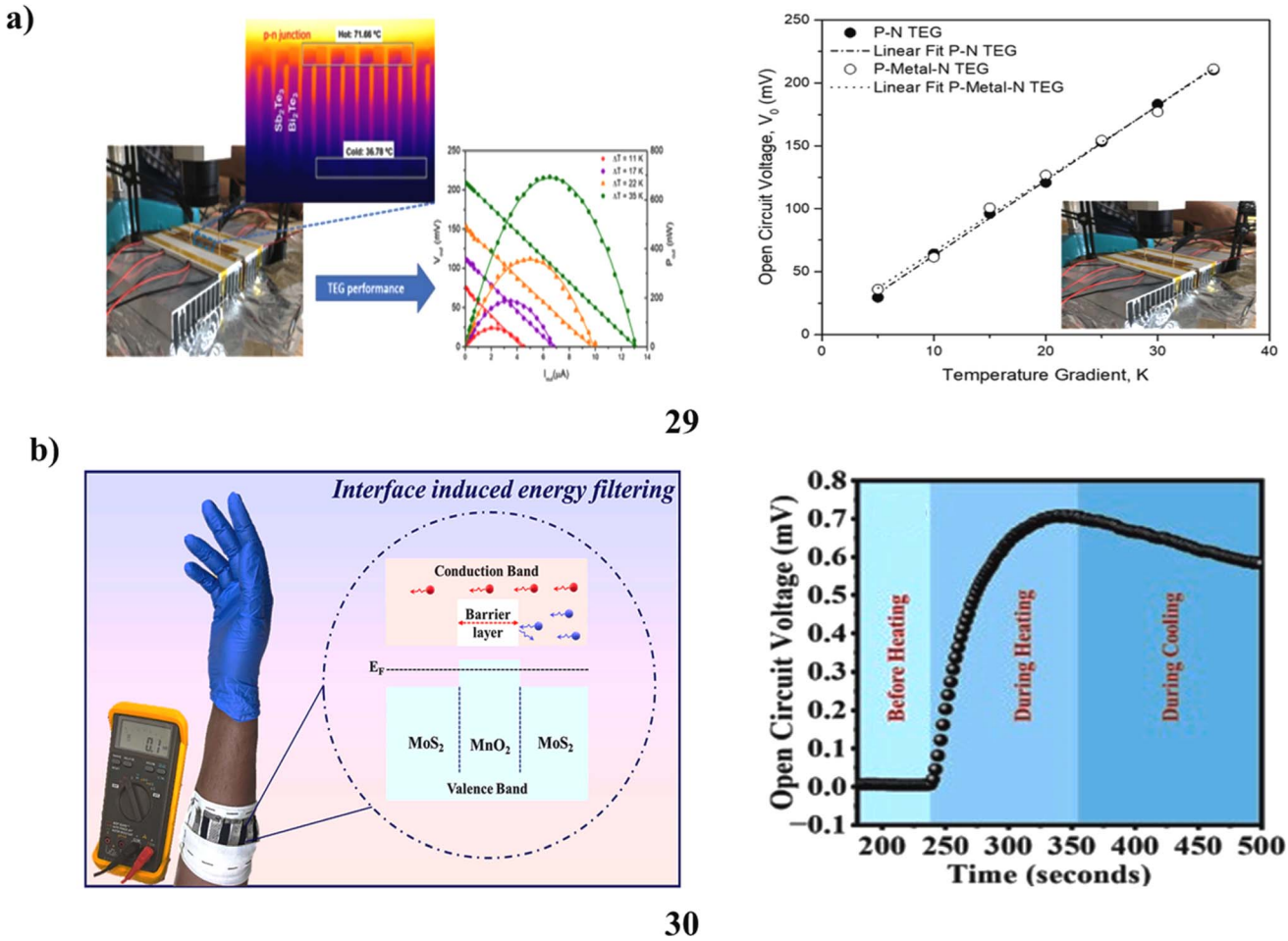

Fig. 16 (a) Thermoelectric device study of Bi_2Te_3/Sb_2Te_3 p–n junctions (**29**). (b) MoS_2/CF based interface induced energy filtering of TE device (**30**).

diminishes to only 20% of its original value under similar conditions. Furthermore, $AuCl_3$-doped P3HT is used in the slot-die coating process to develop an organic thermoelectric generator (OTEG) that is flexible. The OTEG exhibits a notably high open-circuit voltage (V_{oc}) of 7.96 mV and a short-circuit current (I_{sc}) of 0.93 μA yielding a power density of 18.5 nW cm^{-2} under a temperature gradient of 10 °C (Fig. 17a).[50] A compact, high-power, and flexible thermoelectric device constructed from a bulk thermoelectric (TE) material. To enable flexibility in thermoelectric devices based on bulk TE materials. The eutectic gallium–indium (EGaIn) (**32**) is a liquid metal encapsulated in poly-dimethylsiloxane (PDMS) that is used as electrodes on one side above the bending neutral axis in flexible thermoelectric devices (FTED). Flexible printed circuit boards (FPCB) serve as electrodes positioned below the bending neutral axis. Therefore, the stretchability of the liquid metal electrode and the flatness of the FPCB are maximized to minimize thermal contact resistance. Moreover, the use of PDMS and flexible wires as holders eliminates the requirement for filler materials, which could impede thermal bypass. Theoretical analysis suggests that refrigeration powered by portable batteries can lower the skin temperature by 5.4 K, a decrease significant enough for humans to feel a sensation of coldness. In the context of human body-heat harvesting, the open-circuit voltage and output power density were measured at 7.38 mV and 8.32 mW cm^{-2} or 123.74 mW, respectively. These results suggest that the FTED holds potential for dual applications serving as both a portable refrigerator and a wearable body-heat harvester (Fig. 17b).[51]

The enduring chemical stability of the Bi_2Te_3/Ni junction particularly concerning the hot side presents a significant concern for Bi_2Te_3-based and other thermoelectric systems due to the potential formation of Ni–Te intermediate compounds. The implementation of diffusion barrier layers has emerged as a viable solution with the barriers necessitating both excellent chemical inertness and slow diffusion properties. Among 13 metals screened, titanium (Ti) has been identified as an effective barrier material between p-type $Bi_{0.5}Sb_{1.5}Te_3$ thermoelectric materials and Ni electrodes. This selection is attributed to Ti's low diffusion coefficient and long-term interfacial stability. The p-type $Bi_{0.5}Sb_{1.5}Te_3$/Ti/Ni single-leg devices (**33**) as fabricated demonstrate a conversion efficiency exceeding 6% at a temperature difference of 200 K. Notably, these devices exhibit no observable degradation over 1860 cycles of measurements

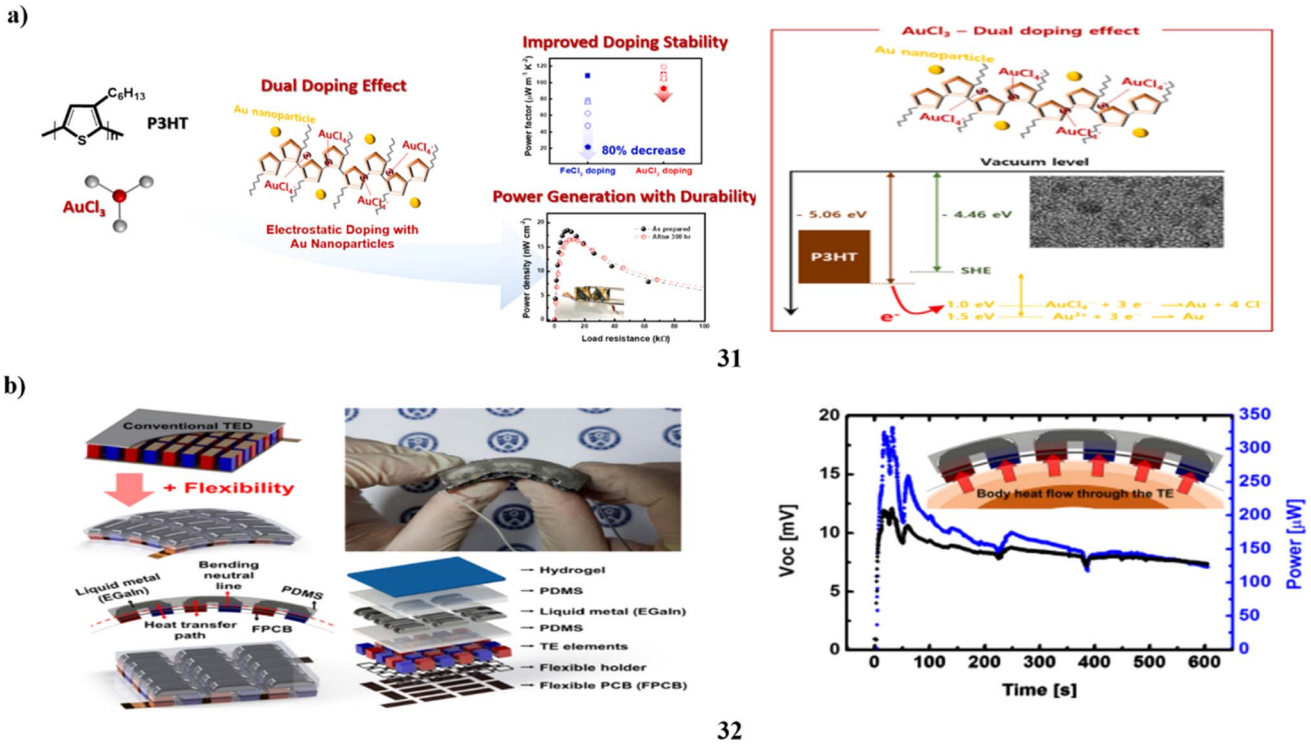

Fig. 17 (a) Thermoelectric devices application of Au–metal precursors (31). (b) High-power TE device study of liquid–metal composites (32).

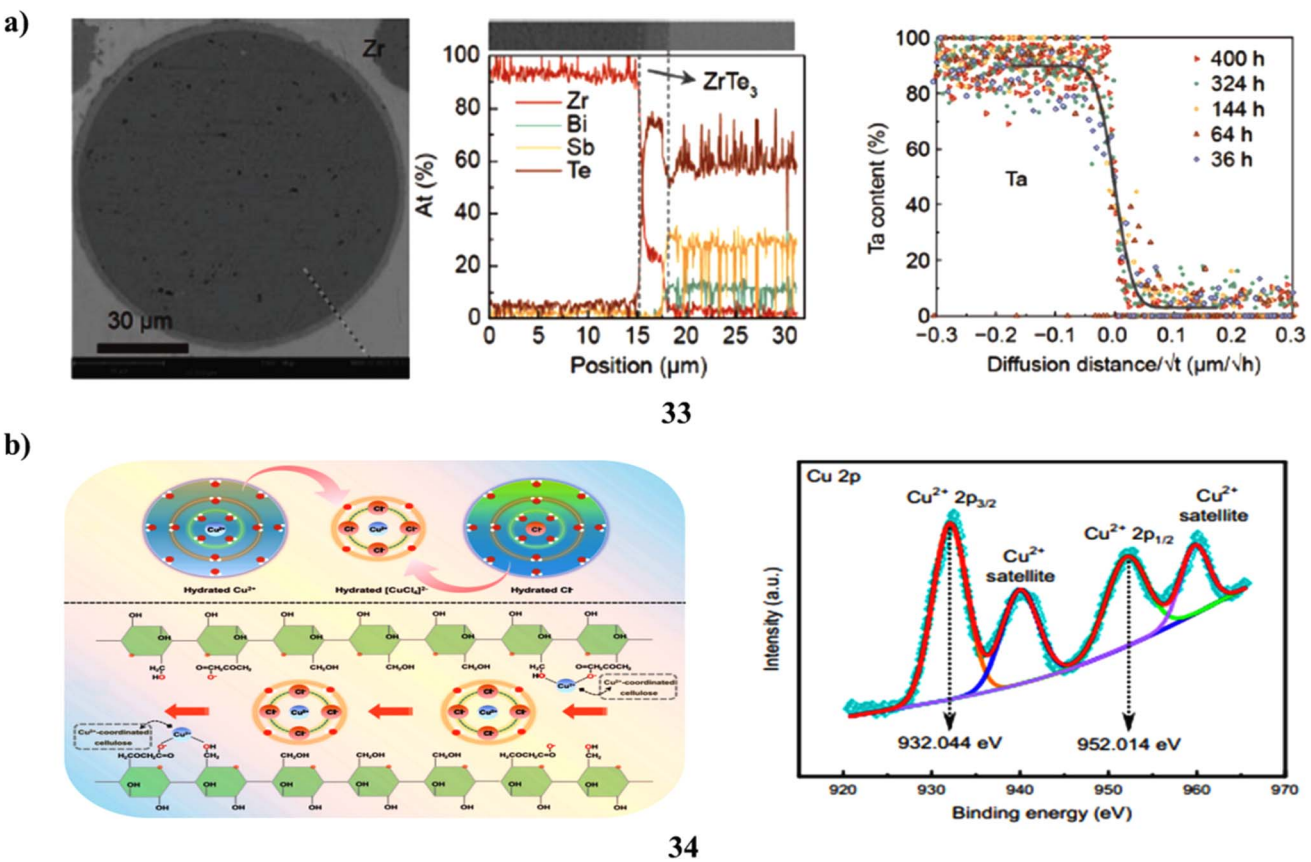

Fig. 18 (a) Metal diffusion barrier screening for thermoelectric $Bi_{0.5}Sb_{1.5}Te_3$ (33). (b) Thermoelectric properties of metal chloride complexes (34).

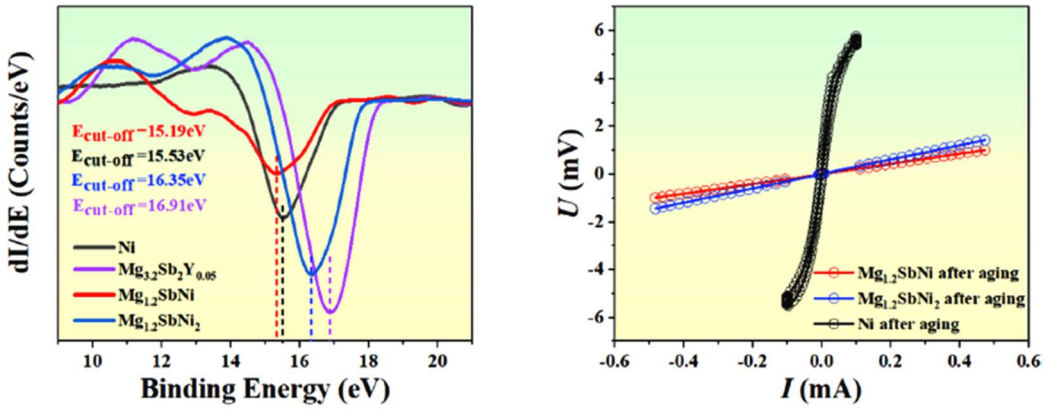

35

Fig. 19 Improvement of the conversion efficiency of Mg_3Sb_2 thermoelectric devices through optimizing the resistivity of the MgSbNi barrier layer (**35**).

spanning a period of 10 days. This study presents a valuable strategy for the development of efficient and long-lasting thermoelectric devices (Fig. 18a).[52] A hydrated membrane composed of polyvinyl alcohol (PVA) and cellulosic material exploits the thermal gradient diffusion of transition metal and chloride complex $[CuCl_4]^{2-}$ (**34**). This diffusion is enhanced through the incorporation of copper-coordinated carboxylated cellulose. Under similar conditions, the PVA-cellulosic membrane displays an impressive thermopower of -26.25 mV K^{-1} positioning it as one of the top-performing n-type ionic thermoelectric materials. The heightened thermally generated voltage can be attributed to the highly coordinated configuration of Cu^{2+}–Cl^- within the membrane. This configuration facilitates the conversion of the individual thermal motions of Cu^{2+} and Cl^- into enhanced ion transport heat of the $[CuCl_4]^{2-}$ anion facilitated by carboxylated cellulose. Notably, this phenomenon is not observed with other transition metal chlorides. The distinct heat transport behavior exhibited by $[CuCl_4]^{2-}$ holds significant implications for the design of high-performance ionic thermoelectric materials (Fig. 18b).[53]

The Mg_3Sb_2-based thermoelectric materials (**35**) have garnered significant attention for their potential in waste heat harvesting. Ensuring interface stability and long-term service performance are critical factors for their successful commercial application. The incorporation of $Mg_{4.3}Sb_3Ni$ as a barrier layer aimed to enhance the thermal stability of Mg_3Sb_2-based devices. However, its inherent high resistivity had a detrimental effect on the desired performance of the device. The findings indicate a 33% increase in the efficiency of the $Mg_{1.2}SbNi$/$Mg_{3.2}Sb_2Y_{0.05}$/$Mg_{1.2}SbNi$ joint compared to barriers with higher Mg content, attributed to the lower resistivity. Moreover, the system demonstrated favorable interfacial compatibility and minimal changes after aging at 673 K for 20 days (Fig. 19).[54]

Metal composites combine the high electrical conductivity of metals with other materials to enhance thermoelectric performance. These composites can achieve a balance between electrical and thermal conductivity, making them valuable in improving the efficiency of thermoelectric devices.

5. Nanoparticle-based thermoelectric devices

A new approach has been devised to enhance the efficiency of commercial thermoelectric generators. This method involves the application of a carbon nanoparticle (**36**) coating through a straightforward process utilizing a candle flame. This innovative technique aims to optimize the performance of thermoelectric generators by harnessing the unique properties of carbon nanoparticles. Utilizing a newly synthesized carbon layer characterized by a three-dimensional porous structure the coated thermoelectric generator demonstrates enhanced light-capturing capabilities. In contrast to the uncoated generator, the CNP-generator exhibits a remarkable 18-fold increase in power output. Further enhancements were achieved by integrating a cooling system and heat sink resulting in a staggering 34-fold improvement in power output compared to the baseline configuration. Leveraging a sunlight concentrator in outdoor conditions the optimized generator consistently supplied electricity to power both an electromotor and an electrochemical cell for chemical fuel production. This showcases the generator's commendable energy output capability affirming its practical suitability for diverse energy conversion applications. The synthesis process for the carbon layer is not only simple and scalable but also opens doors to explore various other applications. As a nano-generator, this advancement offers a promising alternative avenue to tackle the pressing energy crisis while also serving as a viable power source for portable devices. Its versatility and ease of production make it a compelling solution with far-reaching potential impacts on energy generation and device functionality (Fig. 20a).[55] Furthermore, a combination of two physical vapor deposition methods, high-power impulse magnetron sputtering, and a nano-particle gun was employed to embed Fe nanoparticles (**37**) into a CrN matrix. Combining these techniques enabled the generation of nanocomposites where the integrity of Fe nanoparticles remained intact distinct from any interaction with the matrix. The electrical and thermal transport properties of the

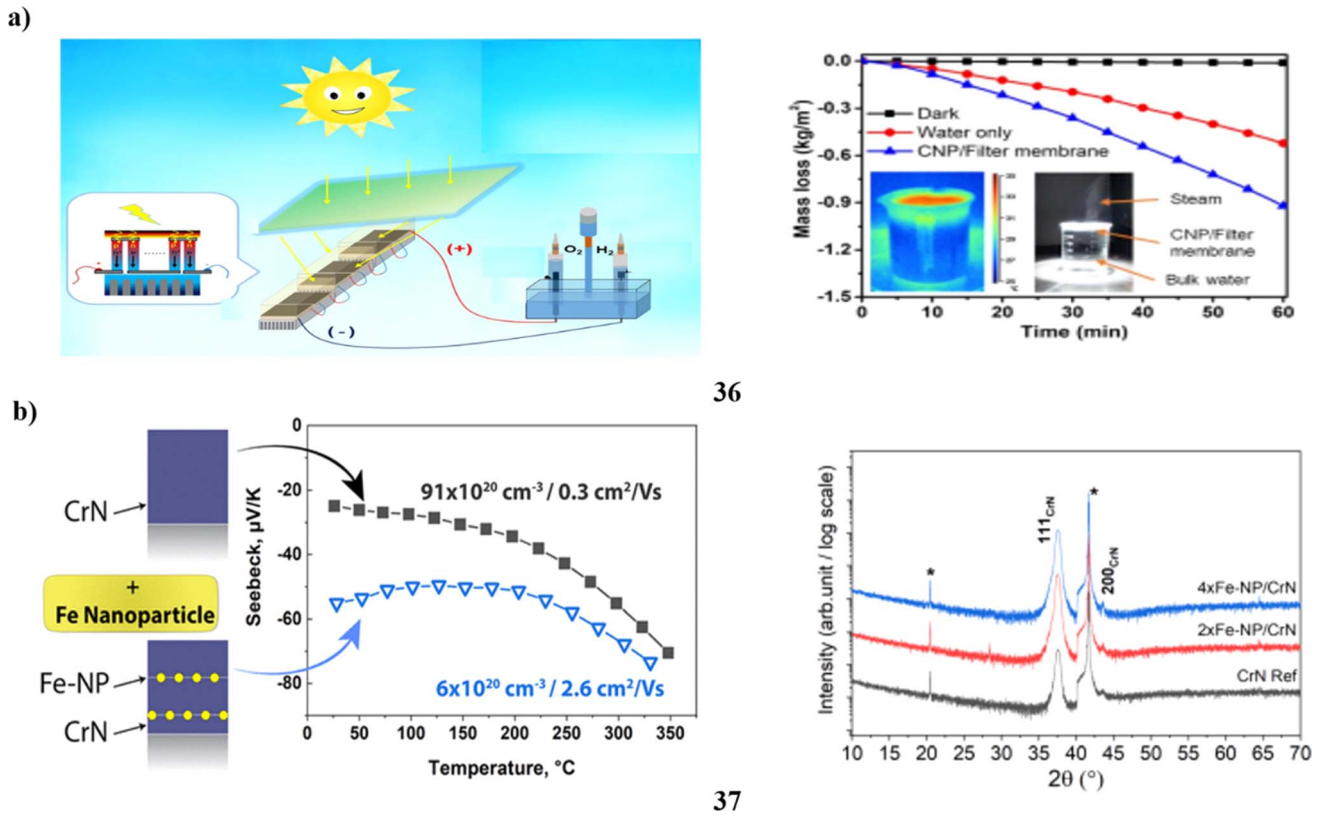

Fig. 20 (a) Electrochemical study of carbon nanoparticle (36). (b) Thermoelectric study Fe nanoparticles (37).

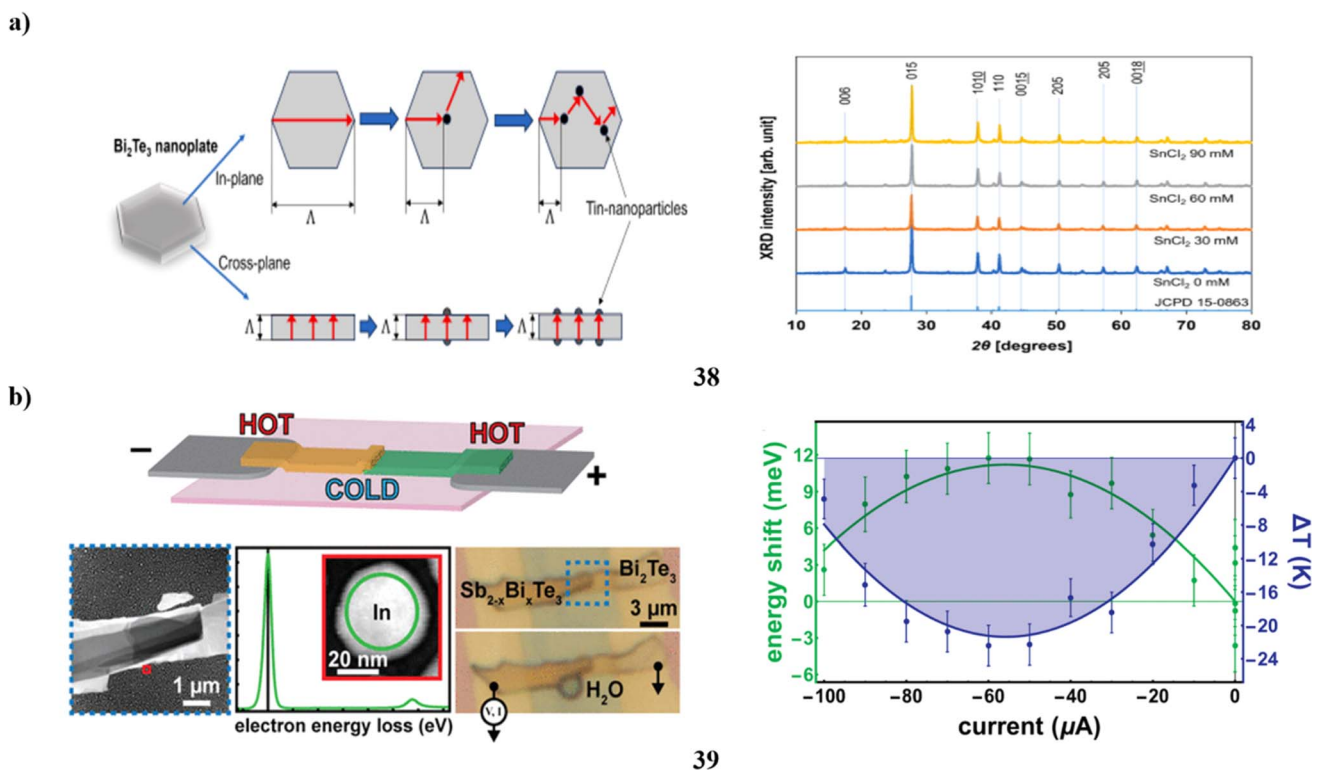

Fig. 21 (a) Skutterudite-based Fe–Ni metallization layers of TE device (38). (b) Electron-transparent thermoelectric coolers study of Bi_2Te_3 nanoparticle (39).

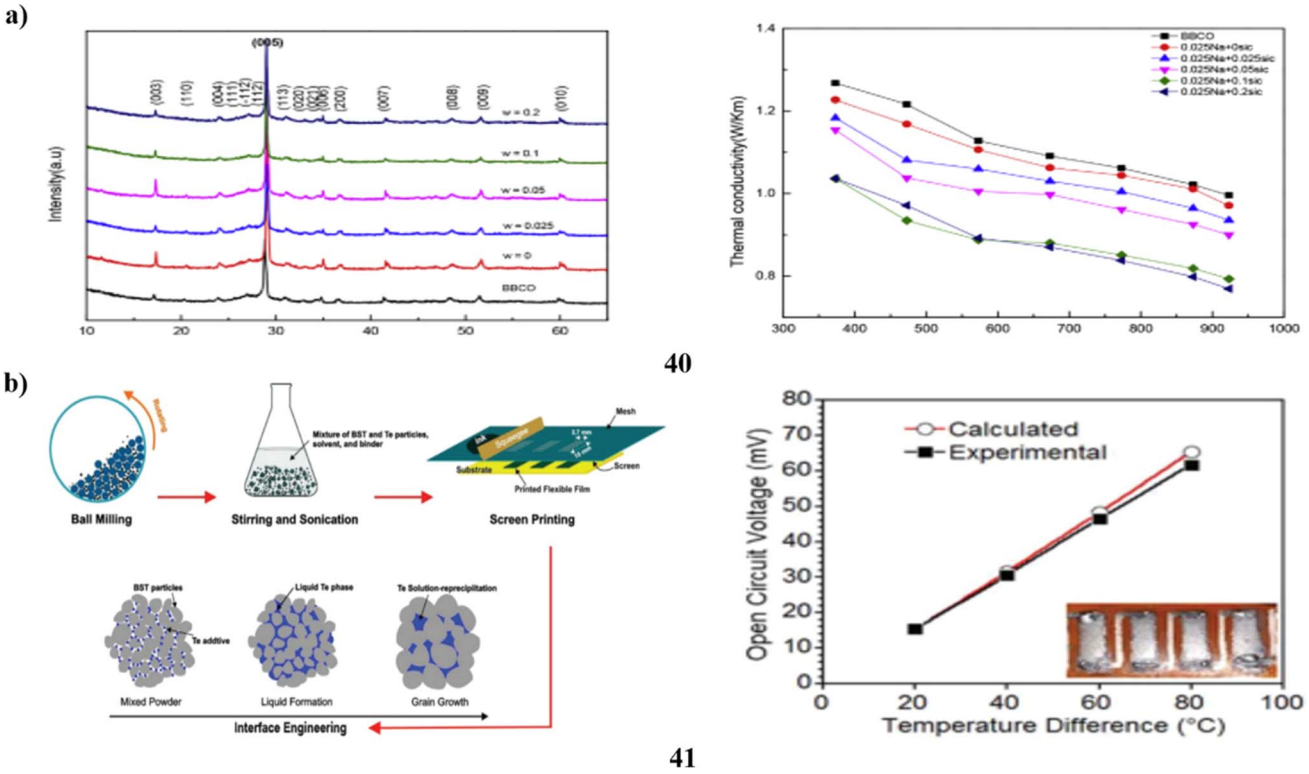

Fig. 22 (a) Thermoelectric properties of $Bi_2Ba_2Co_2O_y$-SiC nanoparticles (**40**). (b) BiSbTe particles based flexible thermoelectric devices (**41**).

nanocomposites were scrutinized and juxtaposed against those of a monolithic CrN film. The observed thermoelectric characteristics exhibited an elevation in the Seebeck coefficient alongside a reduction in Hall carrier concentration and an enhancement in electron mobility. These changes are attributed to energy filtration facilitated by internal phases formed at the interface between the nanoparticles and the matrix. The thermal conductivity of the resultant nanocomposite decreased from 4.8 W m^{-1} K^{-1} to a minimum of 3.0 W m^{-1} K^{-1}. This investigation demonstrates the potential of nanoparticle-based nanocomposite synthesis processes to enhance the thermoelectric characteristics of coatings (Fig. 20b).[56]

Hexagonal Bi_2Te_3 nanoplates (**38**) were produced using a solvothermal synthesis method, followed by the deposition of tin nanoparticles onto the nanoplate surface through electroless plating at different concentrations of $SnCl_2$ surface morphology and composition analyses have identified the presence of tin (Sn) on the surface of the nanoplates. However, X-ray diffraction (XRD) analysis did not detect tin. This could be due to either trace amounts of tin or its low crystallinity. Stated differently, it might be difficult to detect with this approach because the tin concentration is too low to show up in the XRD analysis or because the tin that is there has a poorly defined crystalline structure. To emulate the thermal properties of a single nanoplate as closely as possible the nanoplates were compacted at 300 K. Increasing concentrations of $SnCl_2$ led to a decrease in the in-plane lattice thermal conductivity, while the cross-plane lattice thermal conductivity remained low. This suggests that the deposition of tin on the nanoplate surface hampers phonon flow primarily in the in-plane direction likely due to increased phonon scattering (Fig. 21a).[57] Enhancing the efficiency of thermoelectric devices holds immense potential to revolutionize both refrigeration and energy production. It's anticipated that low-dimensional thermoelectric materials will outperform their bulk counterparts in terms of efficiency. Functional thermoelectric coolers (TECs) measuring only 100 nm in thickness, crafted from single crystal bismuth telluride (Bi_2Te_3) and antimony/bismuth telluride ($Sb_{2-x}Bi_xTe_3$) flakes (**39**) exfoliated from commercially available bulk materials exhibit thermal gradients at nanoscale lengths. These gradients are beyond the resolution capabilities of conventional thermometry methods. These devices represent a groundbreaking achievement as the smallest thermoelectric coolers (TECs) ever demonstrated surpassing previous sizes by a factor of 104. To accurately measure the heating and cooling effects produced by these ultra-small TECs indium nanoparticles were deposited to function as nanothermometers. The temperature decrease of $\Delta T = -21 \pm 4$ K from room temperature was revealed by the exact temperature measurements made possible by the use of plasmon energy expansion thermometry (PEET). Additionally, they introduced the concept of condensation thermometry a novel technique enabling quantitative mapping of temperature changes with a spatial precision of approximately $\lesssim$300 nm, thereby establishing another milestone in nanoscale thermal measurement (Fig. 21b).[58]

The synthesis yielded ceramic samples of $Bi_2Ba_2Co_2O_y$ + v wt% SiC and $Bi_{1.975}Na_{0.025}Ba_2Co_2O_y$ + w wt% SiC compositions. The introduction of a small quantity of Na element

doping increased the carrier concentration leading to a reduction in resistivity and Seebeck coefficients. The introduction of Na element doping induces lattice distortion consequently lowering the thermal conductivity of the samples. Incorporating SiC nanoparticles (**40**) further decreases the resistivity with a notable impact on reducing thermal conductivity. This effect is primarily attributed to the increased scattering of phonons by the additional grain boundaries resulting in a more significant reduction in thermal conductivity. The introduction of SiC particles in conjunction with Na element doping leads to a slight increase in the Seebeck coefficients due to the low energy carrier scattering effect. This synergistic effect effectively enhances the thermoelectric performance of $Bi_2Ba_2Co_2O_y$-based samples by reducing resistivity and thermal conductivity thus improving overall efficiency. The addition of 0.1 wt% SiC to the $Bi_{1.975}Na_{0.025}Ba_2Co_2O_y$ sample leads to a significant enhancement in its thermoelectric performance resulting in a maximum *ZT* value of 0.21 at 923 K. This represents a remarkable improvement compared to the $Bi_{1.975}Na_{0.025}Ba_2Co_2O_y$ sample alone with a 26.6% increase in *ZT* value, and a staggering 93% increase compared to the pure $Bi_2Ba_2Co_2O_y$ sample (Fig. 22a).[59] To create high-performance and flexible thermoelectric devices a scalable screen-printing technique is utilized. This method incorporates the tellurium-based nano solder approach as outlined in reference (**41**) to effectively bridge interfaces between the BiSbTe particles during the post-printing sintering process. The flexible films of BiSbTe produced through printing exhibit exceptional room-temperature power factors reaching an ultrahigh value of 3 mW m^{-1} K^{-2} along with a remarkable *ZT*. Additionally, a fully printed thermoelectric generator achieves an impressive power density of 18.8 mW cm^{-2} demonstrating high performance even with a relatively small temperature gradient of 80 °C. A significant step towards making thermoelectrics economically feasible for a variety of energy harvesting and cooling applications is the novel screen-printing technology, which directly transforms thermoelectric nanoparticles into high-performance and flexible devices (Fig. 22b).[60]

The high thermoelectric figure-of-merit is achieved in skutterudite nanocomposites through precise tailoring of interface carrier filtering. These nanocomposites consist of single-filled skutterudite ($Dy_{0.4}Co_{3.2}Ni_{0.8}Sb_{12}$) matrices incorporating rare-earth oxides nanoparticles such as Yb_2O_3, Sm_2O_3, and La_2O_3 (**42**). In the skutterudite nanocomposites, the interfaces between nanoparticles and the skutterudite serve as efficient carrier filters. This tailored structure substantially increases the Seebeck coefficient while maintaining high electrical conductivity. Consequently, the nanocomposites attain an impressive power factor of approximately 6.5 W m^{-1} K^{-2}. The presence of nonuniform strain distribution near the nanoparticles attributed to local lattice misfit and concentration fluctuations exerts an influence on heat carriers resulting in a reduction in lattice thermal conductivity. Moreover, the analysis using three-dimensional atom probe techniques unveils the formation of Ni-rich grain boundaries within the skutterudite matrix. These grain boundaries further contribute to the reduction of lattice

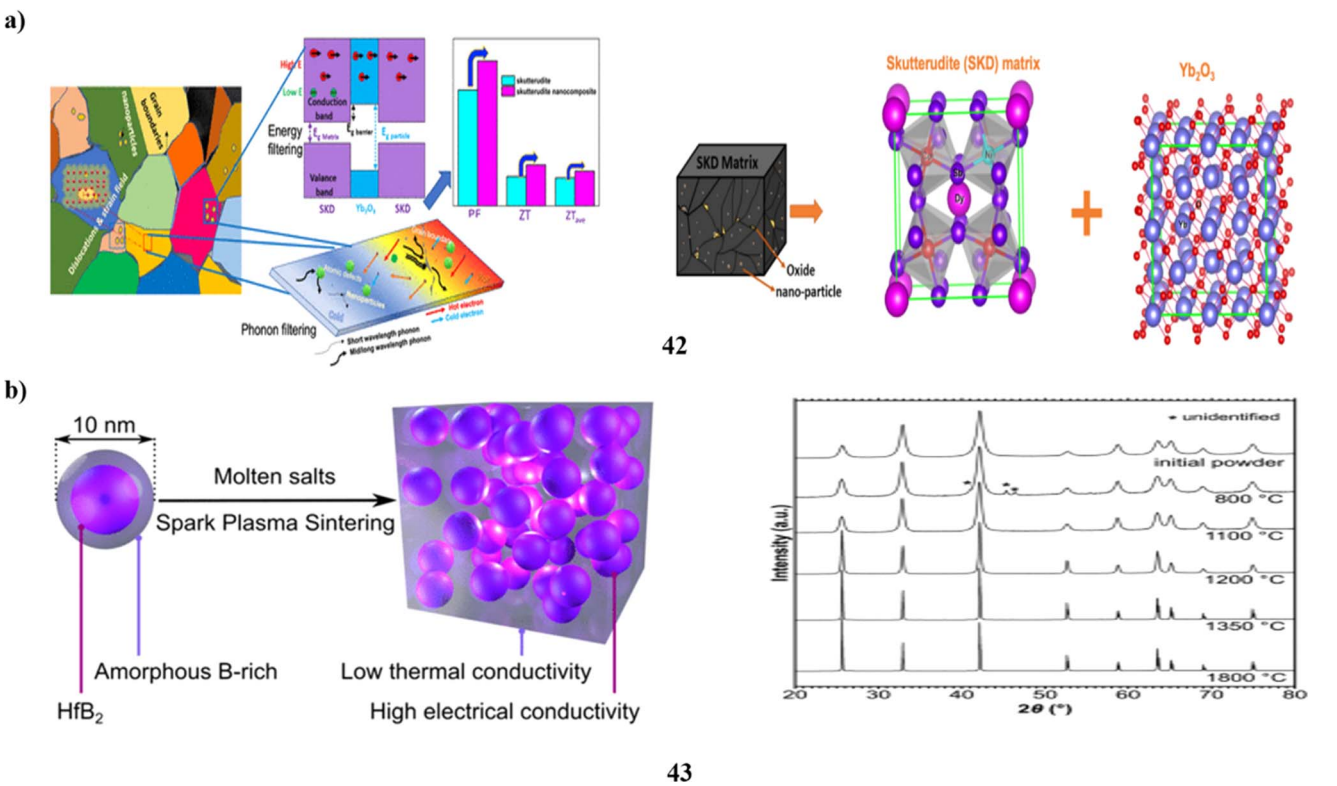

Fig. 23 (a) Skutterudite-Yb_2O_3 nanocomposites based thermoelectric device (**42**). (b) Transport properties of nanoparticle-based boron-rich composites (**43**).

thermal conductivity. The combined effects of decreased lattice thermal conductivity and enhanced power factor result in a remarkable increase in the thermoelectric figure of merit (ZT) of up to approximately ~1.84 at 723 K. Additionally, the average ZT reaches around 1.56 in the temperature range of 523 to 723 K (Fig. 23a).[61] Nanostructuring boron-rich materials have the potential to profoundly affect their thermal and electrical transport properties. However, nanostructured monoliths of such materials within the 10 nm range have remained elusive. This challenge arises due to the substantial temperatures needed for the synthesis and production of boron-rich compounds. A nanocomposite consisting of metallic HfB_2 nanocrystals (**43**) distributed in an insulating amorphous boron-rich matrix is synthesized in a single pot using inorganic molten salts. The synthesis allows for precise control over the volume fraction of nanocrystals, ranging from 16 to 56 vol%. This controlled liquid-phase synthesis method can be integrated with spark plasma sintering to achieve densification while preserving the nanostructure of the material. The study emphasizes the correlations between the reagent ratios utilized in the liquid-phase synthesis the sintering parameters employed, and the resulting transport properties of the densified nanocomposites. The nanocomposite demonstrates metallic electrical conductivity, which is attributed to the presence of HfB_2 nanocrystals. Additionally, it exhibits enhanced thermal dissipation, which can be attributed to the nanostructured amorphous boron matrix (Fig. 23b).[62]

The thermoelectric carbon nanoparticle (CNP)–carbon nanotube (CNT) heterostructures (**44**) as a highly favorable flexible thermoelectric materials. The Seebeck coefficient (S) of the heterostructures is enhanced by optimizing the barrier energy between the CNP and CNT leveraging the energy filtering effect. To achieve peak thermoelectric performance precise control over the work function of the CNPs allows effective tuning of the CNP–CNT barrier energy. The optimized p-type CNP–CNT heterostructures demonstrated a Seebeck coefficient (S) and power factor (PF) of $50.6 \pm 1.4\ \mu V\ K^{-1}$ and $400 \pm 26\ \mu W\ m^{-1}\ K^{-2}$, respectively. Conversely, the n-type CNP–CNT heterostructures optimized for a different CNP work function exhibited S and PF values of up to $-37.5 \pm 3.4\ \mu V\ K^{-1}$ and $214 \pm 42\ \mu W\ m^{-1}\ K^{-2}$ respectively. Moreover, p-and n-type CNP–CNT heterostructures with precisely calibrated barrier energies demonstrate the thermoelectric generator's potential for energy harvesting. At a ΔT of 5 K, the thermoelectric generator including 10 p-type and 9 n-type thermoelectric elements demonstrated a maximum output power of 0.12 μW. This work provides a simple method for creating thermoelectric CNP–CNT heterostructures with customised energy filtering properties. The use of these heterostructures in thermoelectric devices on paper substrates is also investigated (Fig. 24a).[63] The Bi_2Te_3-based compounds are widely recognized as the most established and commonly utilized thermoelectric materials. However, the manufacturing of industrial devices unavoidably yields substantial amounts of Bi_2Te_3 scraps resulting in the

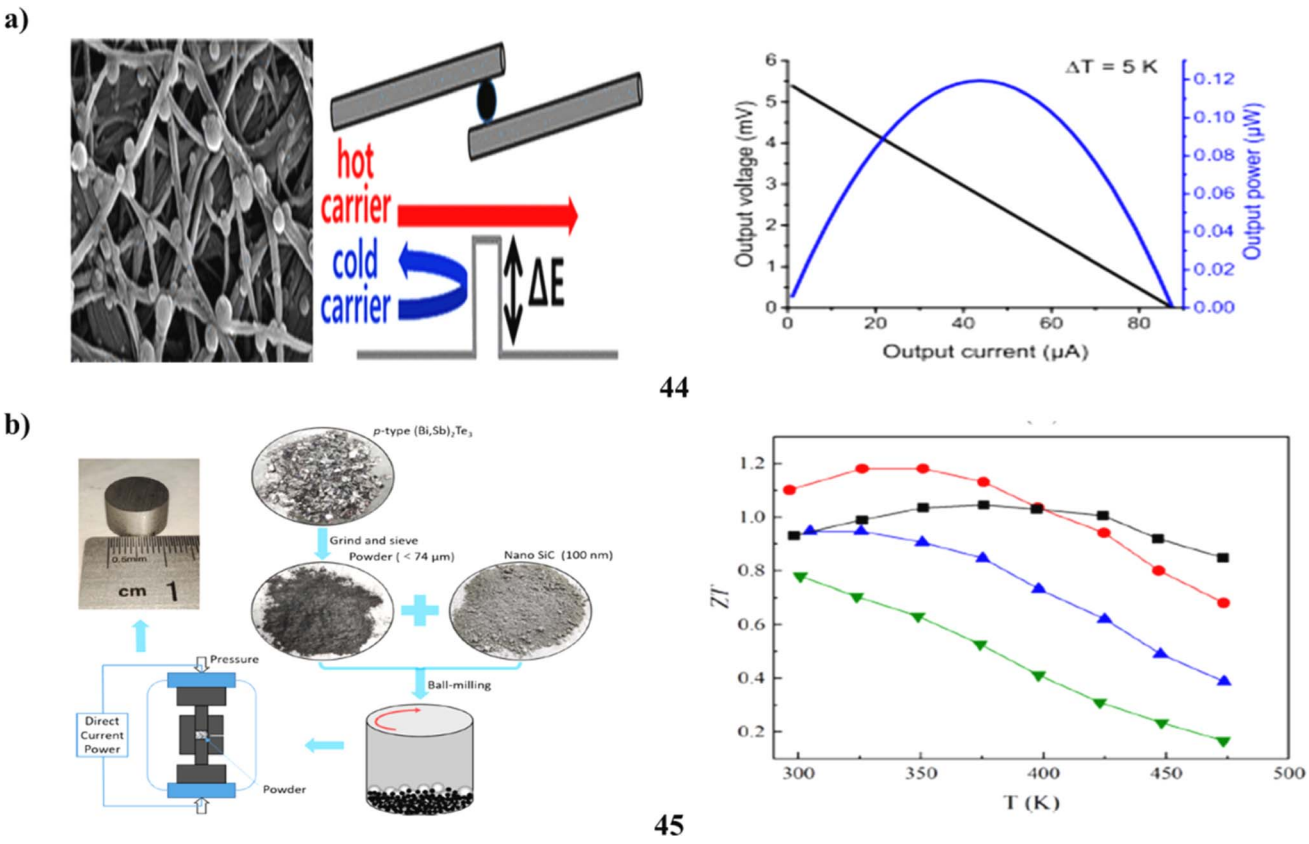

Fig. 24 (a) CNP-CNT heterostructures based Thermoelectric device (**44**). (b) $(Bi,Sb)_2Te_3$-based thermoelectric nano-composites (**45**).

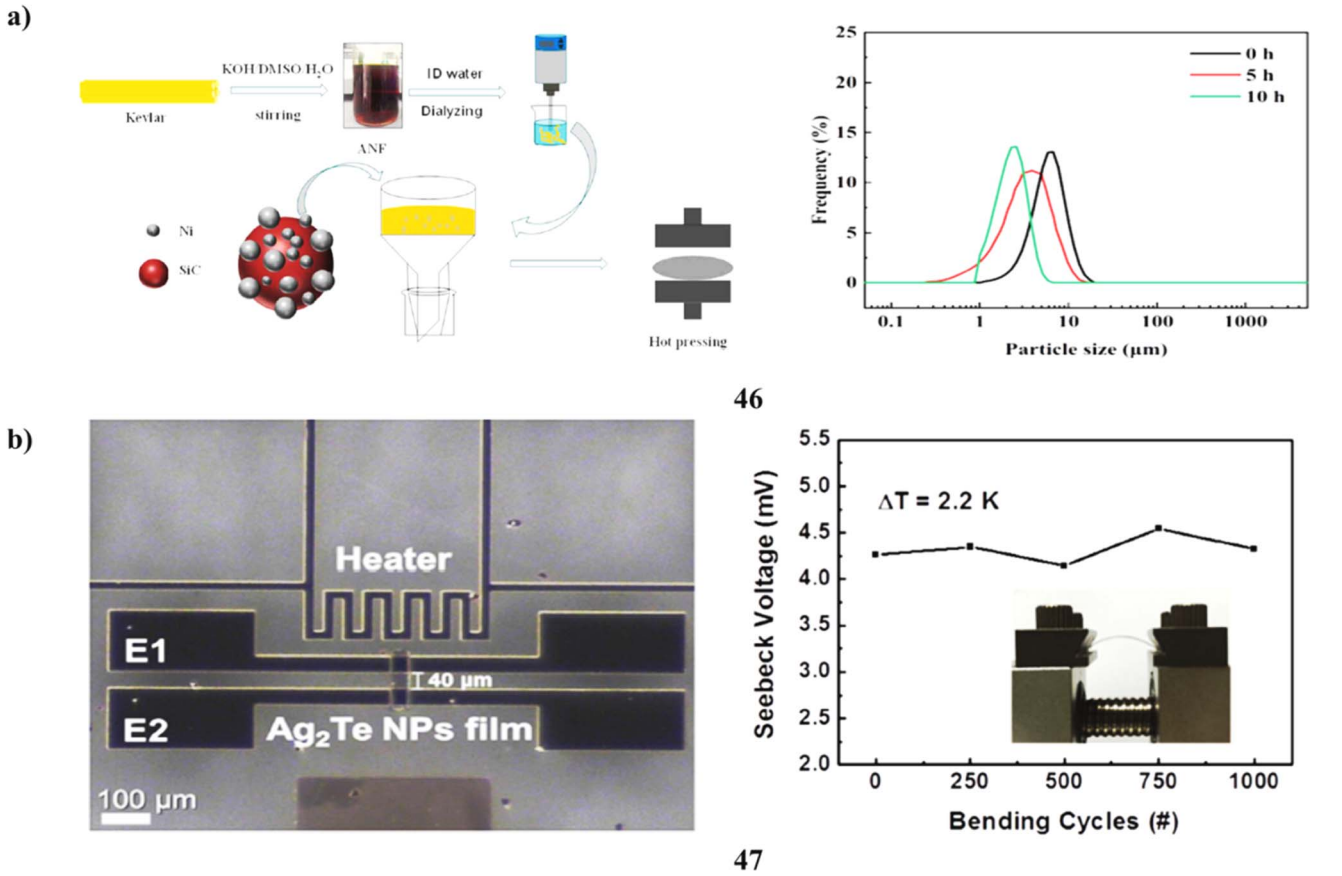

Fig. 25 (a) SiC-nickel nanoparticle-based thermal conductive applications (**46**). (b) Thermoelectric characteristics of γ-Ag_2Te nanoparticle (**47**).

depletion of valuable material resources. The p-type $(Bi,Sb)_2Te_3$ scraps were repurposed by transforming them into nanocomposites through incorporation with nano-SiC (**45**). The thermoelectric performance saw enhancement achieving a notable *ZT* value of 1.07 representing a substantial improvement compared to commercial p-type $(Bi,Sb)_2Te_3$ ingots. Furthermore, there was a notable increase in hardness, which is advantageous for device fabrication. A higher *ZT* value of 1.2 was also attained by optimizing the amount of Bi/Te in the commercial p-type $(Bi,Sb)_2Te_3$ scraps, which better thermoelectric performance (Fig. 24b).[64]

The method involved using nickel (Ni) nanoparticles to coat the silicon carbide (SiC) filler employing a rapid and environmentally friendly process. This process entailed mixing nickel acetate tetrahydrate ($Ni(CH_3COO)_2 \cdot 4H_2O$) and SiC followed by heating under an inert atmosphere. The resulting composites serving as thermal fillers were then utilized to fabricate an aramid nanofiber (ANF) (**46**)-based composite film. The decoration of silicon carbide (SiC) with an appropriate amount of nickel (Ni) nanoparticles significantly enhances various properties of the aramid nanofiber (ANF) composite film. Specifically, it improves thermal conductivity, hydrophobicity, thermal stability, and puncture resistance. The optimization of balling time to 10 hours resulted in an enhanced thermal conductivity of 0.502 W m^{-1} K^{-1} for the ANF film, which represents a 298.4% increase compared to the original film. The addition of thermal fillers up to 30 wt% resulted in a significant enhancement in thermal conductivity reaching 0.937 W m^{-1} K^{-1}, a remarkable 643.7% increase compared to the pristine ANF film. Additionally, the ANF-composite films showed a noticeable improvement in thermal stability and the compatibility of the ANFs with the thermal fillers. The effective heat transfer capabilities of the composite films were further validated through experiments involving an LED lamp and a thermoelectric device. Additionally, the composite films exhibited enhanced mechanical properties and superior hydrophobicity highlighting their potential for applications in electronic devices (Fig. 25a).[65] The γ-Ag_2Te nanoparticles (NPs) (**47**) were synthesized, and their thermoelectric properties were studied within a thin film configuration deposited onto a flexible plastic substrate. The thermoelectric properties demonstrate typical p-type behavior, with the Seebeck coefficient of the γ-Ag_2Te NP thin film measuring 1330 μV K^{-1}, markedly higher than that of α- or β-Ag_2Te NP thin films. At room temperature in air the power factor is determined to be 0.66 μW m^{-1} K^{-2}. Additionally, the stability in thermoelectric characteristics persists even after subjecting the films to 1000 bending cycles. These findings indicate that γ-Ag_2Te NP thin films are exceptionally well-suited for flexible thermoelectric devices capable of operating reliably under real-life conditions (Fig. 25b).[66]

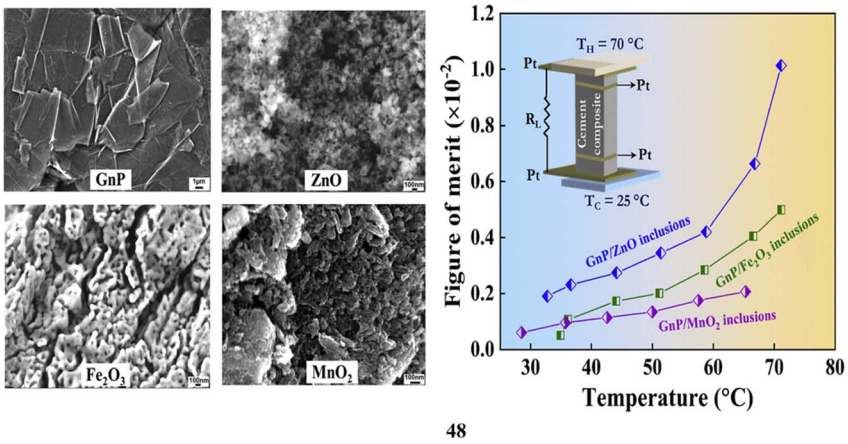

Fig. 26 Thermoelectric figure of merit study of graphene-based metal oxide nanoparticles (48).

The Seebeck coefficient of cement composites incorporating transition metal oxide nanoparticles (**48**) and graphene has been measured to exceed 100 mV K^{-1}. This value represents a significant improvement approximately three times higher than previously reported graphene-enhanced cement composites. The elevated Seebeck coefficient in these cement composites is primarily attributed to the presence of metallic oxides, which play a dominant role. This enhancement is largely driven by the quantum confinement effect exhibited by the nanoparticles. The notable increase in the Seebeck coefficient significantly contributes to improving the thermoelectric figure of merit of the composite material. The highest figure of merit reaching 1.01×10^{-2} is attained when incorporating ZnO inclusions into the composite. In comparison, the addition of Fe_2O_3 yields a figure of merit of 0.5×10^{-2}, while MnO_2 incorporation results in a figure of merit of 0.2×10^{-2}. The peak figure of merit achieved by these cement composites holds promising implications for efficient energy harvesting in buildings offering significant potential for advancements in the near future (Fig. 26).[67]

Nanoparticles have the potential to significantly boost the thermoelectric efficiency of materials by enhancing their electrical properties while reducing thermal conductivity. The ability to engineer nanoparticles at the atomic level allows for precise control over their thermoelectric characteristics, opening new avenues for high-performance applications.

6. Polymer based thermoelectric devices

The conducting polymers present novel opportunities for the creation of soft, flexible, and lightweight thermoelectric textile generators. These generators can seamlessly blend into garments offering unobtrusive integration while providing efficient energy harvesting capabilities. The polyelectrolyte complex poly(3,4-ethylenedioxythiophene):poly(styrene sulfonate) (PEDOT:PSS) (**49**) serves as the p-type material for the creation of electrically conducting sewing threads. These threads are integrated into thick wool fabrics enabling the formation of out-of-plane thermoelectric textile generators. Detailed discussion on the influence of device design highlights that the performance of e-textile devices can be effectively predicted and optimized using modeling techniques developed for conventional thermoelectric systems. This prediction accuracy is contingent upon incorporating electrical and thermal contact resistances into the model. At last, a breakthrough in thermoelectric textile devices has been achieved demonstrating unprecedented power generation for polymer-based devices. Specifically, it has attained an impressive power output of 1.2 μW when subjected to a temperature gradient (ΔT) of 65 K. Even at a more modest temperature gradient of 30 K, it still yields over 0.2 μW of power output (Fig. 27a).[68] The incorporation of thermoelectric generators (TEGs) into textiles presents an appealing prospect for harvesting body heat to power wearable electronics. Textile-integrated TEGs offer the advantage of seamlessly conforming to the body ensuring efficient heat transfer without restricting movement. Utilizing additive printing techniques and solution-processable polymer-based thermoelectric (TE) materials holds promise for creating textile thermoelectric generators (TEGs). Nonetheless, several fabrication challenges hinder the realization of a printed polymer-based textile TEG through a cost-effective, scalable, and textile-compatible process. Stencil and transfer printing techniques have proven effective in fabricating a 32-leg device on a commercial sports fabric substrate. This device boasts a modest fill factor of approximately 30%. The polymer materials utilized in this process include PEDOT:PSS as the p-type material and poly[Na(NiETT)] (**50**) as the n-type material formulated into inks for printing. The textile-integrated thermoelectric (TE) device exhibits an open circuit voltage of approximately 3 mV when subjected to a temperature gradient (ΔT) of 3 K. Scaling up the fabrication process an 864-leg device is demonstrated yielding a voltage output of approximately 47 mV. This study marks the pioneering demonstration of a textile thermoelectric generator (TEG) utilizing both p- and n-type conducting polymers enabling effective through-plane body heat harvesting. Serving as a crucial proof-of-concept this advancement lays the groundwork for integrating

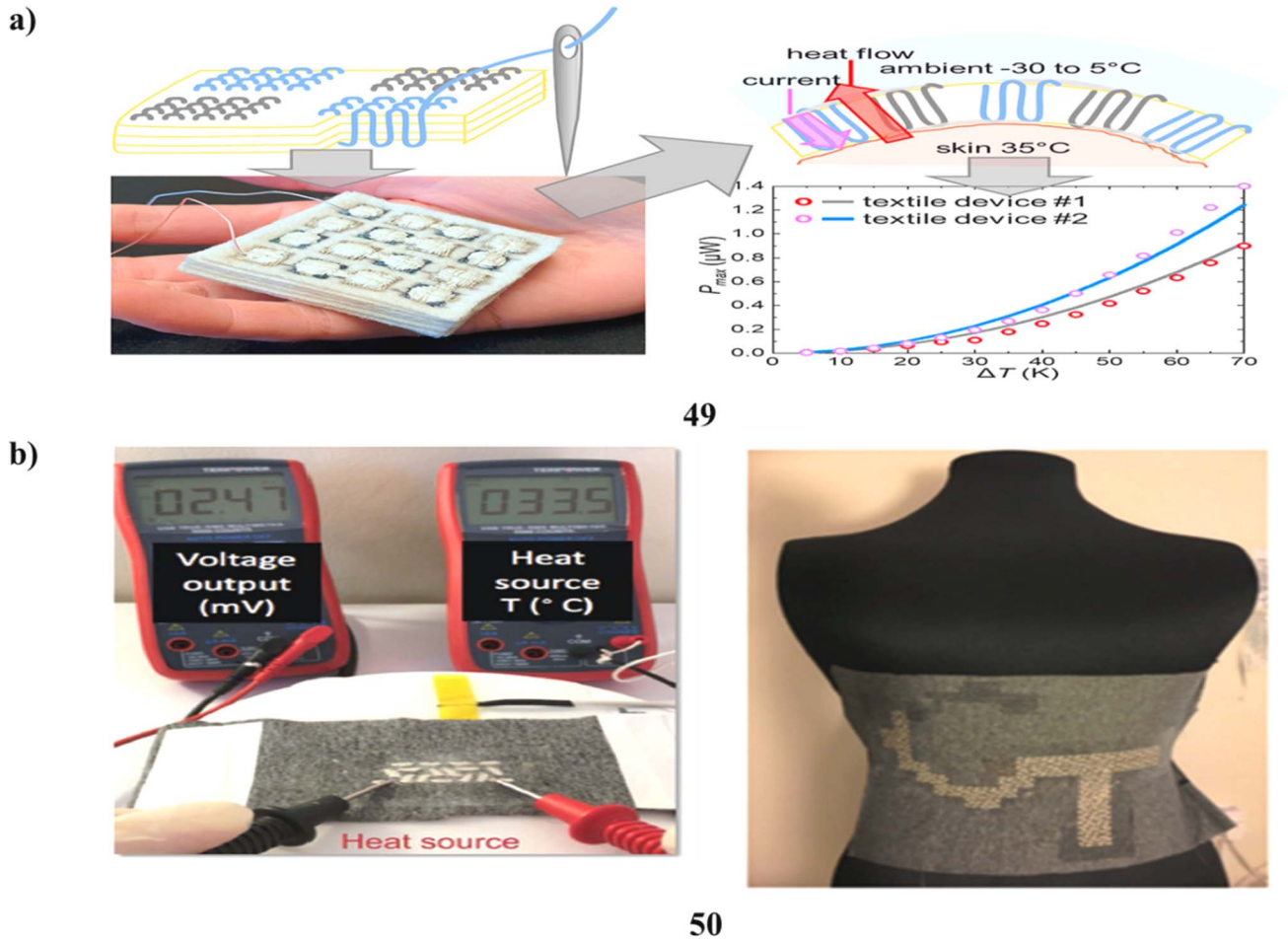

Fig. 27 (a) PEDOT:PSS-based textile TE generator (**49**). (b) Textile-integrated polymer-based TE generator (**50**).

thermoelectric devices into mainstream fabrics and clothing (Fig. 27b).[69]

The study explores the impact of incorporating nickel oxide (NiO) into the polyaniline (PANI) backbone to enhance charge transport within the polymeric system. This approach serves the dual purpose of improving the material's conductivity and tailoring it for thermoelectric (TE) applications. Polyaniline/nickel oxide (PANI/NiO) nanocomposites (**51**) have been effectively synthesized through a combination of sol–gel and *in situ* chemical oxidative polymerization methods. Ammonium persulfate is used in the procedure as a polymerizing agent in an acidic media. The synthesized nanocomposites underwent comprehensive characterization *via* techniques including XRD, SEM, FTIR, and UV-Vis-NIR absorbance measurements. An observable shift in the band gap attributed to p–p* electronic transition was detected during optical measurements. The polymer chain exhibits enhanced carrier transport facilitated by its ordered chain orientation and heightened conjugation resulting in elevated electrical conductivity. Additionally, the incorporation of NiO nanoparticles within the polymer chain matrix serves to reduce barriers to both interchain and intrachain hopping. An impressive enhancement in thermoelectric electromotive force (thermo emf) and Seebeck coefficient (S) has been observed upon the incorporation of NiO into pure PANI (Fig. 28a).[70] Flexible composite films consisting of Ag_2Se nanowires (NW) (**52**) and PEDOT:PSS are fabricated in this study. The Ag_2Se nanowires are initially synthesized through solution mixing. The first step in the synthesis of Ag_2Se nanowires is solution mixing. The Ag_2Se NW/PEDOT:PSS composite film is then produced by a simple drop-casting technique. The thermoelectric properties of these composites are thoroughly analyzed across varying Ag_2Se contents to assess their potential applications. Strategies for optimizing the thermoelectric power factor are also deliberated upon to maximize the efficiency of the composite materials. The composite film achieves its maximum room-temperature power factor of 178.59 μW m^{-1} K^{-2} with 80 wt% Ag_2Se nanowires. Moreover, it exhibits exceptional durability maintaining its integrity even after undergoing 1000 repeated bending cycles. The development of high-performance flexible thermoelectric composite films represents a significant advancement with broad implications for both inorganic and organic composite materials. This innovation is poised to catalyze further advancements and applications in the field of thermoelectrics (Fig. 28b).[71]

A wearable thermoelectric device is developed using a cost-effective deposition technique to coat PANI/G nanocomposite

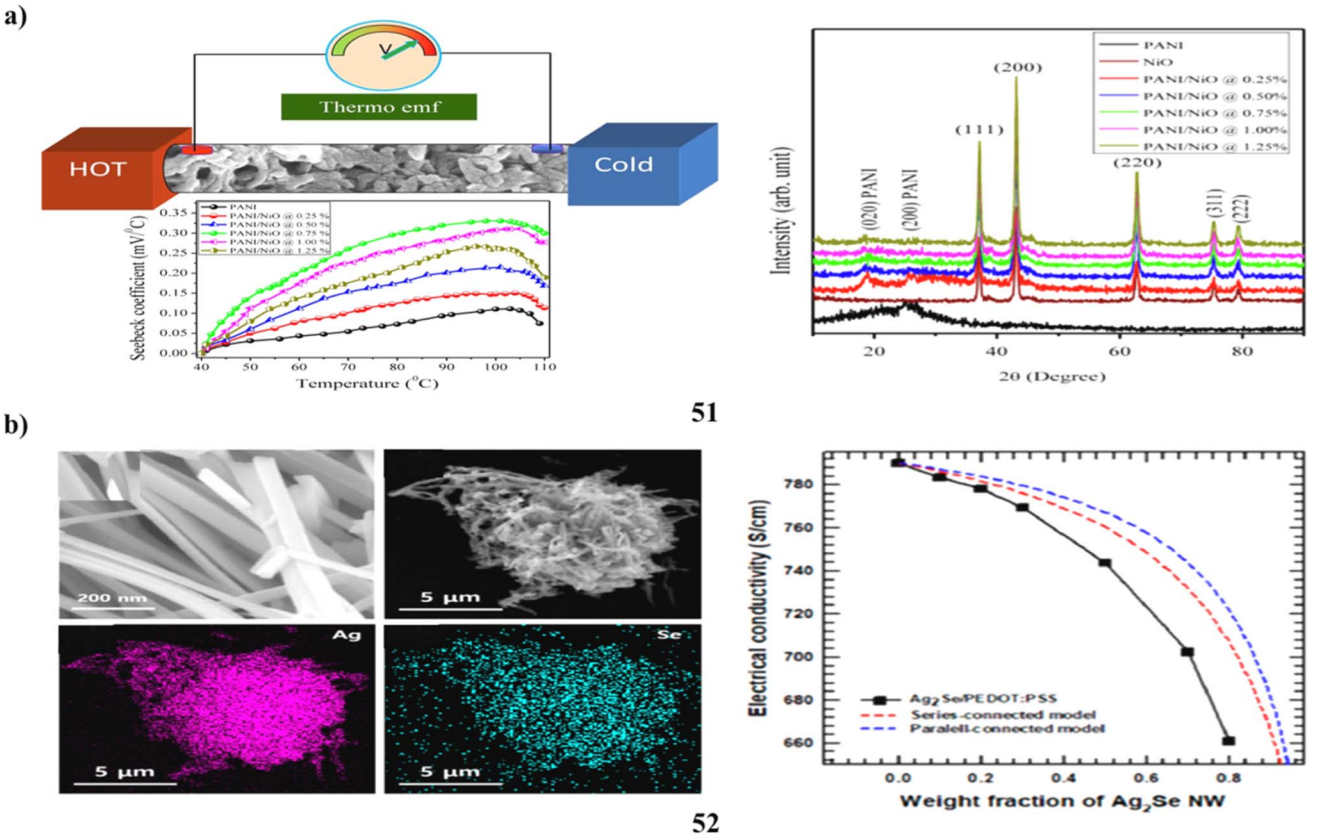

Fig. 28 (a) Polyaniline/nickel oxide-based thermoelectric generator (**51**). (b) PEDOT:PSS/Ag_2Se nanowires based thermoelectric applications (**52**).

(**53**) onto carbon fabric. The resulting sample, comprising polyaniline/graphene-coated on carbon fabric exhibits an electrical conductivity of 1.98×10^2 S m^{-1} at 373 K and a Seebeck coefficient of 18.3 ± 0.02 μV K^{-1} at the same temperature. Moreover, the transport mechanism observed in the polyaniline-graphene nanocomposite coated on carbon fabric was predominantly governed by a variable range hopping process. For the fabrication of a thermoelectric (TE) device, four couples of TE materials were utilized with a PGCF2 sample serving as the p-type material and copper wire employed as the n-type material. By connecting the n and p-type legs with copper tape a voltage of 0.40 mV was generated at a temperature difference (ΔT) of 321 K. This innovative approach opens up new possibilities in the realm of wearable thermoelectric devices. The potential applications of these thermoelectric devices extend to portable and interactive devices promising advancements in various fields (Fig. 29a).[72] A solution-processable TEG is introduced featuring exclusively polymers as active materials. This TEG combines the high-mobility n-type polymer poly[[*N*,*N*-bis(2-octyldodecyl)-naphthalene-1,4,5,8-bis(-dicarboximide)-2,6-diyl]-*alt*-5,5-(2,2-bithiophene)] (P(NDI2OD-T2)) with the well-studied p-type polymer blend PEDOT:PSS (**54**) to form a thin-film TEG. The versatility of this device design extends beyond its current application encompassing a wide range of organic materials that can be processed from solution. Moreover, its scalability facilitates the seamless transition to fully flexible devices offering adaptability across various systems and contexts (Fig. 29b).[73]

A comprehensive investigation was carried out on free-standing flexible composites comprising carbon nanotubes (CNTF) and polyaniline (PANI) (**55**). These composites, fabricated with varying PANI polymerization times underwent thorough analysis to assess their morphologies, chemical compositions, thermoelectric properties, and mechanical behaviors systematically. At a PANI polymerization time of 5 hours, the CNTF/PANI composites exhibited notable thermoelectric properties with a Seebeck coefficient of 63.3 μV K^{-1}, electrical conductivity of 1338.4 S cm^{-1}, and a power factor of 536.8 μW m^{-1} K^{-2} at 360 K. Even after undergoing bending 500 times, the electrical conductivity of the CNTF/PANI composites remained robust maintaining 93.3% of its initial value. Moreover, these CNTF/PANI composites exhibited superior mechanical properties. Compared to CNTF alone the composites demonstrated tensile strength, Young's modulus, and toughness that were 3.5, 2.6, and 2.1 times higher, respectively. With enhanced thermoelectric and mechanical properties the CNTF/PANI composites become highly suitable for intelligent wearable applications. Their robustness and superior performance make them ideal for integration into wearable devices offering improved functionality and durability (Fig. 30a).[74] A gram-scale polymer-based thermoelectric module was designed and fabricated by laminating ultrathin half-dried PEDOT/PSS

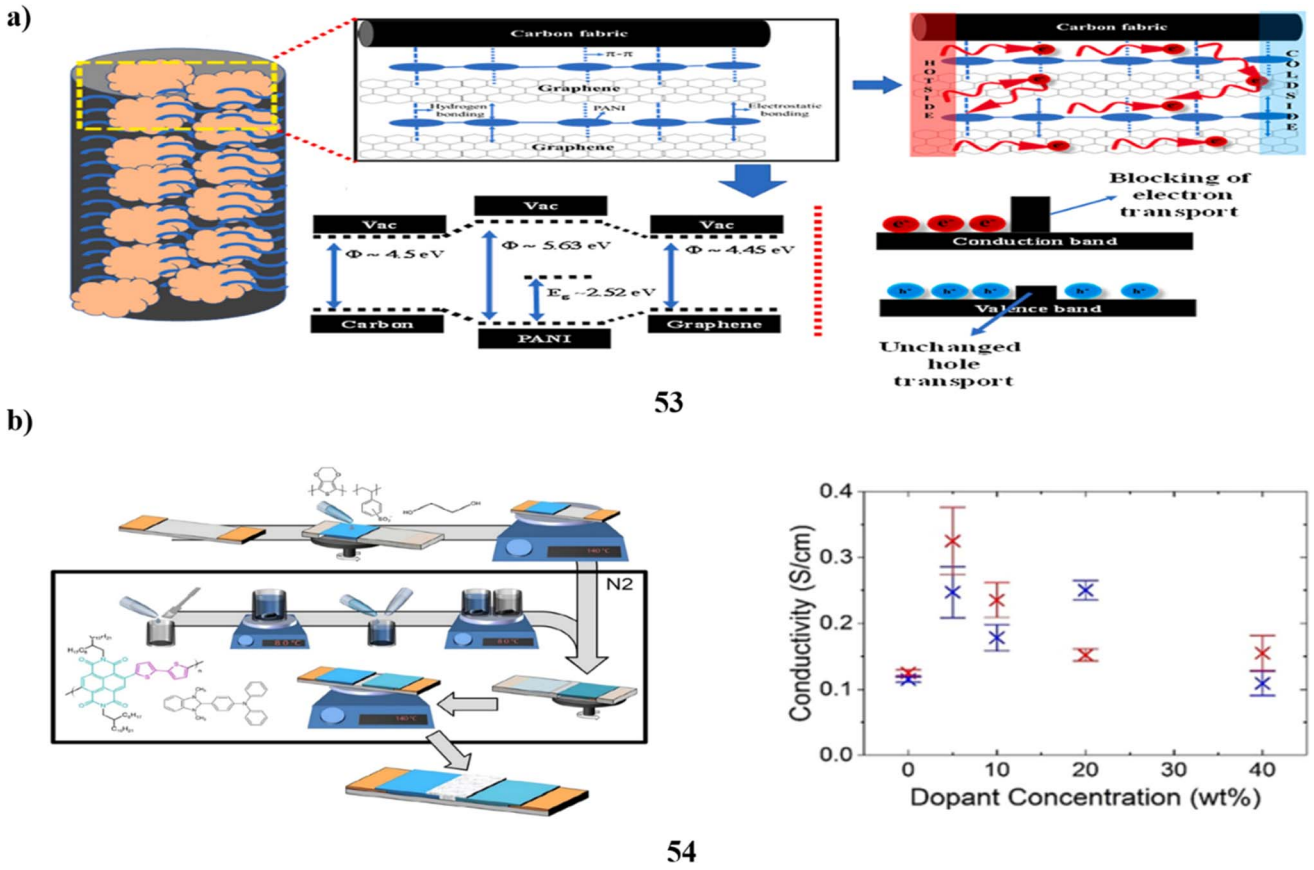

Fig. 29 (a) Polyaniline anchored graphene based TE generators (**53**). (b) P(NDI2OD-T2)-based thin-film thermoelectric generator (**54**).

films (**56**) with nickel foils. Hot pressing a partially dried PEDOT/PSS film results in a dual effect. It enhances the film's electrical conductivity while simultaneously reducing its contact resistance. Under natural cooling conditions and without the need for a heat sink these devices demonstrate an impressive power density of 72 μW cm^{-2} at 100 °C. With this capability, a 5 g device can fully charge a commercial Li-ion battery within a span of just 2 days. The organic thermoelectric device produced is a viable alternative to CR2032 coin cells for powering a range of commercial sensors, including those for acceleration, geomagnetism, temperature, humidity, atmospheric pressure, and illuminance. Impressively, these devices demonstrate exceptional stability reliably operating for over 2 months under continuous operation conditions (Fig. 30b).[75]

Lightweight thermoelectric materials that are adaptable and simple to produce are becoming more and more sought after for energy harvesting applications. Thermoplastic polyvinylidene fluoride (PVDF) and elastomer styrene–ethylene/butylene–styrene (SEBS) polymers (**57**) have been used to address this need by reinforcing them with a combination of electrically conductive carbon nanotubes (CNT) and thermoelectric ceramics like bismuth sulphide (Bi_2S_3), bismuth telluride (Bi_2Te_3), and antimony telluride (Sb_2Te_3). This approach allows for tailored thermal and electrical properties, making these materials well-suited for thermoelectric device applications. In semicrystalline PVDF composites, the inclusion of thermoelectric ceramic fillers leads to an increase in the Seebeck coefficient. Nonetheless, a tiny drop in the Seebeck value is noted for amorphous SEBS composites as the amount of thermoelectric ceramic filler increases. In the polymer composites, the thermoelectric power factor and figure-of-merit experience a remarkable increase of up to 9 orders of magnitude compared to the pristine polymer. In the PVDF/CNT/Bi_2Te_3 composite, this increase achieves a peak value of 10^{-3} μW m^{-1} K^{-2} and 10^{-6}, respectively. Utilizing two printable p–n thermocouples each based on PVDF/50Bi_2S_3 and PVDF/50Bi_2Te_3 a device is capable of generating power at the nanoWatt scale. This generated power is sufficient to charge a capacitor to 5 V. Theoretical modeling enables the evaluation of various thermoelectric configurations the impact of the number of thermocouples, and the influence of temperature gradients on the device's performance (Fig. 31a).[76] A new n-type yarn for thermoelectric textiles based on conjugated polymers is presented. These thermoelectric textile devices hold promise as intriguing power sources for wearable electronic devices. Employing yarns containing conjugated polymers is highly favored due to their potentially superior mechanical properties when compared to alternative thermoelectric materials. In this approach, a regenerated cellulose yarn is coated with an n-type conducting polymer-based ink comprising poly(-benzimidazobenzophenanthroline) (BBL) and poly(-ethyleneimine) (PEI) *via* the spray-coating method. The n-type

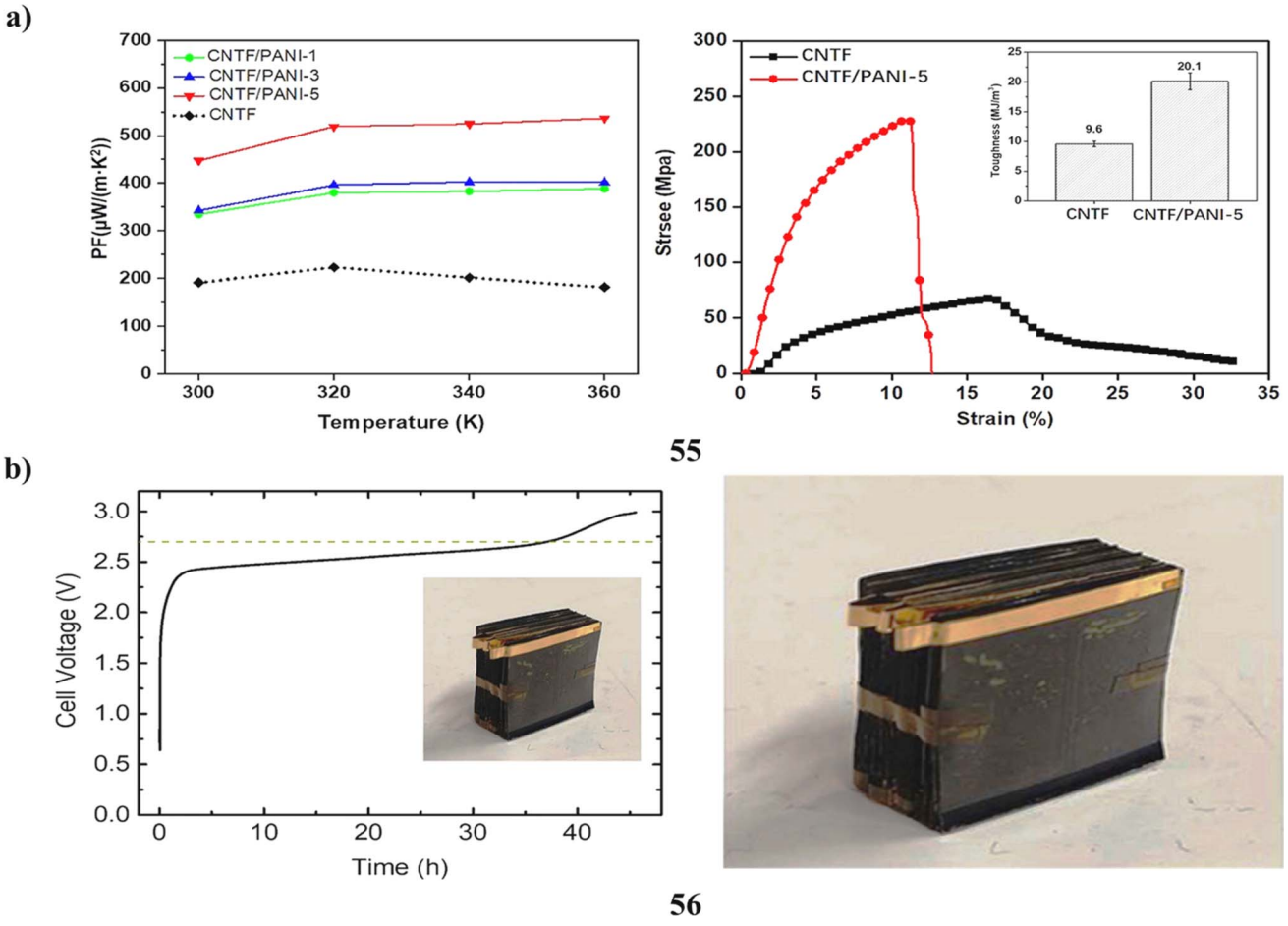

Fig. 30 (a) Polyaniline/carbon nanotube film-based thermoelectric composites (**55**). (b) Gram-scale polymer-based thermoelectric device (**56**).

yarns have an impressive Seebeck coefficient of −79 μV K^{-1} and a bulk electrical conductivity of 8 × 10^{-3} S cm^{-1}. To enhance their air stability an additional coating of thermoplastic elastomer can extend their performance duration to at least 13 days, showing promising stability. Making use of the developed n-type and p-type yarns, which are composed of PEDOT:PSS (**58**) coated regenerated cellulose a prototype in-plane thermoelectric textile is successfully fabricated. This prototype demonstrates stable device performance in ambient air for a minimum of 4 days. It achieves an open-circuit voltage per temperature difference of 1 mV per °C, indicating promising thermoelectric performance. Polymer-based n-type yarns represent a viable and essential component in the construction of thermoelectric textile devices (Fig. 31b).[77]

The popularity of wearable electronics has increased demand for environmentally friendly ways to power these gadgets, which has led to research into potential substitutes including thermoelectric generators that can turn waste heat into electricity. To address this challenge, PEDOT (**59**) polymerization is undertaken using three distinct counterions: $LiClO_4$, 1-butyl-3-methylimidazolium hexafluorophosphate (PF_6), and 1-ethyl-3-methylimidazolium bis(trifluoromethylsulfonyl)imide (BTFMSI). This method provides a comprehensive understanding of how the counterion affects the material's thermoelectric properties. The counterion that is utilized affects both the electrical conductivity and the Seebeck coefficient. Notably, the highest figure of merit (*ZT*) was achieved for PEDOT polymerized in the presence of BTFMSI attributed to the enhanced carrier mobility facilitated by this specific counterion (Fig. 32a).[78] PEDOT:PSS films (**60**) are significantly improved in thermoelectric characteristics using a multi-step production approach. Initially, these films are produced *via* spray coating followed by a sequential two-step post-treatment process involving ethylene glycol (EG) and a methylammonium iodide (MAI) solution. The first step utilizing ethylene glycol (EG) treatment notably enhances the electrical conductivity of the PEDOT:PSS film reaching up to 1752.1 S cm^{-1}, while maintaining an unchanged Seebeck coefficient within the range of 15–17 μV K^{-1}. Subsequently, the optimal utilization of 0.05 M methylammonium iodide (MAI) in a DMSO/DI water solution during the second step results in a high power factor of 122.3 μW m^{-1} K^{-2}. Additionally, this step further enhances the conductivity to 2226.8 S cm^{-1} and increases the Seebeck coefficient to 22.8 μV K^{-1}. The as-fabricated PEDOT:PSS on a plastic substrate demonstrates high thermoelectric performance evidenced by a facile proof-of-concept thermoelectric generator capable of generating a maximum power density of 12.1 nW cm^{-2}. These polymer

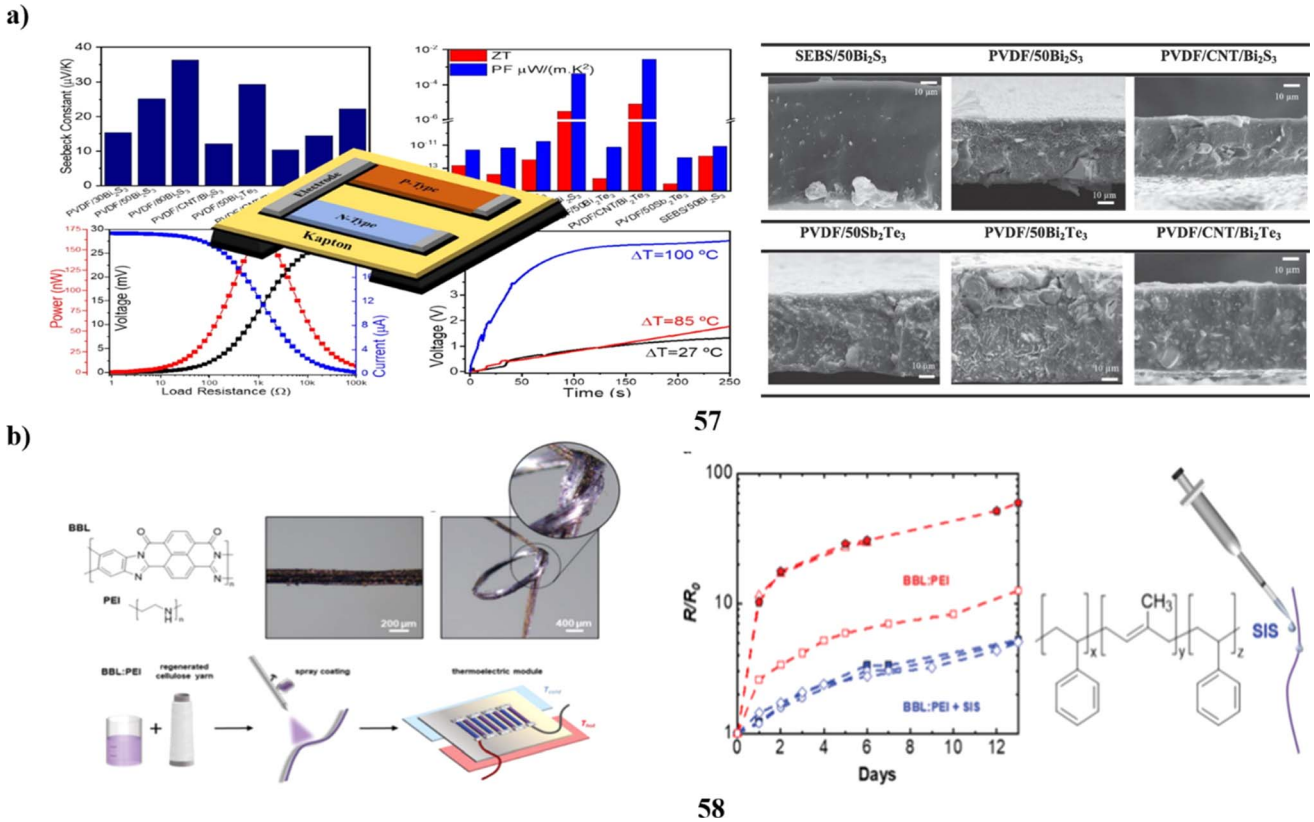

Fig. 31 (a) PVDF/CNT/Bi_2Te_3 composite based flexible thermoelectric energy (**57**). (b) Polymer-based n-type yarn for organic TE textiles (**58**).

thermoelectric materials exhibit significant potential for application in wearable thermoelectric devices (Fig. 32b).[79]

Thermoelectric polymers offer a lightweight, flexible alternative to traditional materials, with the added benefit of low thermal conductivity. Recent developments in polymer chemistry have enhanced their electrical properties, making them increasingly viable for use in flexible and wearable thermoelectric devices.

7. Silicon-based thermoelectric devices

The selection of an adequate electrode that provides smooth electrical conduction across the module is crucial to optimizing the performance of Mg_2(Si,Sn) (**61**) based thermoelectric generators. Through meticulous functionalization the TE legs are augmented to exhibit impressively low electrical contact resistances below 10 μΩ cm^2 for both p- and n-type materials. Even after annealing processes, these values remain consistent or are further reduced showcasing the efficacy of the chosen electrode in maintaining optimal electrical connectivity within the thermoelectric system. Moreover, the stability of the p-type material has been affirmed within the Mg_2(Si,Sn)-based module with no evidence of charge carrier compensation due to the electrode observed in the n-type material. This underscores the suitability of aluminum as the preferred electrode material ensuring stable performance and efficient electrical conduction throughout the system. As a result, aluminum emerges as the optimal choice bolstering the potential of Mg_2(Si,Sn)-based modules for diverse thermoelectric applications in industries ranging from automotive to aerospace. These advancements signify a significant step forward in achieving sustainable and efficient energy conversion poised to shape the future of energy utilization and conservation (Fig. 33a).[80] Additionally, Mg_2(Si,Sn) (**62**) stands out as a compelling material class owing to its exceptional thermoelectric (TE) properties evidenced by a remarkable maximum power density of 0.9 W cm^{-2} at $\Delta T =$ 375 °C. However, accurately determining the efficiency of these devices poses challenges due to uncertainties in heat flow measurements and parasitic heat losses. Thus, it becomes imperative to validate measurement reliability by comparing experimental data against theoretical calculations. This is addressed by comparing observed data with predicted values using thermoelectric generator (TEG) device simulations that use a constant property model. Remarkably, the results reveal a close alignment between experimental and theoretical outcomes underscoring the robustness and accuracy of the measurement technique. This validation process ensures confidence in the reported efficiency of Mg_2(Si,Sn)-based thermoelectric systems bolstering their potential for various energy conversion applications with enhanced reliability and performance (Fig. 33b).[81]

The SiGe nanowires offer a straightforward yet powerful solution for thermoelectric generation. They are perfect for

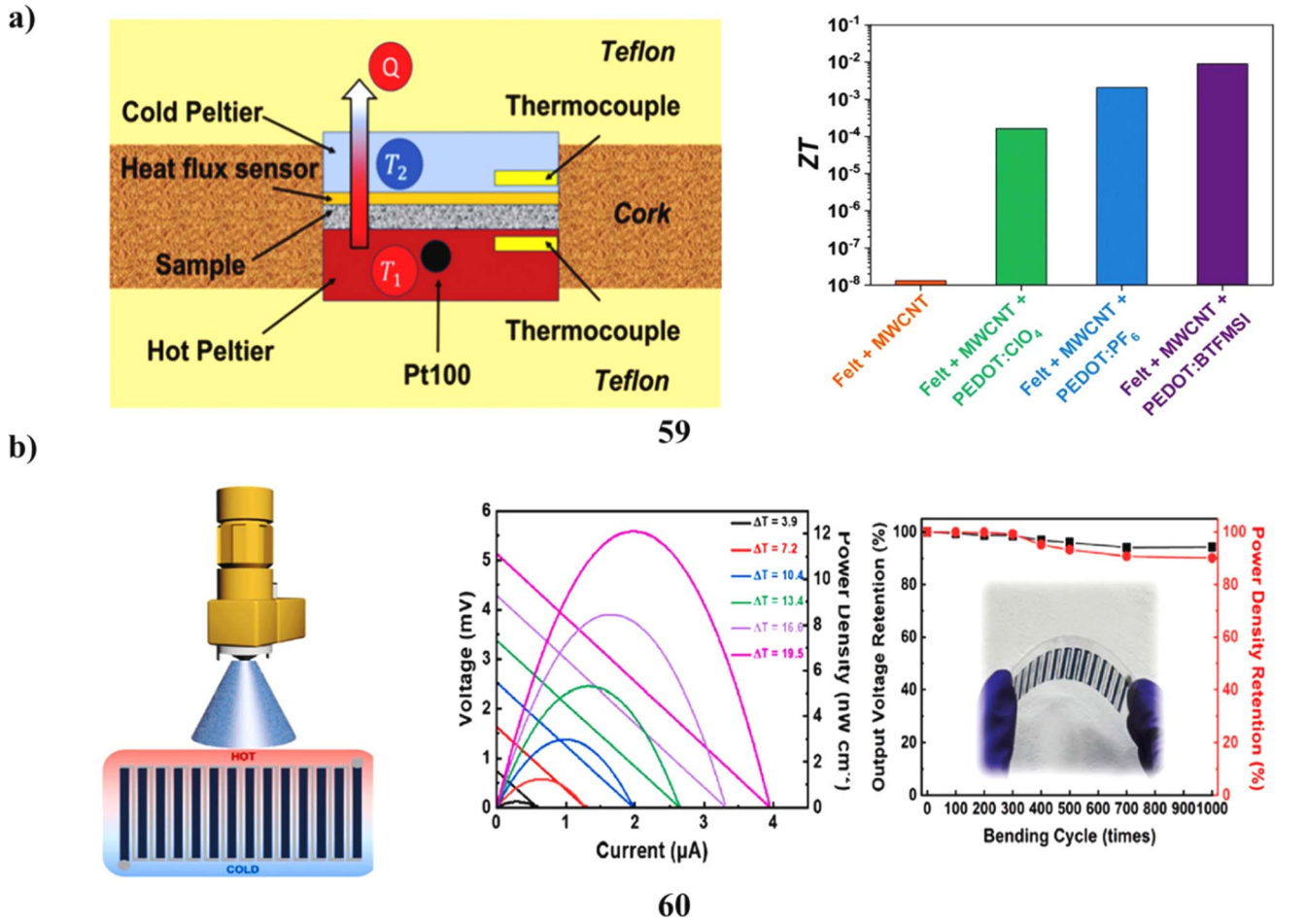

Fig. 32 (a) Electrochemical polymerization based thermoelectric generator (**59**). (b) Seebeck coefficient study of PEDOT-PSS based high thermoelectric device (**60**).

effectively turning heat into electricity because of their special qualities. Their flexibility to be adjusted allows them to be more widely applied across a range of sectors by optimizing them for varied temperature differentials. The SiGe nanowires (**63**) might revolutionize energy harvesting systems as research advances offering a low-tech yet efficient way to generate sustainable electricity. In the pursuit of enhancing thermoelectric generator efficiency, a bottom-up vapor–liquid–solid chemical vapor deposition method is utilized to incorporate heavily boron-doped SiGe nanowires onto the generators. These nanowires undergo comprehensive characterization of their thermoelectric properties across a temperature range spanning from 300 to 600 K. This thorough analysis facilitates the complete determination of the figure of merit (*ZT*), which stands as a crucial metric for thermoelectric performance evaluation. Impressively, the obtained *ZT* values reach 0.4 at 600 K for nanowires that are optimally doped. This breakthrough underscores the potential of heavily boron-doped SiGe nanowires as a key component in advancing thermoelectric generator technology, offering significant strides toward more efficient energy harvesting systems. Using advanced elemental mapping techniques researchers establish a direct link between doping levels, thermoelectric performance, and elemental distribution in heavily boron-doped SiGe nanowires. They also present p-doped SiGe nanowires function in silicon micromachined thermoelectric generators. These generators are tested both individually and in series- and parallel-connected arrays of nanowires. This straightforward approach provides valuable insights into optimizing thermoelectric performance and understanding device functionality under various configurations. Micro-thermoelectric generators based on SiGe nanowires can provide power outputs of up to 15.6 μW cm^{-2} in parallel and series topologies with a maximum open circuit voltage of 13.8 mV. These results are obtained using thermal gradients generated with hot sources at 200 °C and air flows of 1.5 m s^{-1}. This advancement paves the way for the direct application of these generators in IoT devices offering a sustainable energy solution for powering various applications in IoT ecosystems (Fig. 34a).[82] The thermoelectric properties of a Si thin-film (**64**) integrated into a planar micro thermoelectric generator (TEG) are investigated using phosphorus (n) and boron (p) doping to form thermocouples. These thermocouples, defined through selective ion implantation doping on a 100 nm thin Si film undergo thorough characterization at various temperatures.

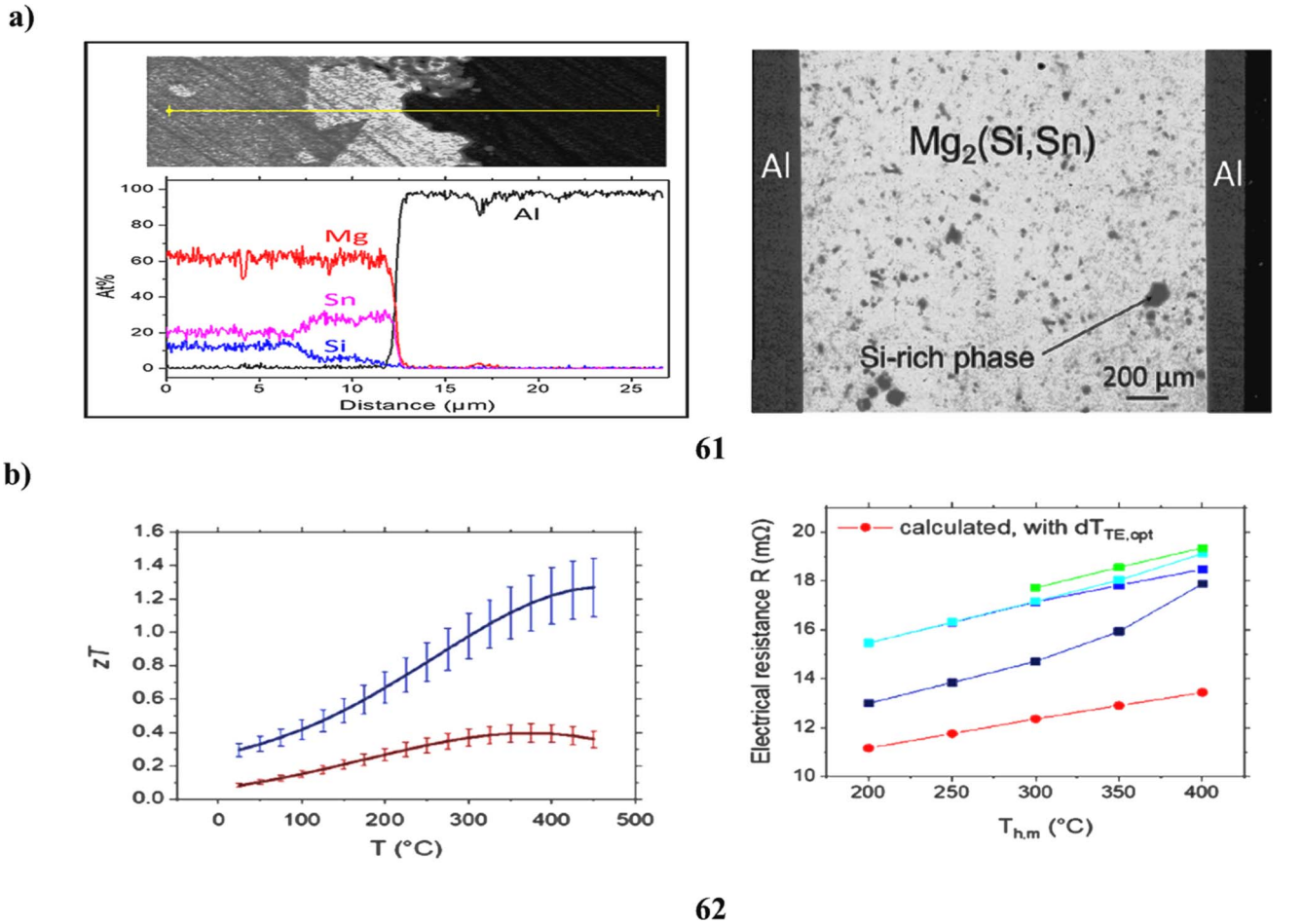

Fig. 33 (a) Seebeck coefficient study of $Mg_2(Si,Sn)$-based thermoelectric devices (**61**). (b) Thermoelectric characteristics of the thermoelectric generator based on $Mg_2(Si,Sn)$ (**62**).

The thermal conductivity, Seebeck coefficient, and electrical resistivity of each Si thermocouple are experimentally determined using built-in heater/sensor probes. The obtained values are further refined through finite element modeling (FEM). The results reveal a thermoelectric figure of merit (*ZT*) for the Si thin films of 0.0093 at room temperature representing a notable 12% improvement compared to bulk Si. Additionally, the overall thermoelectric performance of the TEG is assessed yielding a figure of merit of 0.0046 at room temperature. This research demonstrates the efficacy of utilizing selective doping and thin-film integration techniques to enhance the thermoelectric properties of Si-based micro TEGs. The achieved *ZT* values signify a significant advancement in the efficiency of Si thin-film thermoelectric materials holding promise for applications in energy harvesting and conversion technologies (Fig. 34b).[83]

The $Mg_2(Si,Sn)$-based solid solutions (**65**) offer a promising solution for mid-to-high temperature waste heat recovery due to their efficient thermoelectric conversion, non-toxicity, low density, and cost-effectiveness. However, challenges arise from the degradation of n-$Mg_2(Si,Sn)$ at temperatures ≥400 °C attributed to magnesium loss and charge carrier reduction, particularly in Sn-rich compositions. To address these challenges and develop a thermoelectric generator (TEG) stable up to 400 °C a solution is proposed. By employing $Ni_{45}Cu_{55}$ and Ni for electrical contacts the TEG achieves low electrical contact resistance (<5 μΩ cm^2) without compromising the thermoelectric properties of n-Mg_2Si. This approach ensures stable TEG operation at high temperatures while preserving the desirable thermoelectric characteristics of n-Mg_2Si. It represents a significant advancement in waste heat recovery technology offering a reliable and efficient solution for mid-to-high temperature applications (Fig. 35a).[84] Despite bulk silicon crystal's prominence, its thermoelectric performance has been constrained by its high thermal conductivity even with nanostructuring attempts. However, a breakthrough has been achieved with the development of nanostructured silicon material (**66**), boasting a remarkable *ZT* exceeding 0.3 at room temperature. This accomplishment was made possible through a scalable process involving metal-assisted chemical etching and plasma-activated sintering. This innovative approach not only enhances the thermoelectric properties of silicon but also offers a practical and scalable manufacturing method. As a result, nanostructured silicon material holds significant promise for

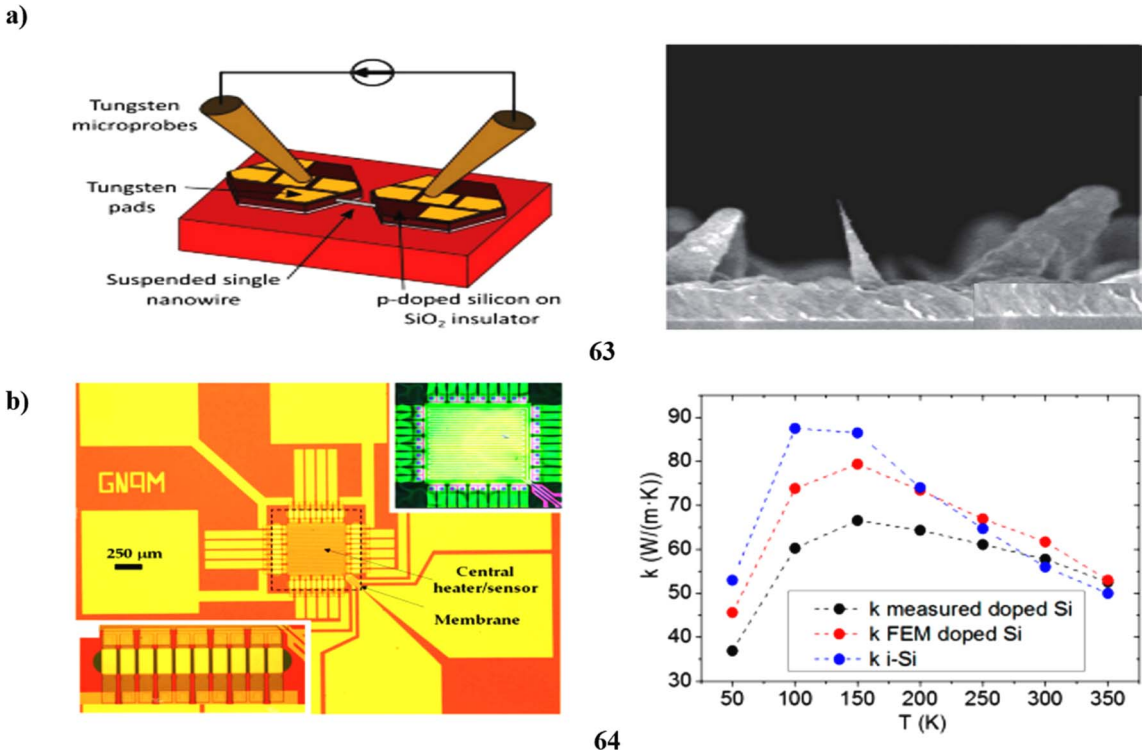

Fig. 34 (a) Microdevice structure of SiGe NWs (63). (b) Thin-film Si-based TE microgenerator (64).

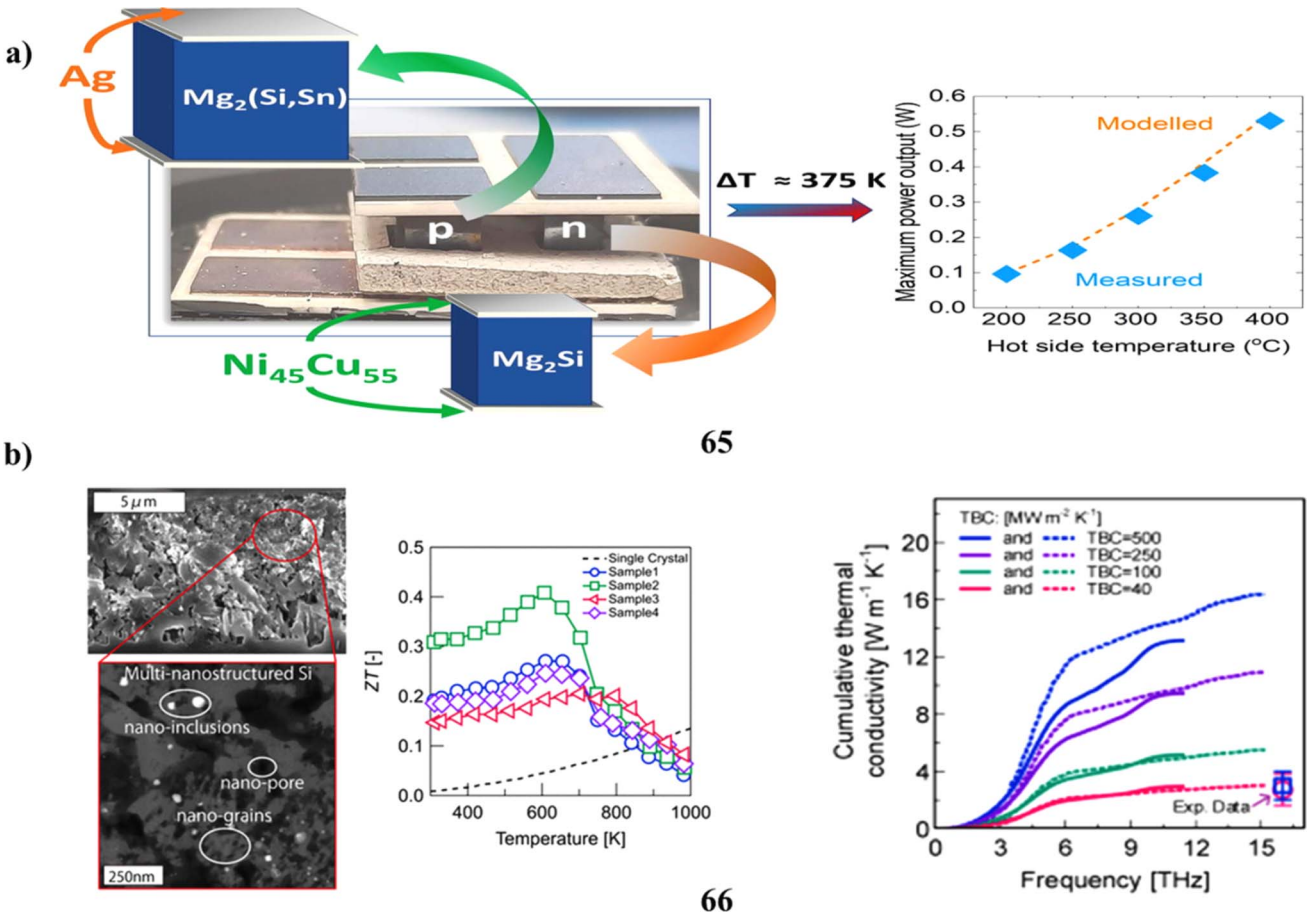

Fig. 35 (a) Thermoelectric study of $Mg_2(Si,Sn)$-based thermoelectric generators (65). (b) Multi-nanostructured silicon based thermoelectrics (66).

advancing thermoelectric technology opening doors to efficient energy conversion and waste heat recovery applications. Heat conductivity is greatly reduced without significantly losing electrical conductivity due to the very complex material structure consisting of hierarchically sized metal nano-precipitates, randomly dispersed nanograins, and nanopores. Further research, both theoretical and experimental reveals that the softening of grain boundaries, which severely reduces interfacial phonon transmission is the primary source of the decrease. By reducing the prices of materials and processes, the created high-performance silicon nanocomposite is anticipated to significantly improve the application of thermoelectrics (Fig. 35b).[85]

Microelectronic thermoelectric generators (TEGs) utilizing nanostructured silicon thermopiles (**67**) have been developed on an industrial silicon complementary metal-oxide-semiconductor (CMOS) process line. These TEGs demonstrate a high specific power generation capacity near room temperature comparable to typical $(Bi,Sb)_2(Se,Te)_3$-based TEGs. The extraordinary power capacity is ascribed to CMOS processing's ability to precisely manage electrical and thermal impedances and create thermocouples with a high surface density and low packing fraction. Remarkably, TEG power was shown to rise dramatically with decreasing thermocouple width providing a route for further improvements. While silicon-integrated circuit TEGs may be inexpensively added to large-scale silicon CMOS microelectronic circuits, they are not as easily integrated as $(Bi,Sb)_2(Se,Te)_3$ TEGs. This innovation represents a significant advancement in microelectronic TEG technology offering a promising avenue for efficient and cost-effective energy harvesting in various applications (Fig. 36a).[86] Strong fracture resistance in flexible thermoelectric materials has intriguing prospects for wearable thermoelectric device applications. In this regard, an environmentally friendly two-dimensional (2D) magnesium-silicon monolayer (**68**) was designed using the CALYPSO package and first-principles calculations. Notably, this stable 2D Mg Si monolayer exhibits a semiconductor behavior with an in-plane negative Poisson's ratio of −0.364. More impressively, the thermoelectric figure of merit (ZT) values for the p-type doped Mg Si monolayer in the x direction achieve 2.51 at room temperature and 3.92 at 500 K surpassing the conventional thermoelectric material threshold of 2.0. This exceptional thermoelectric performance is attributed to resonant bonds between magnesium and silicon atoms strong coupling between acoustic and optical phonon modes, leading to pronounced phonon anharmonicity, and effective reduction

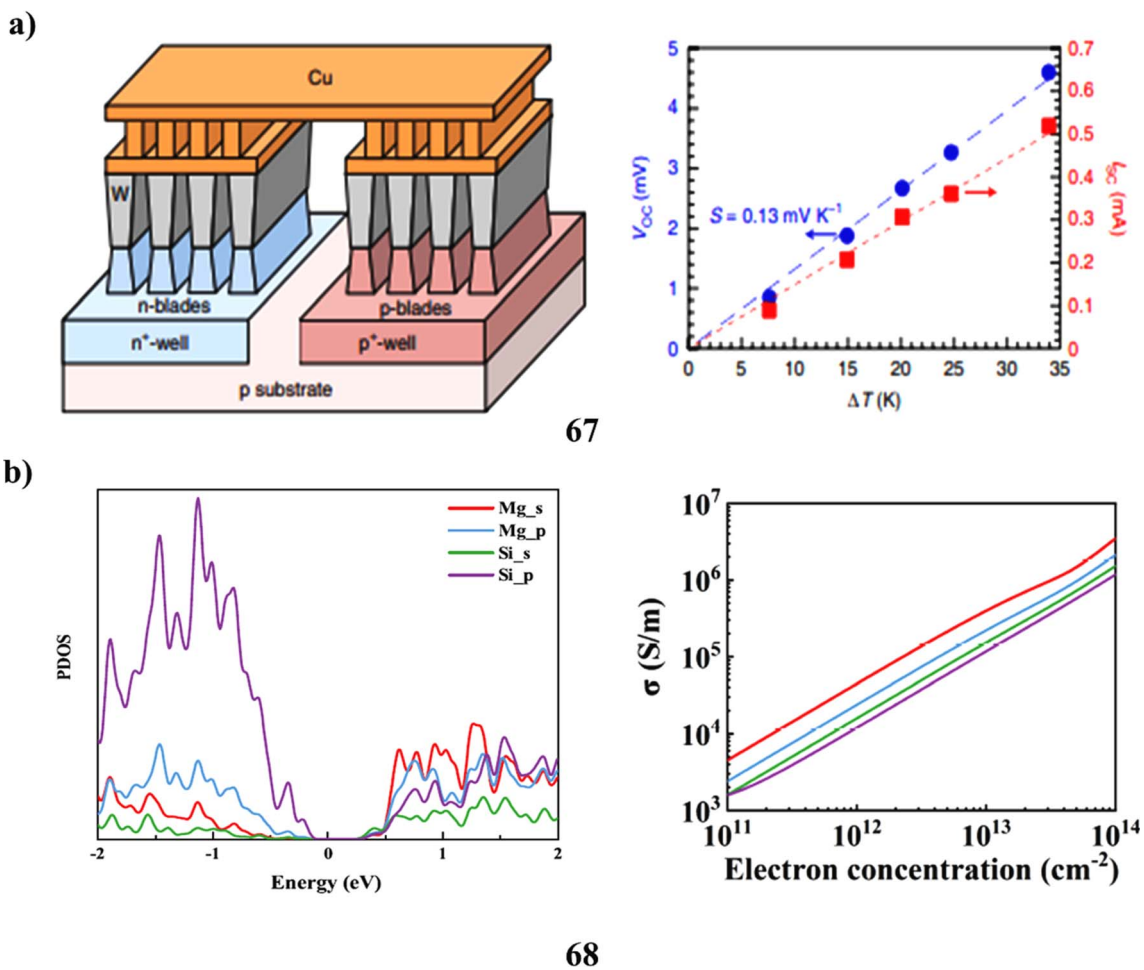

Fig. 36 (a) Silicon CMOS-based thermoelectric generators (**67**). (b) Mg–Si monolayer-based thermoelectric device (**68**).

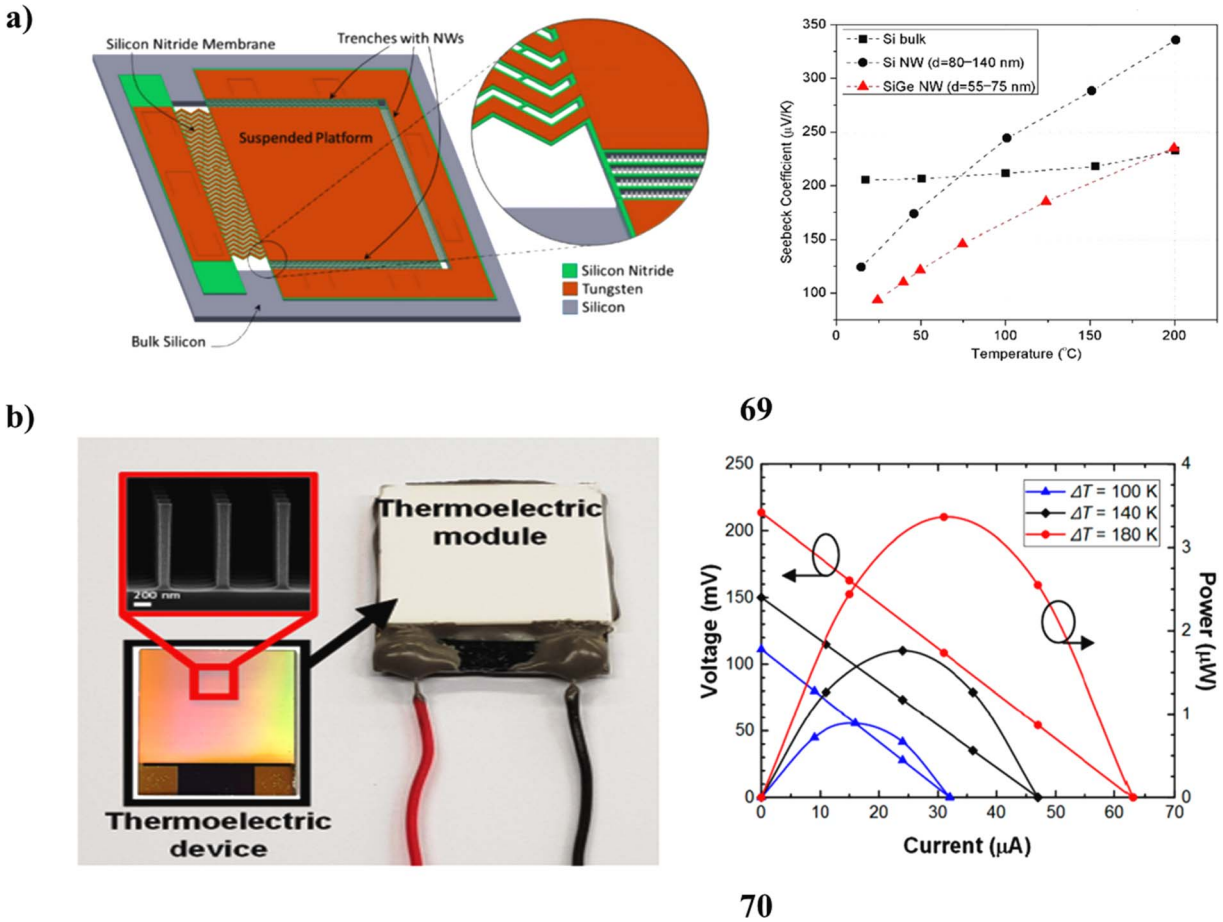

Fig. 37 (a) SiGe nanowires-based thermoelectric microgenerators (**69**). (b) Thermoelectric properties of Si-NWs (**70**).

of lattice thermal conductivity through four-phonon scattering processes. Moreover, considering that a portion of phonon mean free paths falls below the Ioffe-Regel limit a two-channel model is employed to calculate lattice thermal conductivity. These findings offer valuable insights into the diverse structural, thermoelectric, and mechanical properties of the Mg Si monolayer thereby paving the way for the development of wearable thermoelectric devices with enhanced performance and durability (Fig. 36b).[87]

Functional device-level comparisons have been made between the thermoelectric performance of nanostructured low-dimensional silicon and silicon-germanium (**69**). Arrays of nanowires of both materials grown using a VLS-CVD method were monolithically integrated into a silicon micromachined structure to leverage the enhanced thermoelectric properties of nanostructured silicon-based materials. A vertical temperature gradient may be translated into a lateral temperature differential across the nanowires more easily because of the device design. A thin film metal leg in a uni-leg form completes each thermocouple. The device operates independently and can be efficiently replicated using standard IC and MEMS technologies. Despite SiGe nanowire devices exhibiting a lower Seebeck coefficient and higher electrical resistance compared to silicon nanowires, they demonstrate superior performance with larger open circuit voltages and overall power supply. This is attributed to the lower thermal conductance of the nanostructured SiGe ensemble, enabling a significantly larger internal temperature difference for the same external thermal gradient. As a result, these devices can achieve power densities in the μW cm^{-2} range when placed on hot surfaces within the 50–200 °C range under natural convection even without the presence of a heat exchange mechanism (Fig. 37a).[88] Thermoelectric modules utilizing silicon nanowires (Si-NWs) have garnered significant interest for their improved thermoelectric efficiency attributed to reduced thermal conductivity. A top-down fabrication approach has been developed to substantially decrease the thermal conductivity of vertical Si-NWs. This reduction is achieved through increased surface roughness, decreased diameter, and elevated doping concentration, leading to enhanced phonon scattering dependent on phonon wavelength. Boron- and phosphorus-doped rough Si-NWs (**70**) with a diameter of 200 nm and surface roughness of 6.88 nm exhibit remarkably low thermal conductivity of 10.1 and 14.8 W m^{-1} K^{-1}, respectively. These values are 5.1- and 3.6-fold lower than those of smooth intrinsic nanowires and 14.8- and 10.1-fold lower than bulk silicon. Utilizing this doped rough Si-NW array a thermoelectric module has been fabricated demonstrating exceptional performance with an open circuit voltage of 216.8 mV cm^{-2} and a maximum power output of 3.74 μW cm^{-2} under a temperature difference of 180 K representing the

Table 1 This table provides a structured overview of different materials are synthesized, their controlled properties, key observations, underlying principles, and typical applications in the field of thermoelectric materials

Materials	Synthesis parameters	Controlled properties	Key observations	Principles	Device design	Performance	Applications
Gels	Sol–gel method	Temperature, pH, aging time	Nanostructured morphology, film thickness	Nanoscale chemistry, thin film deposition	Scaffold structures for tissue engineering	Controlled release rates, mechanical integrity	Thermoelectric devices, sensors
Ceramics	Solid–state reaction	Temperature, atmosphere, doping elements	Grain boundaries, crystalline structure	Crystal growth, phase control	Thin films for electronics, porous structures for implants	High dielectric strength, biocompatibility	High-temperature applications
Metals	Arc melting, alloying	Temperature, atmosphere, doping elements	Band structure, electron mobility	Metallurgy, solid-state physics	Conductive wires, structural frameworks	High conductivity, tensile strength	Energy harvesting, cooling
Nanoparticles	Chemical reduction, solvothermal	Temperature, surfactants, precursors	Size effects, surface chemistry, stability	Quantum mechanics, surface science	Nanoscale drug carriers, sensor elements	Enhanced reactivity, target specificity	Catalysis, nanocomposites
Silicon	Czochralski method, ion implantation	Crystal growth rate, doping concentration	Defect engineering, carrier mobility	Semiconductor physics, crystallography	Microchips, photovoltaic cells	High efficiency, low power consumption	Electronics, energy conversion
Polymers	Solution casting, electrospinning	Solvent choice, processing temperature	Mechanical flexibility, molecular alignment	Polymer chemistry, material science	Flexible films, adhesive layers	Durability, flexibility, biocompatibility	Flexible electronics, wearables

highest reported values for Si-NW thermoelectric modules (Fig. 37b).[89]

Silicon, a widely used semiconductor, is being explored for its potential in thermoelectric devices due to its abundance and compatibility with existing technology. Advances in nanostructuring and doping have significantly improved its thermoelectric properties, making it a promising material for future applications.

Future research on thermoelectric materials should focus on enhancing material properties and developing scalable production methods. For ceramics, the emphasis should be on improving mechanical and thermal stability and integrating them into hybrid systems for automotive, aerospace, and industrial applications. Thermally conductive gel-like materials require advancements in flexibility, durability, biocompatibility, and scalable fabrication for wearable electronics and medical devices. Metal-based thermoelectric materials should optimize alloy compositions and nanostructuring techniques, with a focus on integration into existing infrastructures. For nanoparticles, research should optimize synthesis and assembly for uniform and stable materials, with applications in flexible and wearable devices. Polymers need improved doping strategies and nanocomposites, focusing on sustainable and flexible applications. Silicon-based materials should enhance performance through nanostructuring and alloying, with integration into electronic devices and renewable energy systems. These directions aim to advance next-generation thermoelectric technologies for sustainable energy solutions and efficient thermal management.

A summary of materials, synthesis parameters, controlled properties, key observations, principles and applications is found in Table 1 below.

8. Conclusion

The recent trends in thermoelectric devices and applications represent a significant advancement in the field of energy harvesting, waste heat recovery, and thermal management. The exploration of advanced thermoelectric materials, including nanostructured, organic, and hybrid materials, has demonstrated promising potential for enhancing the performance and scalability of thermoelectric devices. Furthermore, the utilization of advanced manufacturing techniques has opened new avenues for the practical implementation of thermoelectric technology in various industries. The emerging applications of thermoelectric devices in automotive, aerospace, wearable electronics, and industrial waste heat recovery underscore their versatility and relevance in addressing contemporary energy and thermal challenges. The potential for thermoelectric devices to contribute to sustainable energy solutions and efficient thermal management systems is increasingly recognized, paving the way for their integration into diverse technological landscapes. Looking ahead, the future prospects of thermoelectric devices and applications are multifaceted and hold great promise for continued innovation and impact. One of the key future prospects lies in the further advancement of thermoelectric materials, with ongoing research focusing on enhancing their efficiency, durability, and cost-effectiveness. The development of novel materials and the optimization of existing ones through advanced synthesis and characterization techniques are expected to drive significant progress in the field. Moreover, the integration of thermoelectric devices into next-generation automotive technologies presents a compelling opportunity for improving fuel efficiency and reducing emissions. As the automotive industry continues to prioritize sustainability and energy efficiency, thermoelectric devices have the potential to play a pivotal role in advancing these

objectives. Similarly, in the aerospace sector, the utilization of thermoelectric technology for waste heat recovery and thermal regulation in aircraft and spacecraft holds promise for enhancing operational efficiency and reducing environmental impact.

In the realm of wearable electronics, the miniaturization and integration of thermoelectric generators into wearable devices offer the potential for self-powered, autonomous systems. This could revolutionize the way we power and interact with wearable technology, enabling greater convenience and sustainability. Additionally, the application of thermoelectric devices in industrial waste heat recovery presents a compelling opportunity for improving energy efficiency and reducing the environmental footprint of industrial processes. The continued exploration of thermoelectric devices for power generation from waste heat sources, such as exhaust gases and industrial processes, holds significant promise for contributing to global efforts to mitigate climate change and reduce reliance on traditional energy sources. By harnessing waste heat that would otherwise be dissipated into the environment, thermoelectric devices have the potential to make a meaningful impact on energy sustainability and resource conservation. Furthermore, the integration of thermoelectric devices into building and HVAC (heating, ventilation, and air conditioning) systems offers the potential for more efficient and sustainable thermal management. By leveraging thermoelectric technology for localized heating and cooling, buildings can reduce their overall energy consumption and environmental impact. This application aligns with the growing emphasis on sustainable building practices and energy-efficient infrastructure. As the field of thermoelectric devices and applications continues to evolve, interdisciplinary collaboration and innovation will be essential for unlocking their full potential. The convergence of materials science, engineering, and energy technology will drive the development of next-generation thermoelectric materials and devices with enhanced performance characteristics. Additionally, the integration of advanced computational modeling and simulation techniques will facilitate the design and optimization of thermoelectric systems for specific applications, further expanding their utility and impact.

In conclusion, the recent trends in thermoelectric devices and applications represent a significant step forward in the pursuit of sustainable energy solutions and efficient thermal management. The advancements in thermoelectric materials, manufacturing techniques, and diverse applications across industries underscore the growing relevance and potential impact of thermoelectric technology. Looking to the future, the continued innovation and integration of thermoelectric devices hold great promise for addressing global energy and environmental challenges, paving the way for a more sustainable and efficient technological landscape.

Data availability

Data will be made available on your request.

Conflicts of interest

There are no conflicts to declare.

Acknowledgements

M. R. acknowledges financial support from the UGC-DAE CSR, Indore, India. M. R. thanks Prof. T. Sasiprabha, Vice-Chancellor, Sathyabama Institute of Science and Technology (deemed to be University), for her encouragement.

References

1 S. Yang, P. Qiu, L. Chen and X. Shi, Recent Developments in Flexible Thermoelectric Devices, *Small Sci.*, 2021, **1**, 2100005.
2 R. Knura, M. Maksymuk, T. Parashchuk and K. T. Wojciechowski, Achieving high thermoelectric conversion efficiency in Bi Te -based stepwise legs through band-gap tuning and chemical potential engineering, *Dalton Trans.*, 2024, **53**, 123–135.
3 S. Mardi, D. Zhao, N. Kim, I. Petsagkourakis, K. Tybrandt, A. Reale and X. Crispin, The Interfacial Effect on the Open Circuit Voltage of Ionic Thermoelectric Devices with Conducting Polymer Electrodes, *Adv. Electron. Mater.*, 2021, **7**, 2100506.
4 C. Zhang, Q. Lai, W. Wang, X. Zhou, K. Lan, L. Hu, B. Cai, M. Wuttig, J. He, F. Liu and Y. Yu, Gibbs Adsorption and Zener Pinning Enable Mechanically Robust High-Performance Bi2Te3-Based Thermoelectric Devices, *Adv. Sci.*, 2023, **10**, 2302688.
5 Y. Hou, Z. Li, Z. Wang, X. Zhang, Y. Li, C. Li, H. Guo and H. Yu, Programmable and Surface-Conformable Origami Design for Thermoelectric Devices, *Adv. Sci.*, 2024, 2309052.
6 A. Ojha, R. K. Sabat and S. Bathula, Advancement in half-Heusler thermoelectric materials and strategies to enhance the thermoelectric performance, *Mater. Sci. Semicond. Process.*, 2024, **171**, 107996.
7 J. S. Yun, S. Choi and S. H. Im, Advances in carbon-based thermoelectric materials for high-performance, flexible thermoelectric devices, *Carbon Energy*, 2021, 1–42.
8 T. Cao, X. L. Shi and Z. G. Chen, Advances in the design and assembly of flexible thermoelectric device, *Prog. Mater. Sci.*, 2023, **131**, 101003.
9 X. L. Shi, T. Cao, W. Chen, B. Hu, S. Sun, W. D. Liu, M. Li, W. Lyu, M. Hong and Z. G. Chen, Advances in flexible inorganic thermoelectrics, *EcoEnergy*, 2023, **1**, 296–343.
10 T. Deng, P. Qiu, T. Yin, Z. Li, J. Yang, T. Wei and X. Shi, High-Throughput Strategies in the Discovery of Thermoelectric Materials, *Adv. Mater.*, 2024, **36**, 2311278.
11 S. Asadikouhanjani, A. Zolfagharian and M. Bodaghi, Design and Fabrication of Microarchitected Thermoelectric Generators: Prospects and Challenges, *Adv. Eng. Mater.*, 2024, **26**, 2301609.
12 J. Gobpant, B. Klongratog, C. Rudradawong, R. Sakdanuphab, P. Junlabhut, P. Nuthongkum, P. Limsuwan and A. Sakulkalavek, High-performance flexible thermoelectric generator based on silicone rubber and cover with graphite sheet, *Appl. Therm. Eng.*, 2024, **236**, 121656.
13 J. Xiao, Z. Zhang, S. Wang, C. Gao and L. Wang, High-Performance thermoelectric generator based on n-Type

flexible composite and its application in Self-Powered temperature sensor, *J. Chem. Eng.*, 2024, **479**, 147569.
14 Y. T. Lin, I. Permana, F. Wang and R. J. Chang, Improvement of heating and cooling performance for thermoelectric devices in medical storage application, *Case. Stud. Therm. Eng.*, 2024, **54**, 104017.
15 A. A. Nikitina, F. V. Lavrentev, V. Yu. Yurova, D. Y. Piarnits, O. O. Volkova, E. V. Skorb and D. G. Shchukin, Layered nanomaterials for renewable energy generation and storage, *Mater. Adv.*, 2024, **5**, 394–408.
16 X. Sun, S. Hou, Z. Wu, J. Wang, Y. Qiao, Z. Tang, X. Liu, J. Mao, Q. Zhang and F. Cao, Self-doping enhancing thermoelectric properties of GeTe thin films, *Appl. Phys. Lett.*, 2024, **124**, 011601.
17 S. Yang, P. Qiu, L. Chen and X. Sh, Recent Developments in Flexible Thermoelectric Devices, *Small Sci.*, 2021, **1**, 2100005.
18 H. Wei, J. Zhang, Y. Han and D. Xu, Soft-covered wearable thermoelectric device for body heat harvesting and on-skin cooling, *Appl. Energy*, 2022, **326**, 119941.
19 D. Zhang, J. Ramiah, M. Cagirici, K. Saglik, S. F. D. Solco, J. Cao, J. Xu and A. Suwardi, Thermoelectric nanowires for dense 3D printed architectures, *Mater. Horiz.*, 2024, **11**, 847–854.
20 Y. Hou, Y. Yang, Z. Wang, Z. Li, X. Zhang, B. Bethers, R. Xiong, H. Guo and H. Yu, Whole Fabric-Assisted Thermoelectric Devices for Wearable Electronics, *Adv. Sci.*, 2022, **9**, 2103574.
21 M. Wolf, M. Abt, G. Hoffmann, L. Overmeyer and A. Feldhoff, Ceramic-based thermoelectric generator processed via spray-coating and laser structuring, *Open Ceram.*, 2020, **1**, 100002.
22 Z. Shia, J. Xua, J. Zhub, Y. Zhanga, T. Gaob, M. Qina, H. Suna, G. Donga and F. Gaoa, Effect of platelet template seeds on microstructure and thermoelectric properties of $Ca_3Co_4O_9$ ceramics, *Ceram. Int.*, 2019, **45**, 1977–1983.
23 Z. Shi, F. Gao, J. Zhu and J. Xu, Influence of liquid-phase sintering on microstructure and thermoelectric properties of $Ca_3Co_4O_9$-based ceramics with Bi_2O_3 additive, *J. Materiomics*, 2019, **5**, 711–720.
24 N. Jaziri, J. Mülle, B. Müller, A. Boughamoura, N. Gutzeit, B. Mezghani, A. B. Kouki and F. Tounsi, Low Temperature Co-fired Ceramic-Based Thermoelectric Generator with Cylindrical Grooves for Harvesting Waste Heat from Power Circuits, *Appl. Therm. Eng.*, 2021, **184**, 116367.
25 D. H. A. Besisaa, E. M. M. Ewaisb, E. A. M. Shalabyc, A. Usenkod and D. V. Kuznetsov, Thermoelectric properties and thermal stress simulation of pressureless sintered SiC/AlN ceramic composites at high temperatures, *Sol. Energy Mater. Sol. Cells*, 2018, **182**, 302–313.
26 S. Bresch, B. Mieller, P. Mrkwitschka, R. Moos and T. Rabe, Glass-ceramic composites as insulation material for thermoelectric oxide multilayer generators, *J. Am. Ceram. Soc.*, 2022, **105**, 2140–2149.
27 X. Li, J. Wu, S. Huang, Y. Gao, D. Liu, J. Liu and H. T. Lin, Enhancing thermoelectric properties of $Ca_3Co_4O_9$ ceramics through oscillatory pressure sintering, *J. Mater. Res. Technol.*, 2024, **28**, 3475–3484.
28 N. M. Ferreira, D. Lopes, A. V. Kovalevsky, F. M. Costa, A. Sotelo, M. A. Madre and A. Rezania, Thermoelectric Modules Built Using Ceramic Legs Grown by Laser Floating Zone, *Ceram. Int.*, 2020, **46**(15), 24318–24325.
29 M. Abt, M. Wolf, A. Feldhoff and L. Overmeyer, Combined spray-coating and laser structuring of thermoelectric ceramics, *J. Mater. Process. Technol.*, 2020, **275**, 116319.
30 M. Shen, K. Liu, G. Zhang, Q. Li, G. Zhang, Q. Zhang, H. Zhang, S. Jiang, Y. Chen and K. Yao, Thermoelectric coupling effect in BNT-BZT-xGaN pyroelectric ceramics for low-grade temperature-driven energy harvesting, *Nat. Commun.*, 2023, **14**, 7907.
31 S. Mardi, D. Zhao, N. Kim, I. Petsagkourakis, K. Tybrandt, A. Reale and X. Crispin, The Interfacial Effect on the Open Circuit Voltage of Ionic Thermoelectric Devices with Conducting Polymer Electrodes, *Adv. Electron. Mater.*, 2021, 2100506.
32 C. Bai, Z. Wang, S. Yang, X. Cui, X. Li, Y. Yin, M. Zhang, T. Wang, S. Sang, W. Zhang and H. Zhang, Wearable Electronics Based on the Gel Thermogalvanic Electrolyte for Self-Powered Human Health Monitoring, *ACS Appl. Mater. Interfaces*, 2021, **13**, 37316–37322.
33 X. Yang, Y. Tian, B. Wu, W. Jia, C. Hou, Q. Zhang, Y. Li and H. Wang, High-Performance Ionic Thermoelectric Supercapacitor for Integrated Energy Conversion-Storage, *Energy Environ. Mater.*, 2022, **5**, 954–961.
34 A. L. Pires, R. S. Costa, C. Pereira and A. Pereira, An Interdigital Planar Energy Harvesting/Storage Device Based On an Ionic Solid-Gel Polymer, *ACS Appl. Electron. Mater.*, 2021, **3**, 696–703.
35 W. Lee, S. Lee, H. Kim and Y. Kim, Organic thermoelectric devices with PEDOT:PSS/ZnO hybrid composites, *Chem. Eng. J.*, 2021, **415**, 128935.
36 M. Li, H. Xu, M. Luo, X. Qing, W. Wang, W. Zhong, Q. Liu, Y. Wang, L. Yang, X. Zhu and D. Wang, Wearable ionogel fiber-based ionic thermoelectric device for low-grade human body heat harvesting, *J. Chem. Eng.*, 2024, 149784.
37 J. Liu, X. Chen, H. Yang, J. Tang, R. Miao, K. Liua and Y. Fang, Gel-emulsion templated polymeric aerogels for solar-driven interfacial evaporation and electricity generation, *Mater. Chem. Front.*, 2021, **5**, 1953–1961.
38 C. G. Han, Y. B. Zhu, L. Yang, J. Chen, S. Liu, H. Wang, Y. Ma, D. Han and L. Niu, Remarkable high-temperature ionic thermoelectric performance induced by graphene in gel thermocells, *Energy Environ. Sci.*, 2024, **17**, 1559–1569.
39 C. Y. Oztan, B. Hamawandi, Y. Zhou, S. Ballikaya, M. S. Toprak, R. Leblanc, V. Coverstone and E. Celik, Thermoelectric Performance of Cu_2Se Doped with Rapidly Synthesized Gel-Like Carbon Dots, *J. Alloys Compd.*, 2021, **8**(64), 157916.
40 D. Cadavid, S. Ortega, S. Illera, Y. Liu, M. Ibanez, A. Shavel, Y. Zhang, M. Li, A. M. Lopez, G. Noriega, O. J. Dura, M. A. Lopez de la Torre, J. D. Prades and A. Cabot, Influence of the Ligand Stripping on the Transport Properties of Nanoparticle-Based PbSe Nanomaterials, *ACS Appl. Energy Mater.*, 2020, **3**, 2120–2129.

41 Y. Liu, L. Yin, W. Zhang, J. Wang, S. Hou, Z. Wu, Z. Zhang, C. Chen, X. Li, H. Ji, Q. Zhang, Z. Liu and F. Cao, A wearable real-time power supply with a Mg_3Bi_2-based thermoelectric module, *Cell Rep.*, 2021, **23**, 100445.

42 N. Kanas, M. Bittner, T. D. Desissa, S. P. Singh, T. Norby, A. Feldhoff, T. Grande, K. Wiik and M. A. Einarsrud, All-Oxide Thermoelectric Module with in Situ Formed NonRectifying Complex p−p−n Junction and Transverse Thermoelectric Effect, *ACS Omega*, 2018, **3**, 9899–9906.

43 D. Li, X. L. Shi, J. Zhu, M. Li, J. Wang, W. D. Liu, Q. Zhao, H. Zhong, S. Li and Z. G. Chen, Ce-filled $Ni_{1.5}Co_{2.5}Sb_{12}$ Skutterudite Thin Films with Record-High Figure of Merit And Device Performance, *Adv. Energy Mater.*, 2023, **13**, 2301525.

44 M. Hong, K. Zheng, W. Lyv, M. Li, X. Qu, Q. Sun, S. Xu, J. Zou and Z. G. Chen, Computer-aided design of high-efficiency GeTe-based thermoelectric devices, *Energy Environ. Sci.*, 2020, **13**, 1856–1864.

45 H. Bark, M. W. M. Tan, G. Thangavel and P. S. Lee, Deformable High Loading Liquid Metal Nanoparticles Composites for Thermal Energy Management, *Adv. Energy Mater.*, 2021, 2101387.

46 J. Zhang, P. Wei, H. Zhang, L. Li, W. Zhu, X. Nie, W. Zhao and Q. Zhang, Enhanced Contact Performance and Thermal Tolerance of Ni/Bi Te Joints for Bi Te -Based Thermoelectric Devices, *ACS Appl. Mater. Interfaces*, 2023, **15**, 22705–22713.

47 S. Berri, Half-metallic and thermoelectric properties of Sr_2EuReO_6, *Comput. Condens. Matter*, 2021, **28**, 00586.

48 E. M. F. Vieira, A. L. Pires, J. P. B. Silva, V. H. Magalhaes, J. Grilo, F. P. Brito, M. F. Silva, A. M. Pereira and L. M. Goncalves, High Performance μ -Thermoelectric Device based on Bi_2Te_3/Sb_2Te_3 p–n Junctions, *ACS Appl. Mater. Interfaces*, 2019, **42**, 38946–38954.

49 C. S. Prasanna, S. Harish, J. Archana, E. S. Kumar, H. Ikeda and M. Navaneethan, Interfacial energy barrier tuning in MnO_2/MoS_2/Carbon fabric integrated with low resistance text rode for highly efficient wearable thermoelectric generator, *Carbon*, 2024, **218**, 118609.

50 Y. H. Kang, S. J. Ko, M. H. Lee, Y. K. Lee, B. J. Kim and S. Y. Cho, Highly efficient and air stable thermoelectric devices of poly (3-hexylthiophene) by dual doping of Au metal precursors, *Nano Energy*, 2021, **82**, 105681.

51 D. Lee, H. Park, G. Park, J. Kim, H. Kim, H. Cho, S. Han and W. Kim, Liquid-metal-electrode-based compact, flexible, and high-power thermoelectric device, *Energy*, 2019, **188**, 116019.

52 M. Liu, W. Li and Y. Pei, Screening metal diffusion barriers for thermoelectric $Bi_{0.5}Sb_{1.5}Te_3$, *Sci. China Mater.*, 2024, **67**, 289–294.

53 B. Chen, J. Feng, Q. Chen, S. Xiao, J. Yang, X. Zhang, Z. Li and T. Wang, Specific behavior of transition metal chloride complexes for achieving giant ionic thermoelectric properties, *npj Flexible Electron.*, 2022, **6**, 79.

54 H. Zhang, Y. Wang, Z. A. Munir, Y. Zhang, W. Fan and S. Chen, Improvement of the conversion efficiency of Mg_3Sb_2 thermoelectric devices through optimizing the resistivity of the MgSbNi barrier layer, *J. Mater. Sci. Technol.*, 2024, **168**, 208–214.

55 X. Zhang, W. Gao, X. Su, F. Wang, B. Liu, J. J. Wang, H. Liu and Y. Sang, Conversion of solar power to chemical energy based on carbon nanoparticle modified photo-thermoelectric generator and electrochemical water splitting system, *Nano Energy*, 2018, **48**, 481–488.

56 D. Pankratova, K. Yusupov, A. Vomiero, S. K. Honnali, R. Boyd, D. Fournier, S. Ekeroth, U. Helmersson, C. Azina and A. Febvrier, Enhanced Thermoelectric Properties by Embedding Fe Nanoparticles into CrN Films for Energy Harvesting Applications, *ACS Appl. Nano Mater.*, 2024, **7**, 3428–3435.

57 K. Kohashi, H. Yamamoto, Y. Okano, K. Kaneko, S. Miyake and M. Takashiri, Low-dimensional heterostructures of tin nanoparticle-decorated Bi_2Te_3 nanoplates for reducing lattice thermal conductivity, *Ceram. Int.*, 2024, **50**, 764–771.

58 W. A. Hubbard, M. Mecklenburg, J. J. Lodico, Y. Chen, X. Y. Ling, R. Patil, W. A. Kessel, G. J. K. Flatt, H. L. Chan, B. Vareskic, G. Bal, B. Zutter and B. C. Regan, Electron-Transparent Thermoelectric Coolers Demonstrated with Nanoparticle and Condensation Thermometry, *ACS Nano*, 2020, **14**, 11510–11517.

59 C. Ruana, M. Fana, Y. Zhanga, H. Songa, X. J. Lia and H. Hao, Enhancing the thermoelectric properties of $Bi_2Ba_2Co_2O_y$ by dispersing SiC nanoparticles based on Na element doping, *Ceram. Interfaces*, 2020, **46**, 6899–6905.

60 T. Varghese, C. Dun, N. Kempf, M. S. Javash, C. Karthik, J. Richardson, C. Hollar, D. Estrada and Y. Zhang, Flexible Thermoelectric Devices of Ultrahigh Power Factor by Scalable Printing and Interface Engineering, *Adv. Funct. Mater.*, 2019, 1905796.

61 V. Trivedi, M. Tiadi, B. S. Murty, D. K. Satapathy, M. Battabyal and R. Gopalan, Giant Thermoelectric Efficiency of Single-Filled Skutterudite Nanocomposites: Role of Interface Carrier Filtering, *ACS Appl. Mater. Interfaces*, 2022, **14**, 51084–51095.

62 G. Gouget, D. Bregiroux, R. Grosjean, D. Montero, S. Maier, F. Gascoin, C. Sanchez and D. Portehault, Liquid-Phase Synthesis, Sintering, and Transport Properties of Nanoparticle-Based Boron-Rich Composites, *Chem. Mater.*, 2021, **33**, 2099–2109.

63 W. Park, H. Hwang, S. Kim, S. Park and K. S. Jang, Optimized Thermoelectric Performance of Carbon Nanoparticle-Carbon Nanotube Heterostructures by Tuning Interface Barrier Energy, *ACS Appl. Mater. Interfaces*, 2021, **13**, 7208–7215.

64 B. Cai, H. L. Zhuang, Q. Cao, H. Hu, J. Dong, K. Asfandiyar and J. F. Li, Practical High-Performance $(Bi,Sb)_2Te_3$-Based Thermoelectric Nano-composites Fabricated by Nanoparticle Mixing and Scrap Recycling, *ACS Appl. Mater. Interfaces*, 2020, **14**, 16426–16435.

65 X. Wang, H. Dong, Q. Ma, Y. Chen, X. Zhao and L. Chen, Nickel nanoparticle decorated silicon carbide as a thermal filler in thermal conductive aramid nanofiber-based composite films for heat dissipation applications, *RSC Adv.*, 2023, **13**, 20984.

66 S. Yang, K. Cho, J. Yun, J. Choi and S. Kim, Thermoelectric characteristics of γ-Ag_2Te nanoparticle thin films on flexible substrates, *Thin Solid Films*, 2017, **641**, 65–68.
67 S. Ghosh, S. Harish, M. Ohtaki and B. B. Saha, Thermoelectric figure of merit enhancement in cement composites with graphene and transition metal oxides, *Mater. Today Energy*, 2020, **18**, 100492.
68 A. Lund, Y. Tian, S. Darabi and C. Müller, A polymer-based textile thermoelectric generator for wearable energy harvesting, *J. Power Sources*, 2020, **40**, 228836.
69 H. M. Elmoughni, A. K. Menon, R. M. W. Wolfe and S. K. Yee, A Textile-Integrated Polymer Thermoelectric Generator for Body Heat Harvesting, *Adv. Mater. Technol.*, 2019, 1800708.
70 K. Sarkar, A. Debnath, K. Deb, A. Bera and B. Saha, Effect of NiO incorporation in charge transport of polyaniline: Improved polymer based thermoelectric generator, *Energy*, 2019, **177**, 203–210.
71 D. Park, M. Kim and J. Kim, Fabrication of PEDOT:PSS/Ag2Se Nanowires for Polymer-Based Thermoelectric Applications, *Polymers*, 2020, **12**, 2932.
72 V. Shalini, R. K. Roghan, N. S. Santhosh, J. Archana, H. Ikeda, S. Harish and M. Navaneethan, Solution processed polyaniline anchored graphene on conductive carbon fabric for high performance wearable thermoelectric generators, *Mater. Chem. Phys.*, 2023, **306**, 128022.
73 R. M. Kluge, N. Saxena and P. M. Buschbaum, A Solution-Processable Polymer-Based Thin-Film Thermoelectric Generator, *Adv. Energy Sustainability Res.*, 2021, **2**, 2000060.
74 J. Huang, X. Liu and Y. Du, Highly efficient and wearable thermoelectric composites based on carbon nanotube film/polyaniline, *J. Mater.*, 2024, **10**, 173–178.
75 M. Mukaida, K. Kirihara, T. Ebihara and Q. Wei, Gram-scale polymer-based thermoelectric module for charging Li-ion batteries, *Mater. Today Energy*, 2023, **32**, 101238.
76 T. R. Marinho, V. Correia, C. R. Tubio, A. A. Pernas, M. J. Abad, S. L. Mendez and P. Costa, Flexible thermoelectric energy harvesting system based on polymer composites, *J. Chem. Eng.*, 2023, **473**, 145297.
77 S. Darabi, C. Y. Yang, Z. Li, J. D. Huang, M. Hummel, H. Sixta, S. Fabiano and C. Muller, Polymer-Based n-Type Yarn for Organic Thermoelectric Textiles, *Adv. Electron. Mater.*, 2023, **9**(4), 2201235.
78 J. F. S. Claumarchirant, M. A. Nasiri, C. Cho, A. Cantarero, M. Culebras and C. M. Gomez, Textile-based Thermoelectric Generator Produced Via Electrochemical Polymerization, *Adv. Mater. Interfaces*, 2023, **10**(8), 2202105.
79 Y. T. Lin, C. Y. Lee, C. Y. Wu, J. M. Lin, T. C. Lee, S. H. Tung and C. L. Liu, High thermoelectric performance of spray-coated Poly(3,4-ethylenedioxythiophene):poly(styrenesulfonate) films enabled by two-step post-treatment process, *J. Power Sources*, 2023, **556**, 232516.
80 J. Camut, N. H. Pham, D. Y. N. Truong, G. C. Hernandez, N. Farahi, M. Yasseri, E. Mueller and J. de Boor, Aluminum as promising electrode for Mg_2(Si,Sn)-based thermoelectric devices, *Mater. Today Energy*, 2021, **21**, 100718.
81 J. Camut, P. Ziolkowski, P. Ponnusamy, C. Stiewe, E. Mueller and J. Boor, Efficiency Measurement and Modeling of a HighPerformance Mg_2(Si,Sn)-Based Thermoelectric Generator, *Adv. Eng. Mater.*, 2023, **25**, 2200776.
82 J. M. S. Gordillo, C. D. Sierra, G. G. Diez, J. S. Ruiz, V. Bonino, M. N. Eroles, J. C. G. Rosillo, D. E. Wiese, M. Salleras, L. Fonseca, A. Morata and A. Tarancon, Superior Thermoelectric Performance of SiGe Nanowires Epitaxially Integrated into Thermal Micro-Harvesters, *Small*, 2023, 2206399.
83 P. F. Villalba, A. P. P. Marin, L. Abad, G. G. Dalkiranis, A. F. Lopeandia, G. Garcia and J. R. Viejo, Measuring Device and Material ZT in a Thin-Film Si-Based Thermoelectric Microgenerator, *Nanomaterials*, 2019, **9**, 653.
84 R. Deshpande, J. Camut, E. Müller and J. Boor, Device level assessment of Ni and $Ni_{45}Cu_{55}$ as electrodes in Mg_2(Si,Sn)-based thermoelectric generators, *Mater. Des.*, 2024, 112757.
85 M. Kashiwagi, Y. Liao, S. Ju, A. Miura, S. Konishi, T. Shiga, T. Kodama and J. Shiomi, Scalable Multi-nanostructured Silicon for Room-Temperature Thermoelectrics, *ACS Appl. Energy Mater.*, 2019, **10**, 7083–7091.
86 G. Hu, H. Edwards and M. Lee, Silicon integrated circuit thermoelectric generators with a high specific power generation capacity, *Nat. Electron.*, 2019, **2**, 300–306.
87 X. Yu, W. Jin, J. Pang, J. Zuo, X. Kuang and C. Lu, A multifunctional Mg Si monolayer with negative Poisson's ratio and ultrahigh thermoelectric performance at room temperature, *J. Mater. Chem. A*, 2024, **12**, 1488–1497.
88 L. Fonseca, I. D. Noyan, M. Dolcet, D. E. Wiese, J. Santander, M. Salleras, G. Gadea, M. Pacios, J. M. Sojo, A. Morata and A. Tarancon, Transitioning from Si to SiGe Nanowires as Thermoelectric Material in Silicon-Based Microgenerators, *Nanomaterials*, 2021, **11**, 517.
89 S. Lee, K. Kim, D. H. Kang, M. Meyyappan and C. K. Baek, Vertical Silicon Nanowire Thermoelectric Modules with Enhanced Thermoelectric Properties, *Nano Lett.*, 2019, **19**, 747–755.